Why does Nb(V) show higher heterolytic pathway selectivity than Ti(IV) in epoxidation with H_2O_2? Answers from model studies on Nb- and Ti-substituted Lindqvist tungstates

Nataliya V. Maksimchuk[†,‡] Irina D. Ivanchikova,[†] Gennadii M. Maksimov,[†] Ilia V. Eltsov,[‡] Vasilii Yu. Evtushok,[†,‡] Oxana A. Kholdeeva,[†,‡,] Daniel Lebbie,[§] R. John Errington,[§,*] Albert Solé-Daura,[‖] Josep M. Poblet,[‖] and Jorge J. Carbó[‖,*]*

[†] Boreskov Institute of Catalysis, Pr. Lavrentieva 5, Novosibirsk 630090, Russia

[‡] Novosibirsk State University, Pirogova str. 2, Novosibirsk 630090, Russia

[§] Chemistry, School of Natural and Environmental Sciences, Bedson Building, Newcastle University, NE1 7RU, UK

[‖] Departament de Química Física i Inorgànica, Universitat Rovira i Virgili, 43005 Tarragona, Spain

RECEIVED DATE

ABSTRACT. Ti- and Nb-monosubstituted tungstates of the Lindqvist structure, $(Bu_4N)_3[(CH_3O)TiW_5O_{18}]$ (**TiW_5**) and $(Bu_4N)_2[(CH_3O)NbW_5O_{18}]$ (**NbW_5**), display catalytic reactivity analogous to that of heterogeneous Ti- and Nb-containing catalysts in alkene oxidation with aqueous hydrogen peroxide. In this work, we make an attempt to rationalize the differences observed in the catalytic performance of Ti and Nb single site catalysts for alkene epoxidation with H_2O_2 using **MW_5** (M = Ti and Nb) as tractable molecular models. In the oxidation of cyclohexene, **NbW_5** reveals higher catalytic activity and heterolytic pathway selectivity than its Ti counterpart while **TiW_5** is more active for decomposition of H_2O_2. The heterolytic and homolytic oxidation pathways have been investigated by means of kinetic and computational tools. The kinetic trends established for **MW_5**-catalyzed epoxidation, comparative spectroscopic studies (IR, Raman, UV-vis, and ^1H and ^{17}O NMR) of the reaction between **MW_5** and hydrogen peroxide, and DFT calculations

implemented on cyclohexene epoxidation over **MW_5** strongly support a mechanism that involves interaction of either **MW_5** or its hydrolyzed form 'MOH' with H_2O_2 to afford a protonated peroxo species 'HMO_2' that is present in equilibrium with a hydroperoxo species 'MOOH', followed by electrophilic oxygen atom transfer from 'MOOH' to the C=C bond to give epoxide and 'MOH'. For both Ti and Nb, the peroxo species 'HMO_2' is more stable than the hydroperoxo species 'MOOH' but the latter is more reactive toward alkenes. For Ti catalyst, which has a rigid and hindered metal center, the hydroperoxo species transfers preferentially the nondistorted β-oxygen whereas for the Nb catalysts the transference of the more electrophilic α-oxygen is favored. Moreover, upon increasing the oxidation state from Ti(IV) to Nb(V) the reaction accelerates and selectivity towards electrophilic products increases. Calculations showed that the Nb(V) catalyst reduces significantly the free-energy barrier for the heterolytic oxygen transfer because of the higher electrophilicity of the metal center. The improved performance of the Nb(V) single-site is due to a combination of a flexible coordination environment with a higher metal oxidation state.

KEYWORDS: *Epoxidation, hydrogen peroxide, niobium, titanium, Lindqvist tungstate, mechanism, DFT*

INTRODUCTION

The selective oxygenation of organic compounds using green oxidants O_2 and H_2O_2 and leach-resistant heterogeneous catalysts is a demanding task in modern oxidation catalysis.[1-4] Aqueous hydrogen peroxide is an atom-efficient, easy to handle, rather safe and relatively cheap oxidant that produces water as the sole by-product.[5-8] The invention of titanium silicalite-1 (TS-1)[9] by ENI in the 1980s had a great impact on the development of the field of heterogeneous oxidation catalysis as TS-1 appeared to be a highly effective and stable catalyst for selective oxidations of small organic substrates, including the epoxidation of linear olefins, with dilute H_2O_2 as terminal oxidant.[10,11] At

the beginning of the 2000s, the needs of the fine chemicals industry for oxidative transformations of bulky organic molecules motivated an intensive research activity directed to the synthesis of mesoporous metal-silicates[12,13] as well as hierarchical micro–mesoporous materials.[14] However, mesoporous titanium-silicates revealed a relatively low H_2O_2 utilization efficiency and a significant contribution from homolytic oxidation routes, which is especially detrimental to selectivity for alkene epoxidation. In addition, the hydrophilic nature of the surface of mesoporous silicates is detrimental to catalyst stability. Although a range of leach-resistant Ti-containing materials have been developed,[12,13,15-18] Ti single sites in a hydrophilic silica environment are generally prone to polymerization when aqueous H_2O_2 is employed.

In the past decade, mesoporous niobium-silicates have attracted growing attention as heterogeneous catalysts for selective oxidations with H_2O_2.[19-30] Some research groups noticed that Nb-silicates possess hydrothermal stability superior to their Ti analogs and, moreover, they are more active and selective in epoxidation of olefins, in particular those with highly reactive allylic hydrogens.[23,27,28,31] Other distinctive features of Nb-silicates include the capability to catalyze epoxidation of C=C bonds in α,β-unsaturated carbonyl compounds and unusual solvent-dependent regioselectivity in epoxidation of terpenes.[23,24,26,28] While epoxidation of electron-deficient C=C bonds was proved to proceed via oxidation of the solvent molecule (CH_3CN) and in situ generation of peroxycarboximidic acid $H_3CC(=NH)OOH$ that acts as the true epoxidizing species,[28] the origins of the higher selectivity in the epoxidation of electron-rich alkenes and the unusual regioselectivity of the Nb catalysts, as compared to Ti analogs, are not completely clear. Recently, we proposed that these phenomena may be considered as an indication of different structures for the active peroxo species responsible for epoxidation over Nb(V) and Ti(IV).[31] Several mechanistic studies aimed to explain the differences in the catalytic properties of Nb and Ti catalysts,[28,31-36] but inconsistencies remain in the conclusions from these studies. The formation of active hydroperoxo species TiOOH is not in doubt for Ti single-site catalysis although there is no agreement yet about the details of

bonding between the hydroperoxo group and titanium.[11,37,38] The nature of the active peroxo species in the case of Nb catalysts is much less understood. Flaherty and co-workers initially suggested that a superoxo Nb species performs alkene epoxidation on Nb(V) sites,[34,35] but subsequently concluded that a peroxo intermediate Nb(η^2-O_2) is responsible for epoxidation.[36] In the meantime, comparative spectroscopic and kinetic studies on Nb- and Ti-silicates allowed us to suggest that, for both Ti and Nb catalysts, a hydroperoxo moiety MOOH is the real epoxidizingspecies.[28,31]

To shed more light on the origin of the catalytic performance of Nb catalysts, we have made an effort to clarify the role of protons in H_2O_2 activation at Nb(V) through experimental and computational investigations of alkene epoxidation with H_2O_2 in the presence of well-defined Nb-monosubstituted polyoxometalates (Nb-POM).[39] Owing to their metal oxide like structure, thermodynamic stability to oxidation and resistance to hydrolysis, adjustable solubility, acidity and redox activity, and possibility of investigation at the atomic (molecular) level, POMs have found applications as tractable molecular models for heterogeneous metal-oxide catalysts,[40,41] including single-site variants.[42–47] Our studies of Nb(V)-monosubstituted Lindqvist tungstates included $(Bu_4N)_3[Nb(O)W_5O_{18}]$ and $(Bu_4N)_4[(\mu\text{-}O)(NbW_5O_{18})_2]$. The higher activity of the latter, which forms $(Bu_4N)_2[(HO)NbW_5O_{18}]$ upon hydrolysis, unambiguously demonstrated that protons play an indispensable role in both the formation of active peroxo Nb species and their reactivity,[39] and a protonated peroxo complex, $(Bu_4N)_2[(O_2)NbW_5O_{18}H]$ has been synthesized and comprehensively characterized for the first time. In contrast to its unprotonated counterpart, $(Bu_4N)_3[(O_2)NbW_5O_{18}]$, the protonated peroxo complex demonstrated reactivity for epoxidation of cyclohexene and other alkenes under stoichiometric conditions.[39] The UV-vis, IR, Raman, and ^{17}O NMR spectroscopic studies together with DFT calculations all indicated that the activating proton in the Nb peroxo intermediate is mainly located at oxygens that bridge between Nb and W atoms. Meanwhile, DFT calculations showed that hydroperoxo 'Nb(η^2–OOH)' exists in equilibrium with protonated peroxo 'HNb(O_2)' and has a lower activation barrier for the oxygen atom transfer to C=C bond in alkene.[39]

The aim of the present work was to gain insights into the differences in the catalytic performances of Ti and Nb single-site catalysts in H_2O_2-based alkene epoxidation through a comparative study of Ti- and Nb-monosubstituted tungstates of the Lindqvist structure, $(Bu_4N)_3[(CH_3O)TiW_5O_{18}]$ (**TiW_5**) and $(Bu_4N)_2[(CH_3O)NbW_5O_{18}]$ (**NbW_5**) by means of kinetic, spectroscopic, and computational techniques. We also compare here the trends observed with those determined previously for mesoporous Ti- and Nb-silicate catalysts[28,31] synthesized by evaporation-induced self-assembly (EISA).[18,26]

EXPERIMENTAL SECTION

Synthesis and Characterization of POMs. The synthesis of **TiW_5** was carried out following the literature protocol[48] (see Supporting Information (SI) for details). The synthesis of **NbW_5** was adapted from ref.[49] Peroxo complex $(Bu_4N)_2[(O_2)NbW_5O_{18}H]$ (**$HNb(O_2)W_5$**) was prepared and characterized as described previously.[39]

Peroxo complex ***$(Bu_4N)_3[(O_2)TiW_5O_{18}H]$*** (**$HTi(O_2)W_5$**) was synthesized by the addition of 30% aqueous H_2O_2 (32.6 μL, 0.375 mmol) to a solution of TiW_5 (150 mg, 0.075 mmol) in 2 mL of CH_3CN. The yellow solution (maximum at 375 nm in UV-vis) was stirred for 30 min at room temperature and diluted with 10 mL of ether. The resulting bright yellow solid (135 mg, ca. 90% yield) was isolated by filtration, washed with ether and dried in air at room temperature. The presence of one peroxo group per molecule of **$HTi(O_2)W_5$** was confirmed by titration with PPh_3.[50] Potentiometric titration of **$HTi(O_2)W_5$** in CH_3CN with aqueous Bu_4NOH gave a $[H^+]/[Ti]$ ratio of 0.75. Anal. calcd (%) for $C_{48}H_{109}N_3TiW_5O_{20}$: C, 28.61; H, 5.45; N, 2.09; Ti, 2.38; W, 45.61. Found: C, 28.13; H, 5.39; N, 2.11; Ti, 2.41; W, 42.1. IR (KBr, 1000-400 cm^{-1}): 953 (s, W=O), 911 (w, sh), 884 (m, OO), 797 (vs, WOW), 750 (vs, WOW), 623 (s, TiO_2), 552 (m), 534 (m, TiO_2), 462 (s).

Interaction with H_2O. Interaction of **TiW_5** with H_2O was performed by the addition of 10 vol% of distilled water to a 0.02 *M* (^1H and ^{17}O NMR monitoring) solution of the POM in dry CD_3CN (0.5 mL) at 20 and 50 ^oC.

Interaction with H_2O_2. Interaction of POMs with aqueous H_2O_2 was performed by the addition of H_2O_2 (2–5 mole-equiv., taken as 30 or 77% solution in water) to a 0.02 *M* (for ^{17}O NMR monitoring) or 0.0005–0.0015 M (for UV-vis monitoring) solution of the POM in dry CH_3CN at 20 ^oC. UV-vis studies of the rate of formation of peroxo complexes were carried out at λ = 375 nm for **TiW_5** and 315 nm for **NbW_5**. Typically, 0.6 mL of 0.0015 *M* solutions of **TiW_5** or **NbW_5** were placed into the cuvette, and an appropriate amount of water (0.25-1.0 μL) was added. To this solution, 0.4 μL of 30% H_2O_2 or 0.15 μL of 77% H_2O_2 was added. The absorbance D at specific λ was measured *ca*. 20 s after the addition of H_2O_2 and thereafter at 1 min intervals.

Reaction between TiW_5 and dried H_2O_2. Aqueous H_2O_2 (40%, 3.5 μL, 0.15 mmol) was dissolved in CH_3CN (5 mL) and the volatiles were removed under vacuum. After repeating this process twice more, CH_3CN (5 mL) was added, followed by **TiW_5** (300 mg, 0.15 mmol). The reaction mixture was stirred for 1 h, then pumped dry and dissolved in CD_3CN for ^1H NMR. The sample was then returned to the flask with CH_3CN (5 mL). This process was repeated after 3 h, 3 days and 4 weeks after which the ^{17}O NMR spectrum was also recorded. After addition of further H_2O_2 (1.50 mmol, dried as above) and stirring for 2 h, the sample was pumped dry and NMR spectra recorded. This process was repeated after addition of the final aliquot (15.00 mmol) of dried H_2O_2.

Instrumentation and Methods. Infrared spectra were recorded in KBr pellets using an Agilent Cary 600 FTIR spectrometer or from powders on a Nicolet Avatar 370 DTGS spectrometer using a Smart Orbit single reflectance ATR attachment. FT–Raman spectra (3600–100 cm^{-1}, 300 scans, resolution 4 cm^{-1}, 180° geometry) were recorded on a RFS 100/S spectrometer (Bruker) with excitation of the 1064 nm line (Nd–YAG laser). Resonance Raman spectra were obtained using a Triplemate Spex spectrometer with a LN-1340PB CCD detector from Princeton Instruments; the 488

nm line of an Ar laser was used for spectral excitation. Electronic absorption spectra were collected using a Cary–50 spectrophotometer in 0.1 cm quartz cells. The content of W, Ti and Nb was determined by ICP–OES on a PerkinElmer Optima–430 DV instrument. CHNO analyzes were carried out using a CHNSO analyzer Vario EL Cube.

NMR spectra for **TiW_5** and $(Bu_4N)_2[W_6O_{19}]$ (**W_6**) were recorded on a Brüker Avance 300 spectrometer at 300.0 (^{1}H) or 67.8 (^{17}O) MHz using 5 mm o.d. glass NMR tubes (0.5 mL solution volume). ^{1}H NMR spectra were referenced to residual CHD_2CN at δ 1.97 ppm in CD_3CN solvent. ^{17}O NMR spectra were referenced to external H_2O. ^{183}W NMR spectrum for **TiW_5** in the presence of H_2O_2 and ^{31}P NMR spectrum run after addition of PPh_3 to **$HTi(O_2)W_5$** were recorded on a Brüker Avance III 500 spectrometer at 20.83 (^{183}W) or 202.42 (^{31}P) MHz using 10 mm o.d. NMR tubes (2.5 mL solution volume) and referenced to K_2WO_4 and 85% H_3PO_4, respectively. ^{93}Nb NMR spectra of **NbW_5** were recorded at 97.94 MHz on an Brüker Avance-400 spectrometer using a high resolution multinuclear probe head with 10 mm o.d. (2.5 mL solution volume) sample tubes. Chemical shifts were referenced to a saturated solution of $NbCl_5$ in CH_3CN (δ 0 ppm). For convenience, 0.05 M $H_5SiW_{11}NbO_{40}$ (δ –975 ppm) was used as a secondary external standard. The ^{1}H spectra of **NbW_5** were measured on a Brüker Avance III 500 spectrometer at 500.0 MHz using 5 mm o.d. glass NMR tubes (0.5 mL solution volume). ^{1}H chemical shifts were referenced to CH_3CN (δ 1.96 ppm).

GC analyses were carried out on a Chromos GH-1000 gas chromatograph equipped with a flame ionization detector and a quartz capillary column (30 m × 0.25 mm) filled with BP-5. GC–MS analyses were performed using an Agilent 7000B system with a triple–quadrupole mass–selective detector Agilent 7000 and a GC Agilent 7890B apparatus.

Full details on the catalytic and stoichiometric oxidation reactions, kinetic experiments as well as computational methodology are provided in the SI.

RESULTS AND DISCUSSION

Cyclohexene oxidation and H_2O_2 decomposition over TiW_5 and NbW_5. To verify the possibility of using the Lindqvist monosubstituted tungstates **MW_5** (M = Ti and Nb) as molecular models of heterogeneous Ti- and Nb-catalysts, we first compared trends observed in the oxidation of cyclohexene (CyH) with equimolar amounts of H_2O_2 over **MW_5** with those for the corresponding mesoporous M-silicates. Oxidation of CyH, an olefin with highly reactive hydrogen atoms in the allylic positions, is widely accepted as a reliable test that helps in evaluation of the relative contributions of hetero- (selective formation of epoxide, *trans*-cyclohexane-1,2-diol (diol), and 2-hydroxycyclohexanone (ketol)) and homolytic (predominant formation of cyclohexenyl hydroperoxide (HP), 2-cyclohexene-1-ol (enol), and 2-cyclohexene-1-one(enone)) oxidation pathways (Scheme 1).

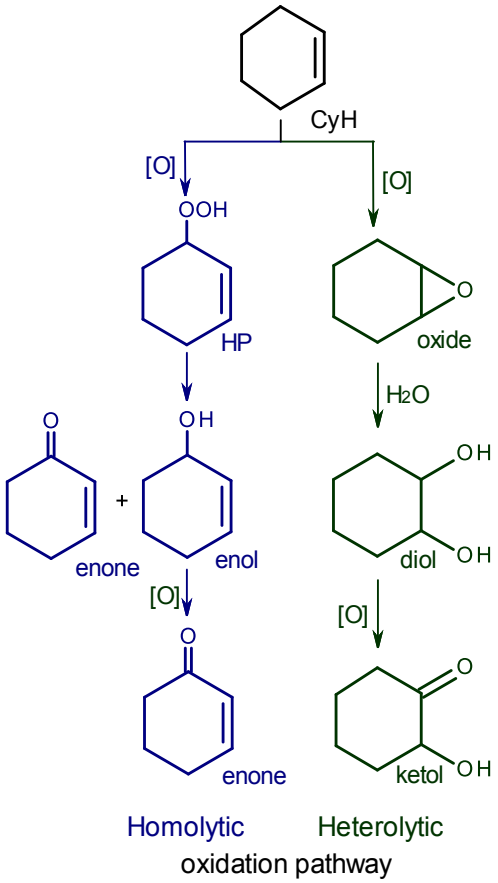

Scheme 1. CyH oxidation products formed via heterolytic and homolytic pathways.

The observed distributions of the CyH oxidation products are presented in Table 1 along with blank experiments. It is evident that both **NbW_5** and Nb-silicate show higher catalytic activity and heterolytic pathway selectivity than their Ti counterparts. Indeed, the same level of CyH conversion was attained much faster for the Nb catalysts than for the corresponding Ti catalysts. Importantly, the Lindqvist tungstate without any heterometal, **W_6**, is completely inactive, which is consistent with its inertness toward H_2O_2 (vide infra).

Table 1. CyH oxidation with H_2O_2 over Nb and Ti catalysts

Entry	catalyst	time, h	CyH conv., %	pathway selectivity, %	
				heterolytic[a] (epoxide/diol/ketol)	homolytic[b]
1	–[c]	5	5	21 (21/traces/0)	77
2	**W_6**[c]	5	2	traces	traces
3	**NbW_5**[c]	0.2	31	86 (23/46/15)	12
		2	67	90 (12/47/31)	10
4	**TiW_5**[c]	3	30	59 (40/10/9)	36
5	Nb,Si[d]	0.3	34	71 (47/15/9)	21
6	Ti,Si[d]	2.5	35	65 (42/12/11)	27

[a] Total selectivity of heterolytic oxidation products based on substrate consumed; individual selectivities are given in parentheses.

[b] Total selectivity of homolytic oxidation products based on substrate consumed (HP + enol + enone).

[c] Reaction conditions: 0.2 mmol CyH, 0.2 mmol H_2O_2, 0.004 mmol POM (when added), 50°C, 1 mL CH_3CN.

[d] Reaction conditions: 0.1 mmol CyH, 0.1 mmol H_2O_2, catalyst 0.003 mmol Ti or Nb, 50°C, 1 mL CH_3CN. Data taken from ref.[31]

On the other hand, the activity of **TiW_5** (Figure 1) and Ti-silicate[31] for hydrogen peroxide decomposition in the absence of organic substrate was observed to be greater than that of their Nb-containing analogs, which corresponds to the higher amounts of allylic oxidation products formed in the presence of Ti catalysts (see Table 1).

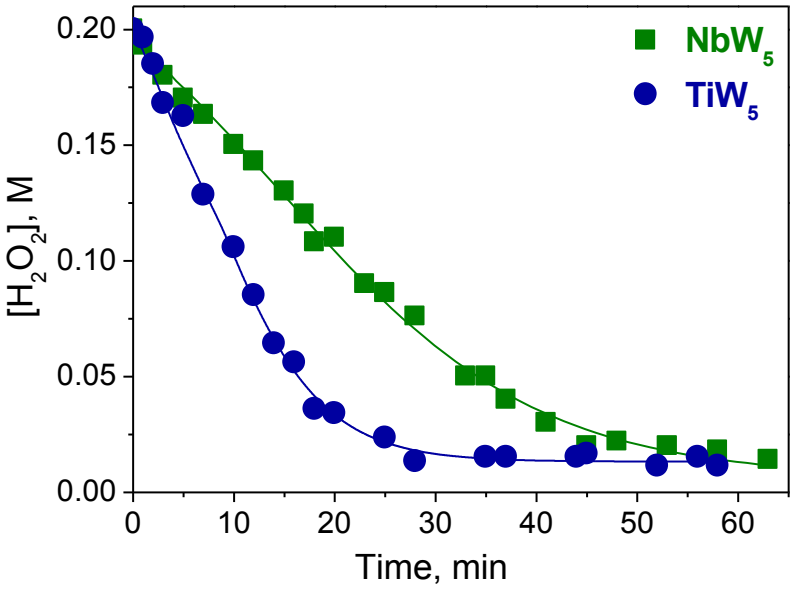

Figure 1. Reaction profiles for H_2O_2 decomposition over **NbW_5** and **TiW_5** in the absence of organic substrate. Conditions: 0.2 *M* H_2O_2, 0.008 *M* POM, 2 mL CH_3CN, 70 °C.

It is important to assess the solvolytic stability of hetero-metal substituted POM structures in order to confirm that any catalytic activity is due to the heterometal M within the POM environment and not to low nuclearity peroxotungstates arising from POM degradation by interaction with aqueous hydrogen peroxide.[51] The structural stability of {NbW_5} Lindqvist tungstates towards, at least, a 50-fold excess of H_2O_2 has been recently demonstrated.[39] ^{17}O NMR spectroscopy confirmed the stability of the **TiW_5** structure under the catalytic conditions of CyH oxidation (Figure S1): no signals with chemical shifts in the range of 621–657 ppm corresponding to low nuclearity peroxotungstates[52] were detected. A slight shift of the TiOW signal from δ 527 to δ 535 ppm is consistent with hydrolysis and condensation of **TiW_5** after the catalysis (note that a peak for TiOTi is not observed as this is derived from non-enriched H_2O).[53] An FTIR spectrum of **TiW_5** isolated after the catalytic reaction of CyH oxidation (Figure S2, spectrum B) retained the main vibrations of the Lindqvist structure in addition to a strong band at 670 cm^{-1} due to ν(TiO) for the TiOTi bridge of the dimer $[(\mu\text{-O})(TiW_5O_{18})_2]^{6-}$.[53] We cannot exclude the possibility that additional dimerization occurred during isolation of the solid from the reaction mixture.

The similarities of the trends observed in CyH oxidation and H_2O_2 decomposition for the **MW_5** and M-silicate catalysts (M = Ti and Nb) coupled with stability of the Lindqvist structure of **MW_5** under the turnover conditions therefore justify the application of **MW_5** as models for mechanistic studies of H_2O_2 activation.

Temperature dependences of epoxidation and H_2O_2 decomposition rates. The rate of cyclooctene (CyOct) epoxidation over both **NbW_5** and **TiW_5** showed typical Arrhenius dependences (Figure 2a). The apparent activation energies (E_a) estimated from the Arrhenius plots of 11.7 and 14.3 kcal/mol for **NbW_5** and **TiW_5**, respectively, are similar to E_a values previously found for Nb-Si and Ti-Si catalysts (11.9 and 14.2 kcal/mol,[31] respectively). At the same time, E_a established for the decomposition of H_2O_2 is lower for **TiW_5** relative to **NbW_5**: 14.6 vs 16.7 kcal/mol (Figure 2b).

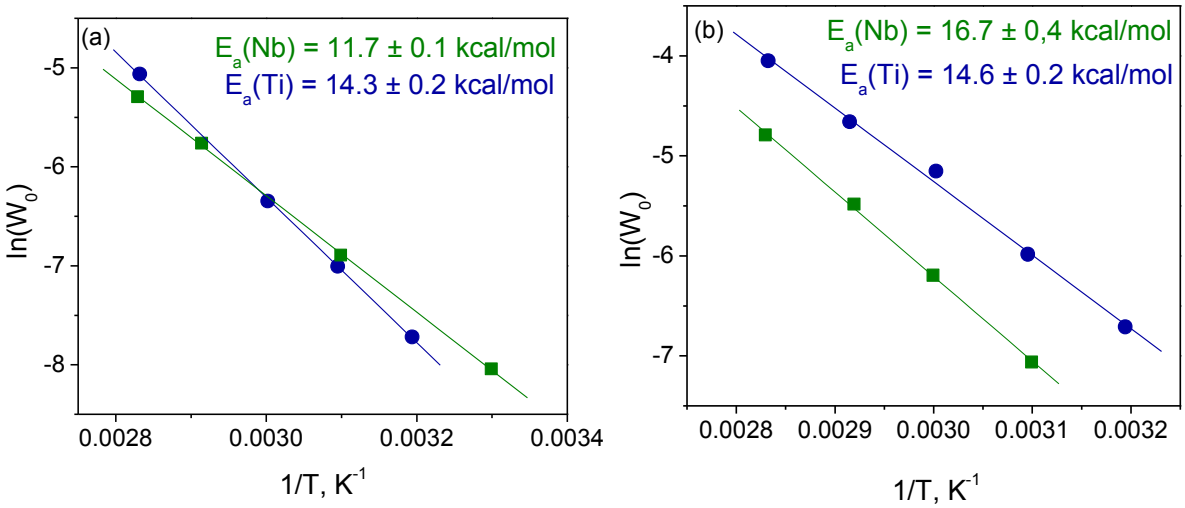

Figure 2. Arrhenius plots for **TiW_5**- and **NbW_5**-catalyzed CyOct epoxidation (a) and H_2O_2 decomposition (b). Reaction conditions: 0.1 *M* CyOct, 0.1 *M* H_2O_2, 0.004 *M* POM, 1 mL CH_3CN (for epoxidation); 0.2 *M* H_2O_2, 0.008 *M* POM, 2 mL CH_3CN (for H_2O_2 decomposition).

A summary on the activation energies determined from the Arrhenius dependences for cyclooctene epoxidation and H_2O_2 decomposition over Ti and Nb catalysts is given in Table 2.

Table 2. Comparison of Arrhenius activation energies (kcal/mol) for CyOct epoxidation and H_2O_2 decomposition over Ti and Nb-catalysts

	NbW_5	**TiW_5**	Nb,Si[a]	Ti,Si[a]
E_a (CyOct epoxidation)	11.7±0.1	14.3±0.2	11.9±0.6	14.2±0.8
E_a (H_2O_2decomposition)	16.7±0.4	14.6±0.2	20.5±0.3	14.8±1.1

[a] Data taken from ref.[31]

The values of E_a for CyOct epoxidation and H_2O_2 degradation are similar for **TiW_5** (14.3 and 14.6 kcal/mol, respectively) whereas the difference between the activation energies for epoxidation and H_2O_2 decomposition for **NbW_5** is significant (11.7 vs 16.7 kcal/mol). The same tendency was previously found for Nb,Si and Ti,Si-catalysts[31] (see Table 2). We therefore suggested that the superior epoxidation selectivity of the Nb-catalysts compared with their Ti analogues is due to (i) a lower energy barrier for the heterolytic pathway leading to epoxidation and (ii) the higher energy cost of homolytic O–O bond splitting in NbOOH intermediates. To verify this assumption, the reaction was further studied by kinetic, spectroscopic and computational methods.

Kinetics of CyOct epoxidation with H_2O_2 over MW_5. Kinetics of alkene epoxidation with H_2O_2 over **TiW_5** and **NbW_5** was investigated using CyOct as a model substrate. Kinetic plots for alkene decay in the presence of **TiW_5** and **NbW_5** showed no induction periods, and the epoxidation rate was not influenced by O_2 or light. 2,6-Di-*tert*-butyl-4-methylphenol, a conventional radical scavenger, did not affect the oxidation rate and product distribution, which is consistent with a non-radical oxidation mechanism or a mechanism with short chains.[54] Without catalyst, the rate of CyOct oxidation was minor.

Figure 3 shows dependences of CyOct consumption over **TiW_5** and **NbW_5** on concentrations of all the reactants. Regardless of the nature of the active metal (Ti or Nb), the reaction rate is first order in alkene (Figure 3a) and catalyst (Figure 3b) and exhibits saturation with increasing

concentration of H_2O_2 (Figure 3c). While the reaction with **NbW_5** was slightly inhibited by H_2O, an opposite effect was observed with **TiW_5** (Figure 3d). At 50 ^oC, similarly to metal-silicates,[31] the epoxidation rate was higher for **NbW_5** relative to **TiW_5** over the full range of concentrations studied.

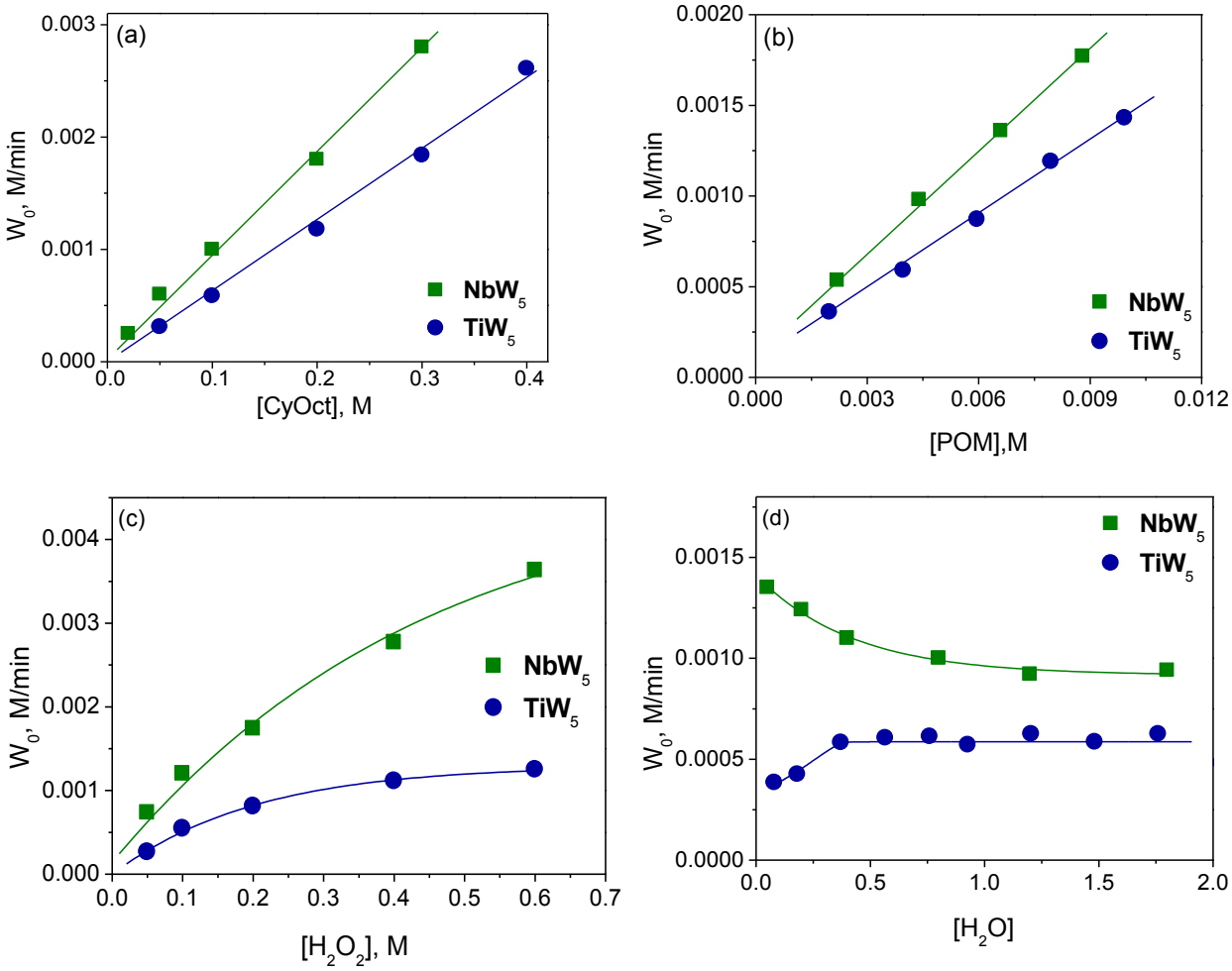

Figure 3. Plots of the initial rate of CyOct oxidation (CH_3CN, 50 ^oC) versus concentration of alkene (a), catalyst (b), oxidant (c), and water (d) in the presence of **NbW_5** and **TiW_5**.

In view of these kinetic results, we suggest that the epoxidation mechanism may involve hydrolysis of the methoxy derivative (Eq. 1) and reversible interaction of **$M(OH)W_5$** with H_2O_2 to produce peroxo complex **$HM(O_2)W_5$** (Eq. 2) followed by oxygen transfer from the peroxo complex to alkene (Eq. 4). In addition, we cannot exclude the possibility that the peroxo complex is formed through direct interaction of **MW_5** with H_2O_2, bypassing the hydrolysis stage (Eq. 3).

$$M(OCH_3)W_5 + H_2O \overset{K_1}{\rightleftharpoons} M(OH)W_5 + CH_3OH \quad (1)$$

$$M(OH)W_5 + H_2O_2 \overset{K_2}{\rightleftharpoons} HM(O_2)W_5 + H_2O \quad (2)$$

$$M(OCH_3)W_5 + H_2O_2 \overset{K_3}{\rightleftharpoons} HM(O_2)W_5 + CH_3OH \quad (3)$$

$$HM(O_2)W_5 + \text{alkene} \xrightarrow{k_4} M(OH)W_5 + \text{epoxide} \quad (4)$$

When all H_2O_2 is consumed at the end of the catalytic reaction, hydroxide **M(OH)W$_5$** formed via reaction (4) tends to dimerize via Eq.5, as evidenced (at least, for M = Ti) by IR and ^{17}O NMR spectroscopy(see above).

$$2\ M(OH)W_5 \overset{K_5}{\rightleftharpoons} (MW_5)_2O + H_2O \quad (5)$$

To investigate steps (1)–(4) we performed independent experiments involving hydrolysis of **MW$_5$**, interaction with H_2O_2, and stoichiometric reactions between **HM(O$_2$)W$_5$** and alkene, as described in the following sections.

Hydrolysis of MW$_5$ and interaction with H$_2$O$_2$. The interaction of **TiW$_5$** with H_2O and aqueous H_2O_2 was probed separately using spectroscopic methods. It was previously shown that hydrolysis of the methoxy group in **TiW$_5$** is relatively slow and, for complete hydrolysis, exposure to 20 equiv. of H_2O under heating is required.[53] Under these conditions, the dimeric Lindqvist polyanion $[(\mu\text{-}O)(TiW_5O_{18})_2]^{6-}$ was formed as a result of hydrolysis and subsequent dimerization of the 'TiOH' derivative.[53] In this work, we studied the reaction between **TiW$_5$** and a larger excess of H_2O by ^{1}H and ^{17}O NMR, *i.e.* conditions more typical of those used in catalytic reactions with aqueous H_2O_2. After the addition of 10 vol% of water (280 molar equiv.) to a 0.02 *M* solution of **TiW$_5$** in dry CH_3CN, the $TiOCH_3$ ^{1}H NMR peak at δ 4.10 disappeared with the simultaneous growth of a peak for free methanol at δ 3.29 ppm (Figure 4), consistent with the conversion of'$TiOCH_3$' to 'TiOH'. This process took 2–4 h at room temperature or 0.5–1 h at 50 ^{o}C.

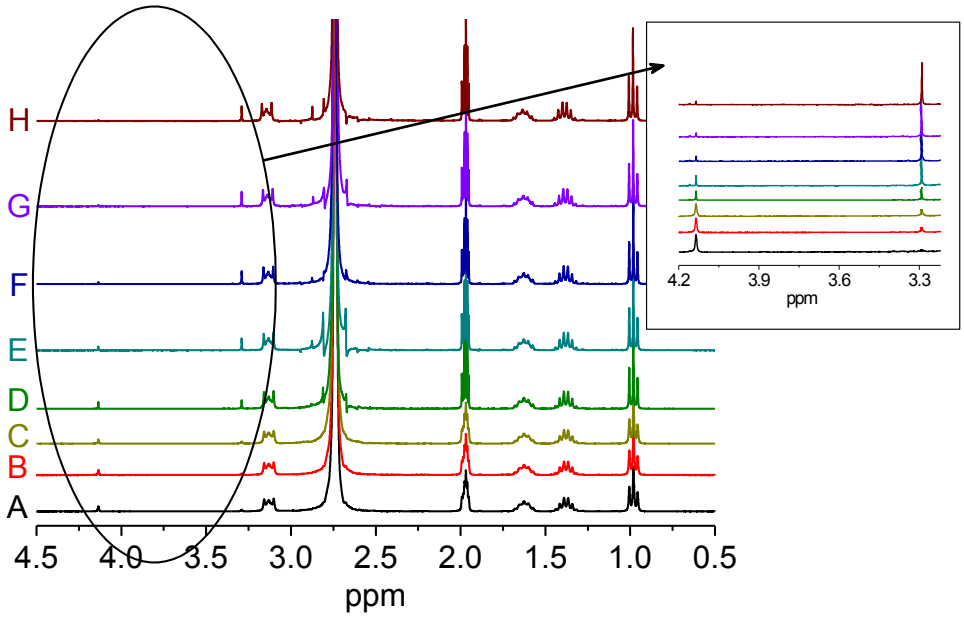

Figure 4. ^{1}H NMR spectra of **TiW_5**: (A) initial **TiW_5**, (B) immediately after addition of H_2O, (C)–(H) 5 min, 30 min, 1 h, 2 h, 4 h, and 24 h after addition of H_2O, respectively. Reaction conditions: 0.02 *M* POM, 10 vol% H_2O, 0.5 mLCH_3CN, 20 ^{o}C.

^{17}O NMR spectra (Figure S3) showed that **TiW_5** preserves the Lindqvist structure upon hydrolysis. No condensation to the dimer $[(\mu\text{-O})(TiW_5O_{18})_2]^{6-}$ occurred under the conditions studied, as shown by the absence of a TiOTi peak at δ 679 ppm and the corresponding shifted TiOW peak.[70] Apparently, a high concentration of water prevents condensation of the 'TiOH' species, favoring hydrolysis of the Ti-O-Ti linkage. Further studies, including isolation and characterization of $(TBA)_3[(HO)TiW_5O_{18}]$ will be published separately. Methoxide **NbW_5** is much more susceptible to trace hydrolysis and, in accordance with the previous work,[48] ^{1}H NMR samples showed the presence of free methanol immediately after dissolution of **NbW_5**.

UV-vis spectroscopic studies showed that interaction of **TiW_5** with H_2O_2 gives rise to the formation of a yellow peroxo species exhibiting a strong absorption band with a maximum at 375 nm ($\varepsilon = 1.85\cdot10^3 M^{-1}cm^{-1}$) (Figure 5a). According to the literature,[55-61] this band can be unambiguously attributed to the $O_2\rightarrow$Ti ligand-to-metal charge transfer in a side-on peroxo titanium complex.

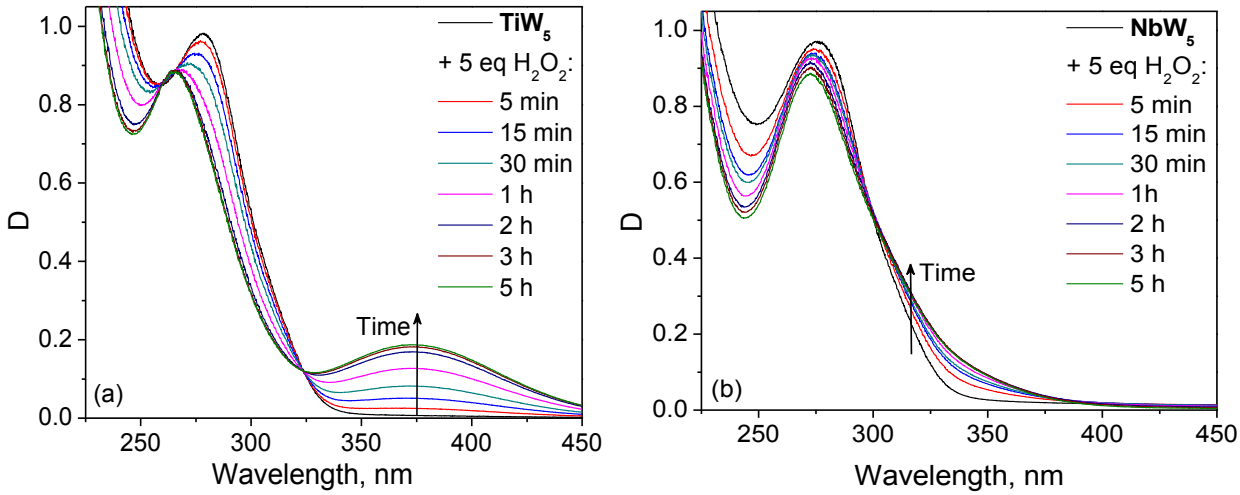

Figure 5. UV spectra of (a) **TiW_5** and (b) **NbW_5** upon interaction with 5 equiv. of 30% H_2O_2. Reaction conditions: 0.0005 *M* POM, 0.0025 *M* H_2O_2, 0.6 mL CH_3CN, 20 °C.

It is noteworthy that, under the same conditions, the niobium peroxo complex is formed significantly faster than the titanium analogue, as evidenced by the dynamics of the characteristic absorptions in the UV-vis spectra of **TiW_5** and **NbW_5** upon addition of H_2O_2 (Figure S4). To establish the importance of the hydrolysis reaction in the formation of the peroxo complex, we checked how the initial rates of increase in the absorbances at 375 nm for **TiW_5** and 315 nm for **NbW_5** (dD/dt at t→0), depend on the concentration of water. If we assumed that the formation of the peroxo species proceeds through direct interaction of the methoxy form **MW_5** with H_2O_2 via Eq. 3, we would expect no dependence of the peroxo complex accumulation rate on the concentration of H_2O. In contrast, if the formation of the peroxo complex requires preliminary hydrolysis of **MW_5** to produce **$M(OH)W_5$** (Eq. 1), the rate of peroxo complex formation rate would be expected to increase with increasing concentration of water, provided the hydrolysis step is rather slow. Figure S5 shows that the formation of the titanium peroxo species was initially slightly accelerated by water but then exhibited saturation with increasing H_2O concentration. On the other hand, the rate of the reaction between **NbW_5** and H_2O_2 was not affected by water concentration (Figure S6). Given that hydrolysis of **TiW_5** takes 2–4 h at room temperature, we may suppose that hydrolysis is rate-limiting for the formation of the Ti peroxo complex at low water concentration. The lack of dependence of the Nb

peroxo complex formation rate on the concentration of water suggests either that this process proceeds directly via Eq. 3 or that the hydrolysis step (Eq. 1) is fast. Indeed, ^{1}H NMR spectra of **NbW_5**.show the presence of free methanol directly after dissolution in acetonitrile and complete disappearance of $NbOCH_3$ signal immediately after addition of 10 vol% of H_2O, which implies facile and rapid hydrolysis. This fact is further supported by DFT calculations, which indicate that the reaction of **NbW_5** either with H_2O or H_2O_2 is fast showing low free energy barriers of 12.2 and 12.6 kcal·mol^{-1}, respectively (vide infra and Figure S16 in the Supporting Information).

Previously, we demonstrated by experimental and computational techniques that the dimer $(Bu_4N)_4[(\mu\text{-}O)(NbW_5O_{18})_2]$ (alternatively, $(Bu_4N)_3[Nb(O)W_5O_{18}] + H^+$) reacts with H_2O/H_2O_2 *via* formation of the monomer $(Bu_4N)_2[(HO)NbW_5O_{18}]$ which interacts with H_2O_2 to produce the protonated η^2-peroxo complex $(Bu_4N)_2[(O_2)NbW_5O_{18}H]$ (**$HNb(O_2)W_5$**).[39] UV-vis (Figure 5b) and ^{93}Nb NMR spectroscopic studies (Figure S7) confirmed that both the dimer and **NbW_5** produce the same peroxo complex **$HNb(O_2)W_5$**, which is not surprising considering the rapid hydrolysis of the methoxy derivative.

The interaction between ^{17}O-enriched **TiW_5** and aqueous H_2O_2 was also investigated by ^{17}O NMR spectroscopy (Figure 6). The addition of 2 mole-equivalents of H_2O_2 resulted in an upfield shift of the TiOW signal from 527 to 409 ppm, which indicates protonation of the TiOW bridging oxygen in the resulting peroxo species.[39,62,63] Indeed, a similar trend was observed in the ^{17}O NMR spectra of **TiW_5** upon addition of $HClO_4$ (Figure S8). Importantly, the heterometal-free Lindqvist tungstate $(Bu_4N)_2[W_6O_{19}]$ does not react with H_2O_2 under the same conditions: no changes were detected in the corresponding UV-vis (Figure S9) and ^{17}O NMR spectra (Figure S10).

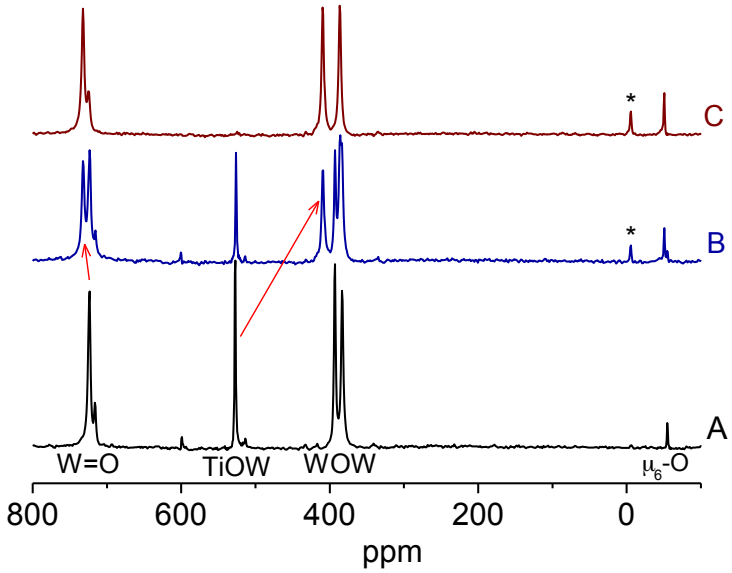

Figure 6. ^{17}O NMR spectra of **TiW$_5$** upon interaction with H_2O_2: (A) initial **TiW$_5$**, (B) immediately after addition of 2 equiv. of 30% H_2O_2, and (C) 15 min after addition of 2 equiv. of 30% H_2O_2. The peak marked with an asterisk corresponds to H_2O.Reaction conditions: 0.02 *M* POM, 0.04 *M* H_2O_2, 0.5 mL CH_3CN, 20 ^oC.

In an attempt to study the reaction between **TiW$_5$** and anhydrous H_2O_2, aliquots of aqueous H_2O_2 were dried by dissolution in CH_3CN and removal of the volatiles under reduced pressure (three times) before addition to the POM solution in dry CH_3CN.The yellow solution produced upon addition of one mole-equivalent of dried $H_2O_2$was monitored over a period of one month by removing the volatiles from the reaction mixture at intervals and recording the ^{1}H NMR spectrum before returning the sample to the reaction flask. The ^{17}O NMR spectrum was then recorded before and after further addition of first ten and then one hundred mole equivalents of dried H_2O_2. Results are shown in Figures S11 and S12. Notably, the characteristic ^{17}O NMR peak at δ 407 ppm assigned to **HTi(O$_2$)W$_5$** appeared only after disappearance of the $TiOCH_3$ peak in the corresponding^{1}H NMR spectrum upon addition of an excess of H_2O_2, and this coincided with the appearance of a new μ_6-O peak at δ –51 ppm. Subsequently, over a period of two days, the peaks for **HTi(O$_2$)W$_5$** diminished and the ultimate ^{17}O NMR spectrum was characteristic of the dimer **(TiW$_5$)$_2$O**. During the initial stages of the reaction, new TiOW and μ_6-O peaks in the ^{17}O NMR spectra at δ 534 and –61 ppm,

respectively, suggest the generation of an intermediate before complete consumption of **TiW_5** and formation of **$HTi(O_2)W_5$**. Whether this intermediate species is the hydroperoxo species **$(HOO)TiW_5$**, which subsequently converts to **$HTi(O_2)W_5$**, or a hydrolysis product resulting from incomplete drying of the H_2O_2 is not clear. The latter is consistent with our conclusions from experiments involving aqueous H_2O_2 that hydrolysis is necessary for the generation of the peroxide species from **TiW_5**, but the formation of a yellow solution immediately upon addition of dried H_2O_2 suggests otherwise.

Synthesis and characterization of Ti peroxo complex. A titanium peroxo complex was isolated from the reaction between **TiW_5** and aqueous H_2O_2 in acetonitrile. The ^{183}W NMR spectrum of **TiW_5** in the presence of 5 equiv. of H_2O_2 (Figure S13) revealed two resonances at δ 53.5 and 45 ppm with the intensity ratio of 4:1, which is characteristic of monosubstituted Lindqvist tungstates. The presence of one peroxo group per POM molecule was confirmed by titration of the peroxo complex with PPh_3 (Figure S14). The elemental analysis data supported the formulation of $(Bu_4N)_3[(O_2)TiW_5O_{18}H]$, while potentiometric titration of **$HTi(O_2)W_5$** with Bu_4NOH specified that the $[H^+]/[Ti]$ ratio is *ca*. 0.75 (Figure S15).

FTIR and Raman spectra of the isolated Ti peroxo complex are given in Figure 7 and Figure 8, respectively (curves B) in comparison with the spectrum of the initial **TiW_5** (curves A). In the IR spectrum of **$HTi(O_2)W_5$** (Figure 7), the bands at 537 and 592 cm^{-1} attributed to ν(Ti-OC)[53] vibrations in **TiW_5** have disappeared. The frequency of ν(W=O) is shifted to higher energy (953 vs 948 cm^{-1}), reflecting a slight increase in terminal oxygen to Ti π-bonding upon protonation at a Ti−O−W bridging oxygen. A higher energy shift of the vibrations of terminal W=O was also detected in the Raman spectrum of **$HTi(O_2)W_5$**: 971 vs 967 cm^{-1} in **TiW_5** (Figure 8). Besides, the band at 777 cm^{-1} attributed to W–O–M (M = W or Ti) stretching vibrations was split in the IR spectrum of the Ti peroxo complex, which might be also rationalized by changes in the polyanion symmetry upon

protonation of one of the Ti–O–W bridges in the solid state. Similar trends were previously observed for $(Bu_4N)_2[(O_2)NbW_5O_{18}H]$.[39]

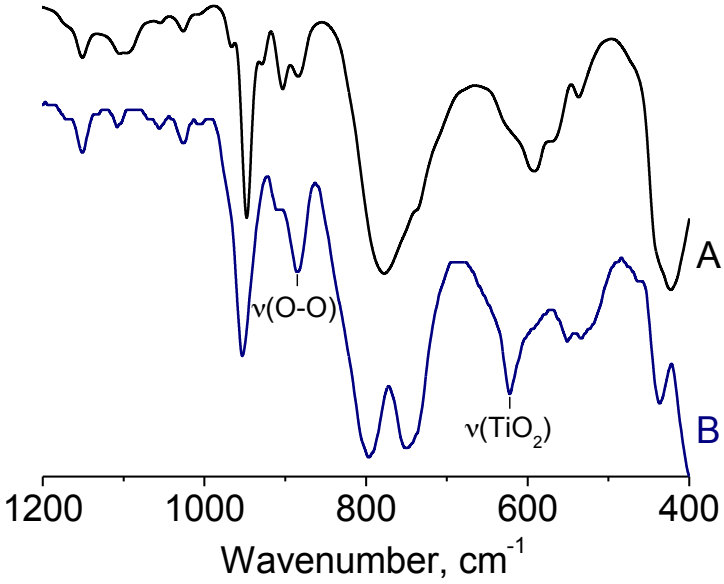

Figure 7. FTIR spectra of (A) **TiW_5** and (B) isolated **TiW_5**-peroxocomplex.

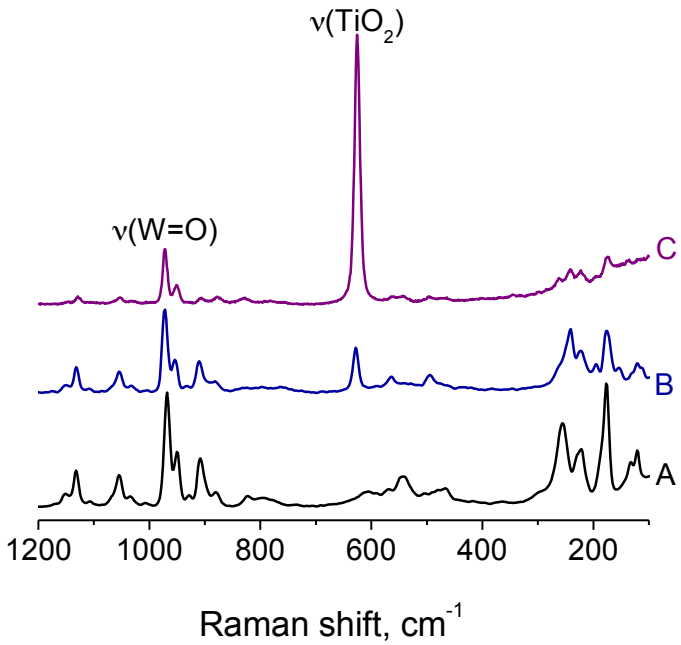

Figure 8. Raman spectra of (A) **TiW_5** and (B)–(C) resonance Raman spectra of isolated **TiW_5**-peroxo complex taken at different excitation λ values: (B) 1064 nm and (C) 488 nm.

Along with the main bands of the Lindqvist tungstate, the IR and Raman spectra of the Ti peroxo complex exhibited new absorption bands at 623 (IR) and 625 (Raman) cm^{-1} that can be assigned to symmetric $\nu(TiO_2)$ vibrations expected for non-bridging η^2-peroxo ligands.[59,64-66] This assignment is confirmed by a strong resonance behavior for this band, the intensity of which greatly increases with decreasing excitation λ (Figure 8, compare curves B and C). The IR spectrum of the Ti peroxo complex also showed a strong band at 884 cm^{-1}, which is not present in the spectrum of peroxo-free **TiW_5** and, according to the literature,[57,59,64,67-70] can be assigned to the stretching fundamental of the O−O bond. Note that the band at 880 cm^{-1} in the Raman spectrum did not undergo any enhancement when the 488 nm excitation source was used. The same behavior was observed for the 898 cm^{-1} feature in the resonance Raman spectra of $[NH_4^+]_3[TiF_5O_2]$, where the ν(O–O) mode (where the Ti center is not directly involved) was not affected by the resonant Raman effect.[71] Hence, vibrational spectroscopy strongly supports a side-on structure for the titanium peroxo complex derived from **TiW_5** and protonation of Ti-O-W bridging oxygen. Previously, protonation of the Nb-O-W bridging oxygen was inferred for **$HNb(O_2)W_5$** on the basis of spectroscopic (IR, Raman, UV-vis and ^{17}O NMR) and DFT studies.[39] Therefore, we may conclude that, for both Ti and Nb compounds, the protonated peroxo species '**$HM(O_2)W_5$**' are the main species observed spectroscopically both in solution and in the solid state.

Reactivity of Ti and Nb peroxo complexes. The stoichiometric interaction of **$HTi(O_2)W_5$** with cyclohexene was studied under conditions of a 5-fold excess of alkene (Scheme 2). Peroxo complex **$HTi(O_2)W_5$** turned out to be active for oxidation of CyH and gave mainly heterolytic oxidation products, such as epoxide (38% selectivity) and diol (41% selectivity), along with some allylic oxidation products (20% total selectivity). The yield of the oxygenated products agreed with the amount of active oxygen in the peroxo complex. The addition of base (1 equiv. TBAOH) completely deactivates **$HTi(O_2)W_5$**, which is typical of Ti peroxo complexes.[11,12,44,45,59]

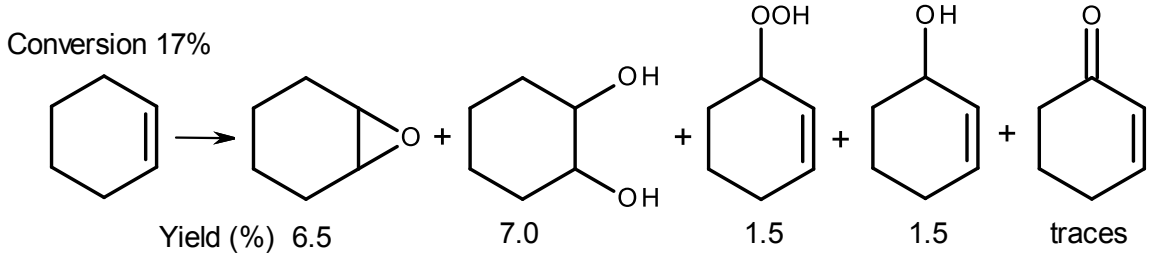

Scheme 2. Cyclohexene oxidation with **HTi(O$_2$)W$_5$**. Reaction conditions: 0.016 *M* POM, 0.08 *M* CyH, 1 mL CH_3CN, 50 ^oC, 5 h.

The stoichiometric interaction between **HTi(O$_2$)W$_5$** and CyH was monitored by UV-vis spectroscopy. The reduction in the characteristic absorption maximum of **HTi(O$_2$)W$_5$** (375 nm) (Figure 9) was much slower in the absence of organic substrate than in the presence of CyH (compare Figure 9a and 9b). This indicates that thermal degradation of the Ti peroxo complex is relatively slow and that the observed decrease in the absorption maximum is caused by the reaction with alkene.

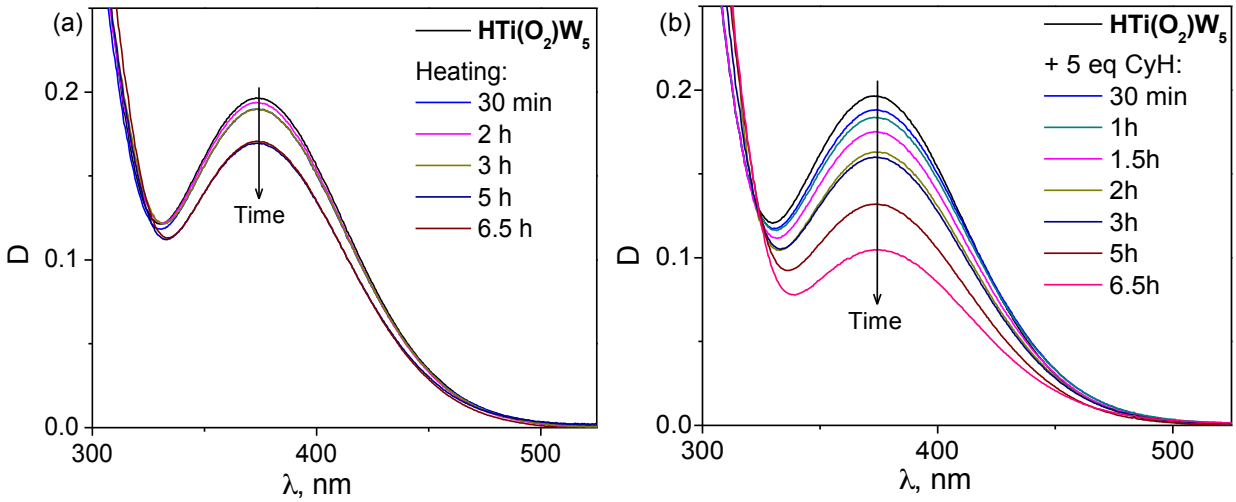

Figure 9. UV−vis spectra of **HTi(O$_2$)W$_5$** (a) in time and (b) in time in the presence of 5 equiv of CyH. Reaction conditions: 0.5 m*M* **HTi(O$_2$)W$_5$**, 2.5 m*M* CyH (if any), 0.6 mL CH_3CN, 50 °C.

Previously, we demonstrated that the peroxo complex **HNb(O$_2$)W$_5$** is also active towards CyH under stoichiometric conditions.[39] However, in contrast to **HTi(O$_2$)W$_5$**, it gave only heterolytic oxidation products, epoxide and diol, and no allylic oxidation products were detected.[39]

Comparison of the rates of the stoichiometric reactions showed that CyH oxidation proceeds faster with **$HNb(O_2)W_5$** than with **$HTi(O_2)W_5$** (Figure 10). As was already mentioned, the rate of catalytic oxidation of CyH with H_2O_2 and the rate of peroxo complex formation were also higher for **NbW_5** relative to **TiW_5**.

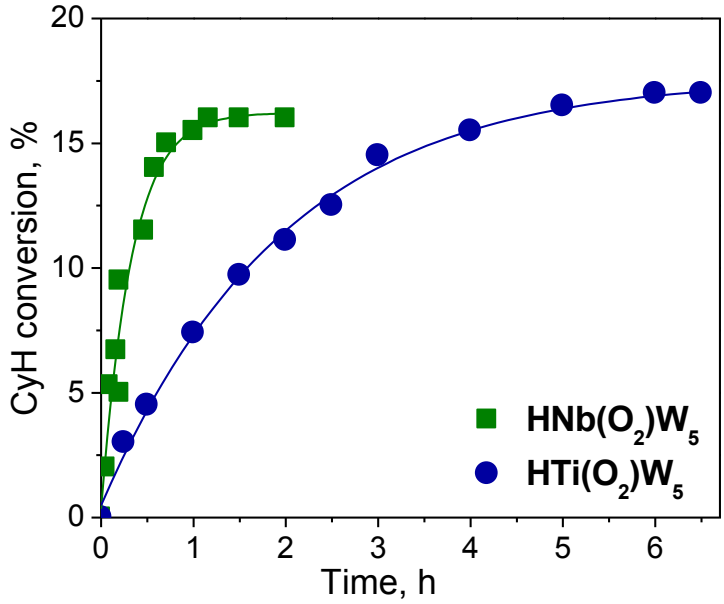

Figure 10. Kinetic curves for CyH stoichiometric oxidation with (A) **$HNb(O_2)W_5$** and (B) **$HTi(O_2)W_5$**. Reaction conditions: 0.016 *M* POM, 0.08 *M* CyH, 1 mL CH_3CN, 50 °C.

DFT comparison of the reaction mechanisms

Our earlier computational studies have analyzed different aspects of the mechanism of selective oxidations with H_2O_2 catalyzed by transition-metal (M) substituted polyoxometalates.[39,72–78] Among them, we showed that the energy barriers for electrophilic oxygen transfer to alkenes from peroxo and hydroperoxo species decrease when we move from Ti down and across to Nb in the periodic table.[75] More recently, we have characterized in detail the reaction mechanism of CyH epoxidation by Nb-substituted Lindqvist anions, showing that reaction occurs mainly through α-oxygen transfer from η^2-hydroperoxo niobium species, while the protonated peroxo species **$HNb(O_2)W_5$** is the resting-sate.[39] Here we perform a detailed comparison of the free-energy landscape for Nb- and Ti-based catalysts on the heterolytic epoxidation of alkenes, using

$[(CH_3O)NbW_5O_{18}]^{2-}$ ($\mathbf{1}^{Nb}$) and $[(CH_3O)TiW_5O_{18}]^{3-}$ ($\mathbf{1}^{Ti}$) complexes, and CyH substrate adopting the same computational level[79] as in the previous contribution. For each M-substituted anion, we have considered three different reaction paths for the electrophilic oxygen transfer to the CyH substrate, namely, the oxygen transfer from the peroxo ligand, and the α- and β-oxygen transfer from the hydroperoxo moiety (see Scheme 3).

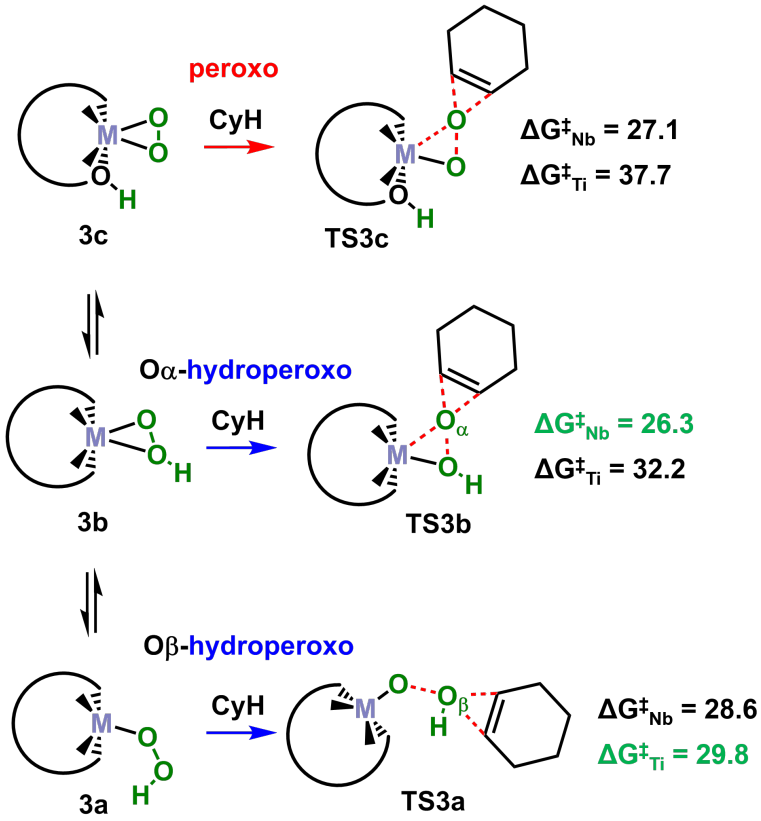

Scheme 3. Possible pathways for oxygen transfer to CyH from peroxo and hydroperoxo species in transition metal-substituted polyoxometalates. Overall free energy barriers for all paths are shown in kcal·mol^{-1}, highlighted in green the most likely mechanism for each metal.

Figure 11 compares the computed free-energy profiles for the most favorable heterolytic pathways in which the transition metal-hydroxo species $[(HO)MW_5O_{18}]^{n-}$ (M = Nb and Ti), $\mathbf{2}^{Nb}$ and $\mathbf{2}^{Ti}$, act as catalysts. Initially, these species can be generated by hydrolysis of the methoxy precursors $[(CH_3O)NbW_5O_{18}]^{2-}$ ($\mathbf{1}^{Nb}$) and $[(CH_3O)TiW_5O_{18}]^{3-}$ ($\mathbf{1}^{Ti}$) anions, both showing accessible, computed free-energy barriers of 12.2 and 23.0 kcal·mol^{-1}, respectively. The hydroxo complex **2** is also

generated after the oxygen transfer step, and although the corresponding methoxy complexes are slightly lower in energy (3.6 and 2.1 kcal·mol^{-1}), the reverse transformation (**2** → **1**) is unlikely because of the low concentration of CH_3OH compared to other reagents. Figure S16 A and B in the Supporting Information shows a complete description of the free-energy profiles for the three heterolytic paths and the interconversion between them. The metal-hydroxo complex **2** can then interact with H_2O_2 through a substitution mechanism assisted by a solvent water molecule acting as proton shuttle (transition state $\mathbf{TS2_w}$) to give the $[(\eta^1\text{-HOO})MW_5O_{18}]^{n-}$ hydroperoxo species **3a** and one water molecule. In agreement with kinetic experiments (*vide supra*), this process was computed to be faster for Nb than for Ti species, $\Delta G^{\ddagger}$(**2** → $\mathbf{TS2_w}$) = 7.2 and 15.5 kcal·mol^{-1}, respectively (see Figure 11). This fact is ascribed to the larger radius of Nb that affords a 7-fold coordination in the transition state geometry more readily than Ti. The same effect might explain the faster hydrolysis of the methoxy precursor (**1** → **2**) observed for Nb as compared to Ti (*vide supra*). It is worth mentioning that in anhydrous conditions, or in low water concentration, the formation of hydroperoxo species **3a** could also occur *via* a 4-membered ring transition state (**TS2**) without the water-assisted H-transfer showing smooth free-energy barriers of 15.3 kcal·mol^{-1} for Nb and 19.3 kcal·mol^{-1} for Ti (see Figure S17).

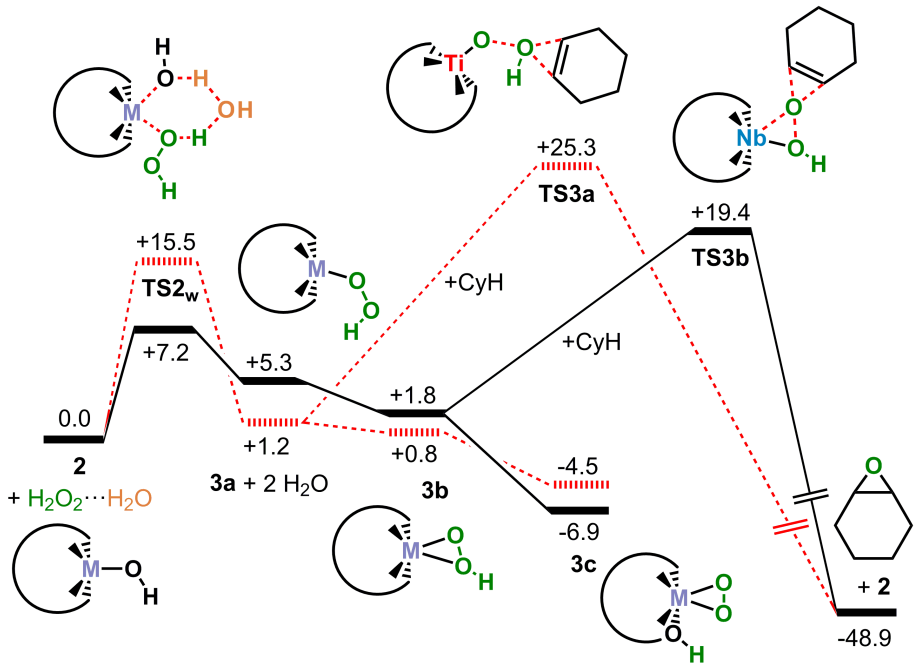

Figure 11. Calculated potential free-energy profile (kcal·mol^{-1}) for cyclohexene epoxidation with H_2O_2 by $[(CH_3O)NbW_5O_{18}]^{2-}$ (**1**^{Nb}) anion (solid black lines) and $[(CH_3O)TiW_5O_{18}]^{3-}$ (**1**^{Ti}) anion (dashed red lines).

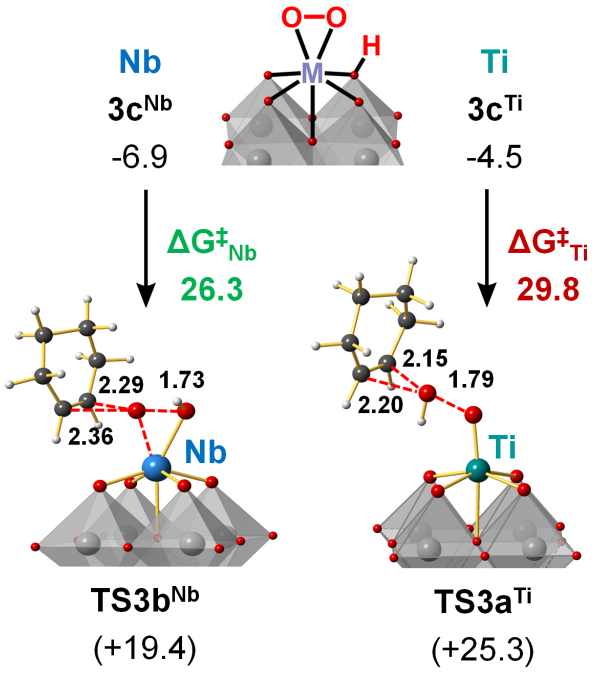

Figure 12. Computed structures of the most favorable transition states for heterolytic oxygen transfer to CyH (α-oxygen for Nb, **TS3b**^{Nb} and β-oxygen for Ti, **TS3a**^{Ti}). Relative free-energies and free-energy barriers in kcal·mol^{-1}, and distances in Å.

The generation of hydroperoxo species **3a** is slightly endergonic (+5.3 and +1.2 kcal·mol^{-1} for Nb and Ti, respectively). However, **3a** can evolve to the corresponding η^2-hydroperoxo species [(η^2-HOO)MW_5O_{18}]$^{n-}$ (**3b**), and then to the protonated peroxo complex [(η^2-O_2)$MW_5O_{18}H$]$^{n-}$ (**3c**). This sequential process is downhill in energy for both metals, resulting in an overall exergonic process where the peroxo complex **3c** lies below the reactants by 6.9 and 4.5 kcal·mol^{-1} for Nb and Ti, respectively. This is consistent with the successful isolation of peroxo complexes by treatment of hydroxo and methoxospecies with H_2O_2. For Nb we had found that the most favorable pathway is the α-oxygen transfer to CyH from Nb-η^2-hydroperoxo complex**3b^{Nb}**, which is formed from the lower-energy Nb-peroxo complex **3c^{Nb}** producing an overall free-energy barrier (**3c^{Nb}** → **TS3b^{Nb}**) of 26.3 kcal·mol^{-1}.[39] In the case of Ti-substituted Lindqvist anion, the β-oxygen transfer pathway (**3c^{Ti}** → **TS3a^{Ti}**) becomes energetically favored over the α-oxygen hydroperoxo (**3c^{Ti}** → **TS3b^{Ti}**) and the peroxo (**3c^{Ti}** → **TS3c^{Ti}**) paths by 2.2 and 7.7 kcal·mol^{-1}, respectively. Although the O_α is more electrophilic than the O_β, it has been demonstrated that when the metal ion is sterically hindered or found in a highly rigid environment (i.e., reluctant to increase its coordination number), the β-oxygen transfer can prevail over the α-oxygen pathway.[77] More interestingly, on going from Nb- to Ti-substituted catalyst the overall free-energy barrier for heterolytic oxygen transfer increases by 3.5 kcal·mol^{-1} in agreement with the conversion values reported in Table 1. Figure 12 compares the key transition state structures and the free-energy barriers for the epoxidation process by Nb- and Ti-substituted catalysts. Decreasing the formal oxidation state of the metal from Nb(V) to Ti(IV), we expect a lower electrophilicity of the M-η^2-OOH moiety towards the attack of the nucleophilic alkene.[78] The metal charge effect is manifested in a higher energy of the σ*O-O orbitals in Ti-η^2-hydroperoxo complex (+0.64 and +1.73 eV for Nb and Ti, respectively), and in a larger free-energy barrier for the α-oxygen transfer ($\Delta G^{\ddagger}$(**3b** → **TS3b**) = 17.6 *vs.* 26.9 kcal·mol^{-1} for Nb and Ti, respectively). Thus, we can explain the higher activity of Nb catalyst and the preference for the β-oxygen transfer path of Ti catalyst. Furthermore, the differences in oxygen transfer mechanisms can

be related to the different regioselectivities observed in H_2O_2-based epoxidation of some alkenes such limonene over Ti- and Nb-silicates.[23,26,31] Thus, the β-oxygen transfer from Ti(η^1-OOH) would favor the epoxidation of the more nucleophilic, internal C=C bond in limonene whereas the α-oxygen transfer from Nb(η^2-OOH) would result in epoxidation of the less sterically hindered, external C=C-bond.

To validate the mechanistic proposal, we compared the Arrhenius activation energies for CyOct epoxidation over the **NbW_5** catalyst (11.7 kcal·mol^{-1}) with computed zero-point corrected energies.[39] We showed that the experimental E_a value lays within the range of computed barriers for the two possible operative paths: direct α-oxygen transfer (8 kcal·mol^{-1}) and reaction from peroxo species **3c^{Nb}**(16 kcal·mol^{-1}).[39] In the case of **TiW_5** catalyst the corresponding computed overall barriers are respectively 12 and 20 kcal·mol^{-1}, whose range also includes the experimental E_a value, 14.3 kcal·mol^{-1}, further supporting the mechanistic proposal. Besides the limitations of the methodology described in Computational Details section, the computed relative rates of reaction paths could be influenced by a counteraction (TBA^+, tetrabutylammonium) effect. Recently, atomistic molecular dynamics simulations on TBA-POM salt in a water-acetonitrile mixture showed that the hydrophobic TBA counter cations are tightly attached to anionic POMs repelling the water molecules around the TBA-POM ion pairs.[80] This effect could slow down the water-assisted H-transfer in hydroperoxo **3b** to form peroxo complex **3c**, favoring the direct oxygen transfer to alkene from **3b**. Nevertheless, and more importantly, calculations are able to reproduce the increase of experimental E_a upon replacement of the metal.

Alternatively, a homolytic cleavage of O–O bond can lead to one-electron oxidation mechanisms producing homolytic oxidation products. In an attempt to understand the higher selectivity of Nb catalyst with respect to the Ti one, we analyzed the tendency of both catalysts to promote homolytic cleavage of the O–O bond. This point had been successfully assessed by estimating the energy cost of forming the metalloxyl and the hydroxyalkane radical from the

hydroperoxo species **3a**.[78] The free-energy cost for homolytic O–O bond cleavage follow the same trend as those for heterolytic oxygen transfer, i.e. the formation of Ti-oxyl radical species (+20.5 and kcal·mol^{-1}) is more disfavored than the corresponding Nb-oxyl species (+19.5kcal·mol^{-1}). Note that these calculations do not provide a detailed description of the radical mechanism but compare the tendency of both metals to form and stabilize radical species. Additionally, we have evaluated the mechanism proposed by Pombeiro, Shul'pin and co-workers for vanadium complexes consisting of the formation of free HOO· radicals in the initial steps.[81,82] The peroxo complex **3c** could incorporate an additional H_2O_2 molecule, followed by H-transfer to a M-O-W bridging oxygen, and elimination of HOO· radical yielding the $[(\eta^2\text{-}O_2)MW_5O_{18}H_2]^{n-}$, in which the spin density is delocalized through the W atoms. The free-energy cost for this process is too high, 36.1 and 39.5 kcal·mol^{-1} for Nb and Ti respectively, and consequently can be discarded. Overall, for the homolytic process the metal nature has a small effect, the energy difference being only 1 kcal·mol^{-1}, suggesting that the selectivity is dominated by the reaction rate of the heterolytic mechanism. Finally, we analyzed the spin density distribution of the Ti(IV)-oxyl and the Nb(V)-oxyl radicals (see Figure S18). The computed spin densities at the terminal oxygen atoms are 0.97 and 0.95 for Ti and Nb species, respectively, indicating that the Nb site delocalizes the spin density better and somewhat favors the homolytic path. Overall, this effect is overcome by the higher electrophilicity of the Nb(V) metal center compared to Ti(IV), which accelerates the heterolytic process to a larger extent than the homolytic process, thereby improving the selectivity for heterolytic pathway.

4. Conclusions

The Ti- and Nb-monosubstituted Lindqvist tungstates **TiW_5** and **NbW** mimic well the catalytic performance of mesoporous Ti- and Nb-silicate catalysts in alkene oxidation with aqueous hydrogen peroxide, and this mechanistic study has clarified important similarities and differences in the mechanisms of H_2O_2 activation at these two metals. The formation of active protonated peroxo

'HMO_2' and hydroperoxo 'MOOH' intermediates is crucial for heterolytic oxygen transfer to alkenes over both Ti(IV) and Nb(V), and these species can be obtained readily by treatment of metal-hydroxo and methoxo species with H_2O_2. For both Ti and Nb, the peroxo form 'HMO_2' is more stable than hydroperoxo 'MOOH' species and 'HMO_2' is observed spectroscopically both in solution and in the solid state. However, DFT calculations showed that hydroperoxo species 'MOOH' (M = Ti or Nb) is more reactive than 'HMO_2' toward epoxidation of alkenes. Depending on the nature of metal and its coordination environment, the hydroperoxo species transfers preferentially the nondistorted β-oxygen (for the Ti, which is more reluctant to increase its coordination number) or the more electrophilic α-oxygen (for the Nb with a nonrigid coordination environment). Moreover, the replacement of Ti by Nb speeds up the reaction and improves the selectivity towards heterolytic products in alkene oxidation by H_2O_2. Calculations showed that increasing the oxidation state from Ti(IV) to Nb(V) makes the metal center more electrophilic, lowering considerably the energy barrier for the heterolytic oxygen transfer to the C=C bond in alkene from 'MOOH', while the homolytic route is much less affected. Thus, the Nb(V) single-site catalyst combines a *flexible* coordination environment with a *high* oxidation state, which increases electrophilicity, resulting in an improved catalytic performance.

AUTHOR INFORMATION

Corresponding Author

* E-mails: khold@catalysis.ru; john.errington@newcastle.ac.uk; j.carbo@urv.cat

Author Contributions

The manuscript was written through contributions of all authors. / All authors have given approval to the final version of the manuscript.

Notes

The authors declare no competing financial interests.

ASSOCIATED CONTENT

Supporting Information. Full details on the POM synthesis and characterization, oxidation reactions, kinetic experiments and computational methodology; ^{183}W, ^{17}O, ^{1}H, ^{31}P and ^{93}Nb NMR, IR and UV-vis spectra; energy profiles; spin densities; and Cartesian coordinates.

ACKNOWLEDGMENTS

We thank Dr. I. Y. Skobelev for preliminary DFT calculations, Dr. I. V. Deliy for CHNO analyzes as well as Dr. Yu. A. Chesalov and Dr. P. A. Abramov for their help in Raman and resonance Raman measurements, respectively. The assistance of Dr. I. E. Soshnikov in ^{1}H NMR measurements for $(Bu_4N)_2[(CH_3O)NbW_5O_{18}]$ is greatly appreciated. This work was supported by the Ministry of Science and Higher Education of the Russian Federation (projectAAAA-A17-117041710080-4). Funding from the European COST Action CM1203, *Polyoxometalates for Molecular Nanoscience* (PoCheMoN) are gratefully acknowledged. DL also thanks Prof. W. G. Klemperer for support during his PhD studentship. This work was supported by the Spanish government (Project CTQ2017-87269-P) and the Generalitat de Catalunya (Grant 2017-SGR629). J.M.P. thanks the ICREA foundation for an ICREA ACADEMIA award.

REFERENCES

(1) *Modern Heterogeneous Oxidation Catalysis: Design, Reactions and Characterization*; Mizuno, N., Ed.; Wiley-VCH: Weinheim, 2009.

(2) *Liquid Phase Oxidation via Heterogeneous Catalysis: Organic Synthesis and Industrial Applications;* Clerici, M.G., Kholdeeva, O.A., Eds.; Wiley: Hoboken, 2013.

(3) *Handbook of Advanced Methods and Processes in Oxidation Catalysis;* Duprez, D., Cavani, F., Eds.; Imperial College Press: London, 2014.

(4) Cavani, F.; Teles, J. H. Sustainability in Catalytic Oxidation: An Alternative Approach or a Structural Evolution? *ChemSusChem* **2009**, *2*, 508–534.

(5) Jones, C.W. *Application of Hydrogen Peroxide and Derivatives*; Royal Society of Chemistry: Cambridge, 1999.

(6) Sheldon, R.; Arends, I. W. C. E.; Hanefeld, U. *Green Chemistry and Catalysis*; Wiley-VCH: Weinheim, 2007.

(7) Strukul, G., Scarso, A. In *Liquid Phase Oxidation via Heterogeneous Catalysis: Organic Synthesis and Industrial Applications*; Clerici, M.G., Kholdeeva O.A., Eds.; Wiley: Hoboken, 2013; pp. 1–20.

(8) Campos-Martin, J. M.; Blanco-Brieva, G.; Fierro, J. L. G. Hydrogen Peroxide Synthesis: An Outlook beyond the Anthraquinone Process.*Angew. Chem. Int. Ed*. **2006**, *45,* 6962–6984.

(9) Taramasso, M.; Perego, G.; Notari, B. Preparation of Porous Crystalline Synthetic Material Comprised of Silicon and Titanium Oxides. *US Patent* 4 410 501, 1983.

(10) Perego*,* C.; Carati, A.; Ingallina, P.; Mantegazza, M. A.; Bellussi, G. Production of Titanium Containing Molecular Sieves and Their Application in Catalysis. *Appl. Catal. A: General* **2001**, *221*, 63–72.

(11) For recent review see: Clerici, M. G.; Domine, M. E. In: *Liquid Phase Oxidation via Heterogeneous Catalysis: Organic Synthesis and Industrial Applications*; Clerici, M. G., Kholdeeva O. A. Eds.; Wiley: Hoboken, 2013; pp. 21–93.

(12) Kholdeeva, O. A. In: *Liquid Phase Oxidation via Heterogeneous Catalysis: Organic Synthesis and Industrial Applications*; Clerici, M. G., Kholdeeva O. A. Eds.; Wiley: Hoboken, 2013; pp. 127–219.

(13) Kholdeeva, O.A. Recent Developments in Liquid-Phase Selective Oxidation Using Environmentally Benign Oxidants and Mesoporous Metal Silicates. *Catal. Sci. Technol*. **2014**, *4*, 1869–1889.

(14) Bellussi, G.; Carati, A.; Rizzo, C.; Millini, R. New Trends in the Synthesis of Crystalline Microporous Materials. *Catal. Sci. Technol.,* 2013, **3**, 833–857.

(15) Kholdeeva, O.A.; Melgunov, M.S.; Shmakov, A.N.; Trukhan, N.N.; Kriventsov, V.V.; Zaikovskii, V.I.; Malyshev, M.E.; Romannikov, V.N. A New Mesoporous Titanium-Silicate Ti-MMM-2: a Highly Active and Hydrothermally Stable Catalyst for H_2O_2-Based Selective Oxidations. *Catal. Today* **2004**, *91-92*, 205–209.

(16) Wu, P.; Tatsumi, T.; Komatsu, T.; YashimaT. Postsynthesis, Characterization, and Catalytic Properties in Alkene Epoxidation of Hydrothermally Stable Mesoporous Ti-SBA-15. *Chem. Mater*. **2002**, *14*, 1657–1664.

(17) Xiao, F.-S. Ordered Mesoporous Materials with Improved Stability and Catalytic Activity. *Top. Catal.* **2005**, *35*, 9–24.

(18) Ivanchikova, I. D.; Kovalev, M. K.; Mel'gunov, M. S.; Shmakov, A. N.; Kholdeeva, O. A. User-Friendly Synthesis of Highly Selective and Recyclable Mesoporous Titanium-Silicate Catalysts for the Clean Production of Substituted *p*-Benzoquinones. *Catal. Sci. Technol*. **2014**, *4*, 200−207.

(19) Nowak, I.; Kilos, B.; Ziolek, M.; Lewandowska, A. Epoxidation of Cyclohexene on Nb–Containing Meso-and Macroporous Materials. *Catal. Today* **2003**, *78*, 487–498.

(20) Nowak, I.; Ziolek, M. Effect of Texture and Structure on the Catalytic Activity of Mesoporous Niobosilicates for the Oxidation of Cyclohexene. *Micropor. Mesopor. Mater*. **2005**, *78*, 281–288.

(21) Somma, F.; Strukul, G. Niobium Containing Micro-, Meso-and Macroporous Silica Materials as Catalysts for the Epoxidation of Olefins with Hydrogen Peroxide. *Catal. Lett*. **2006**, *107*, 73–81.

(22) Feliczak-Guzik, A.; Nowak, I. Mesoporous Niobosilicates Serving as Catalysts for Synthesis of Fragrances. *Catal. Today* **2009**, *142*, 288–292.

(23) Gallo, A.; Tiozzo, C.; Psaro, R.; Carniato, F.; Guidotti, M. Niobium Metallocenes Deposited onto Mesoporous Silica via Dry Impregnation as Catalysts for Selective Epoxidation of Alkenes. *J. Catal*. **2013**, *298*, 77–83.

(24) Tiozzo, C.; Bisio, C.; Carniato, F.; Guidotti, M. Grafted Non–Ordered Niobium–Silica Materials: Versatile Catalysts for the Selective Epoxidation of Various Unsaturated Fine Chemicals. *Catal. Today* **2014**, *235*, 49–57.

(25) Ramanathan, A.; Zhu, H.; Maheswari,R.; Thapa, P. S.; Subramaniam, B. Comparative Study of Nb–Incorporated Cubic Mesoporous Silicates as Epoxidation Catalysts. *Ind. Eng. Chem. Res*. **2015**, *54*, 4236–4242.

(26) Ivanchikova, I. D.; Maksimchuk, N. V.; Skobelev, I. Y.; Kaichev, V. V.; Kholdeeva, O. A. Mesoporous Niobium–Silicates Prepared by Evaporation–Induced Self–Assembly as Catalysts for Selective Oxidations with Aqueous H_2O_2. *J. Catal*. **2015**, *332*, 138–148.

(27) Thornburg, N. E.; Thompson, A. B.; Notestein, J. M. Periodic Trends in Highly Dispersed Groups IV and V Supported Metal Oxide Catalysts for Alkene Epoxidation with H_2O_2. *ACS Catal*. **2015**, *5*, 5077–5088.

(28) Ivanchikova, I. D.; Skobelev, I. Y.; Maksimchuk, N. V.; Paukshtis, E. A.; Shashkov, M. V.; Kholdeeva, O. A. Toward Understanding the Unusual Reactivity of Mesoporous Niobium Silicates in Epoxidation of C=C Bonds with Hydrogen Peroxide. *J. Catal*. **2017**, *356*, 85–99.

(29) Thornburg, N. E.; Notestein, J. M. Rate and Selectivity Control in Thioether and Alkene Oxidation with H_2O_2 over Phosphonate-Modified Niobium(V)–Silica Catalysts. *ChemCatChem* **2017**, *9*, 3714–3724.

(30) Dworakowska, S.; Tiozzo, C.; Niemczyk-Wrzeszcz, M.; Michorczyk, P.; Ravasio, N.; Psaro, R.; Bogdał, D.; Guidotti, M. Mesoporous Molecular Sieves Containing Niobium (V) as Catalysts for the Epoxidation of Fatty Acid Methyl Esters and Rapeseed Oil. *J. Clean. Prod*. **2017**, *166*, 901–909.

(31) Kholdeeva, O. A.; Ivanchikova, I. D.; Maksimchuk, N. V.; Skobelev, I. Y. H_2O_2-Based Selective Epoxidations: Nb-Silicates versus Ti-Silicates. *Catal. Today* **2018** [online early access]. DOI: 10.1016/j.cattod.2018.04.002.

(32) Ziolek, M.; Sobczak, I.; Decyk, P.; Sobanska, K.; Pietrzyk, P.; Sojka, Z. Search for Reactive Intermediates in Catalytic Oxidation with Hydrogen Peroxide over Amorphous Niobium (V) and Tantalum(V) Oxides. *Appl. Catal. B: Environ*. **2015**, *164*, 288–296.

(33) Thornburg, N.E.; Nauert, S.L.; Thompson, A.B.; Notestein, J.M. Synthesis−Structure–Function Relationships of Silica-Supported Niobium(V) Catalysts for Alkene Epoxidation with H_2O_2. *ACS Catal*. **2016**, *6*, 6124–6134.

(34) Bregante, D.T.; Priyadarshini, P.; Flaherty, D.W. Kinetic and Spectroscopic Evidence for Reaction Pathways and Intermediates for Olefin Epoxidation on Nb in *BEA. *J. Catal*. **2017**, *348*, 75–89.

(35) Bregante, D. T.; Flaherty, D. W. Periodic Trends in Olefin Epoxidation over Group IV and V Framework-Substituted Zeolite Catalysts: A Kinetic and Spectroscopic Study. *J. Am. Chem. Soc*. **2017**, *139*, 6888−6898.

(36) Bregante, D. T.; Thornburg, N. E.; Notestein, J. M.; Flaherty, D. W. Consequences of Confinement for Alkene Epoxidation with Hydrogen Peroxide on Highly Dispersed Group 4 and 5 Metal Oxide Catalysts. *ACS Catal*. **2018**, *8*, 2995–3010.

(37) Yoon, C. W.; Hirsekorn, K. F.; Neidig, M. L.; Yang, X.; Tilley T. D. Mechanism of the Decomposition of Aqueous Hydrogen Peroxide over Heterogeneous TiSBA15 and TS-1 Selective Oxidation Catalysts: Insights from Spectroscopic and Density Functional Theory Studies. *ACS Catal*. **2011**,*1*, 1665–1678.

(38) Bordiga, S.; Groppo,E.; Agostini, G.; van Bokhoven, J. A.;Lamberti,C. Reactivity of Surface Species in Heterogeneous Catalysts Probed by *in situ* X-ray Absorption Techniques. *Chem. Rev*. **2013**, *113*, 1736–1850.

(39) Maksimchuk, N. V.; Maksimov, G. M.; Evtushok, V. Yu.; Ivanchikova, I. D.; Chesalov, Yu. A.; Maksimovskaya, R. I.; Kholdeeva, O. A.; Solé-Daura, A.; Poblet, J. M.; Carbó,J. J. Relevance of

Protons in Heterolytic Activation of H_2O_2 over Nb(V). Insights from Model Studies on Nb-substituted Polyoxometalates. *ACS Catal*. **2018**, *8*, 9722–9737.

(40) Fournier, M.; Louis, C.; Che, M.; Chaquin, P.; Masure, D. Polyoxometallates as Models for Oxide Catalysts: Part I. An UV–visible Reflectance Study of Polyoxomolybdates: Influence of Polyhedra Arrangement on the Electronic Transitions and Comparison with Supported Molybdenum Catalysts. *J. Catal*. **1989**, *119*, 400–414.

(41) Chen, Q.; Zubieta, J. Coordination Chemistry of Soluble Metal Oxides of Molybdenum and Vanadium. *Coord. Chem. Rev*. **1992**, *114*, 107–167.

(42) Thomas, J. M. *Design and Applications of Single-site Heterogeneous Catalysts: Contributions to Green Chemistry, Clean Technology and Sustainability;* Imperial College Press: London, UK, 2012.

(43) Kholdeeva, O. A. Titanium–Monosubstituted Polyoxometalates: Relation Between Homogeneous and Heterogeneous Ti–Single–Site–Based Catalysis. *Top. Catal*. **2006**, *40*, 229–243.

(44) Kholdeeva, O. A.; Maksimovskaya, R. I. Titanium–and Zirconium–Monosubstituted Polyoxometalates as Molecular Models for Studying Mechanisms of Oxidation Catalysis. *J. Mol. Catal. A: Chem.* **2007**, *262*, 7–24.

(45) Kholdeeva,O. A. Hydrogen Peroxide Activation over Ti^{IV}: What Have We Learned from Studies on Ti-Containing Polyoxometalates? *Eur. J. Inorg. Chem*. **2013**, 1595–1605.

(46) Guillemot, G.; Matricardi, E.; Chamoreau, L.-M.; Thouvenot, R.; Proust, A. Oxidovanadium (V) Anchored to Silanol–Functionalized Polyoxotungstates: Molecular Models for Single–Site Silica–Supported Vanadium Catalysts. *ACS Catal*. **2015**, *5*, 7415−7423.

(47) Zhang, T.; Mazaud, L.; Chamoreau, L.-M.; Paris, C.; Guillemot, G.; Proust, A. Unveiling the Active Surface Sites in Heterogeneous Titanium–Based Silicalite Epoxidation Catalysts: Input of Silanol–Functionalized Polyoxotungstates as Soluble Analogues. *ACS Catal*. **2018**, *8*, 2330–2342.

(48) Clegg, W.; Elsegood, M. R. J.; Errington, R. J.; Havelock, J. Alkoxide Hydrolysis as a Route to Early Transition-Metal Polyoxometalates: Synthesis and Crystal Structures of Heteronuclear Hexametalate Derivatives, *J. Chem. Soc. Dalton Trans*. **1996**, 681-690.

(49) Lu, Y. J.; Lalancette, R.; Beer. R. H. Deoxygenation of Polynuclear Metal-Oxo Anions: Synthesis, Structure, and Reactivity of the Condensed Polyoxoanion $[(C_4H_9)_4N]_4(NbW_5O_{18})_2O$. *Inorg. Chem*. **1996**, *35*, 2524–2529.

(50) Harrup, M. K.; Kim, G.-S.; Zeng, H.; Johnson, R. P.; VanDerveer, D.; Hill, C. L. Triniobium Polytungstophosphates. Syntheses, Structures, Clarification of Isomerism and Reactivity in the Presence of H_2O_2. *Inorg. Chem*. **1998**, *37*, 5550–5556.

(51) Neumann, R. In: *Transition Metals for Organic Synthesis,* 2nd ed.; Beller, M., Bolm, C., Eds.; Wiley-VCH: Weinheim, 2004; Vol. 2, pp. 415–426.

(52) Howarth, O. W. Oxygen-17 NMR Study of Aqueous Peroxotungstates. *Dalton Trans*. **2004**, 476–481.

(53)Errington, R. J.; Petkar, S. S.; Middleton, P. S.; McFarlane, W.; Clegg, W.; Coxall, R. A.; Harrington, R. W. Non-Aqueous Synthetic Methodology for TiW5 Polyoxometalates: Protonolysis of $[(MeO)TiW_5O_{18}]^{3-}$ with Alcohols, Water and Phenols. *Dalton Trans*. **2007**, 5211–5222.

(54) Sheldon, R. A.; Kochi, J. K. *Metal-Catalyzed Oxidations of Organic Compounds.* Academic Press:New York, 1981.

(55) Yamase, T.; Ozeki, T.; Motomura, S. ^{183}W NMR and X-Ray Crystallographic Studies on the Peroxo Complexes of the Ti-Substituted α-Keggin Typed Tungstophosphates. *Bull. Chem. Soc. Jpn*. **1992**, *65*, 1453–1459.

(56) Reynolds, M. S.; Butler, A. Oxygen-17 NMR, Electronic, and Vibrational Spectroscopy of Transition Metal Peroxo Complexes: Correlation with Reactivity. *Inorg. Chem*. **1996**, *35*, 2378–2383.

(57) Ishikawa, E.; Yamase, T.Kinetics of Epoxidation of Cyclooctene with H_2O_2 by α-Keggin $[PTi_2W_{10}O_{38}(O_2)_2]^{7-}$ Catalyst in Acetonitrile. *J. Mol. Catal. A: Chemical* **1999**, *142*,61–76.

(58) Dakanali, M.; Kefalas, E. T.; Raptopoulou, C. P.; Terzis, A.; Voyiatzis,G.; Kyrikou, I.; Mavromoustakos, T.; Salifoglou, A. A New Dinuclear Ti(IV)−Peroxo−Citrate Complex from Aqueous Solutions. Synthetic, Structural, and Spectroscopic Studies in Relevance to Aqueous Titanium(IV)−Peroxo−Citrate Speciation. *Inorg. Chem.* **2003**, *42*, 4632–4639.

(59) Kholdeeva, O. A.; Trubitsina, T. A.; Maksimovskaya, R. I.; Golovin, A. V.; Neiwert, W. A.; Kolesov, B. A.; López, X.; Poblet, J. M. First Isolated Active Titanium Peroxo Complex: Characterization and Theoretical Study. *Inorg. Chem*. **2004**, *43,* 2284–2292.

(60) Kato, C. N.; Negishi, S.; Yoshida, K.; Hayashi, K.; Nomiya, K. The Strong Influence of Structures Around Titanium Centers in Dimeric Mono-, Di-, and Tri-Titanium(IV)-Substituted Keggin Polyoxotungstates on the Catalytic Epoxidation of Alkenes with H_2O_2. *Appl. Catal. A: General***2005**, *292*, 97–104.

(61) Hayashi, K.; Kato, C. N.; Shinohara, A.; Sakai, Y.; Nomiya, K. Isolation, Characterization, and Reactivity of the Reaction Products of the Dimeric, Ti–O–Ti Bridged Anhydride Form of the 1,2-Di-Titanium(IV)-Substituted α-Keggin Polyoxometalate with Aqueous 30% H_2O_2. *J. Mol. Catal. A: Chemical* **2007**, *262*, 30–35.

(62) Errington, R. J. Nonaqueous Polyoxometalate Synthesis for Systematic Studies of Hydrolysis, Protonation, and Reduction. *Adv. Inorg. Chem*. **2017**, *69*, 287–336.

(63) Pascual-Borràs, M.; López, X.; Rodríguez-Fortea, A.; Errington, R. J.; Poblet, J. M. ^{17}O NMR Chemical Shifts in Oxometalates: From the Simplest Monometallic Species to Mixed–Metal Polyoxometalates. *Chem. Sci.***2014**, *5*, 2031–2042.

(64) Griffith, W. P.; Wickins, T. D. Studies on Transition-Metal Peroxy-Complexes. Part VI. Vibrational Spectra and Structure. *J. Chem. Soc. A* **1968**, 397–400.

(65) Kakihana, M.; Tada, M.; Shiro, M.; Petrykin, V.; Osada, M.; Nakamura, Y. Structure and Stability of Water Soluble $(NH_4)_8[Ti_4(C_6H_4O_7)_4(O_2)_4]\cdot 8H_2O$. *Inorg. Chem.* **2001**, *40,* 891–894.

(66) Rohe, M.; Merz, K. Active Peroxo Titanium Complexes: Syntheses, Characterization and Their Potential in the Photooxidation of 2-Propanol. *Chem. Commun*. **2008**, 862–864.

(67) Mühlebach, J.;Muller, K.; Schwarzenbach, G. Peroxo Complexes of Titanium. *Inorg. Chem.* **1970**, *9*, 2381–2390.

(68) Mimoun, H.; Postel, M.; Casabianca, F.; Fisher, J.; Mitschler, A. Novel Unusually Stable Peroxotitanium (IV) Compounds. Molecular and Crystal Structure of Peroxobis (Picolinato)(Hexamethylphosphoric Triamide) Titanium (IV). *Inorg.Chem.* **1982**, *21*, 1303–1306.

(69) Postel, M.; Casabianca, F.; Gauffreteau, Y. The Structure and Reactivity towards Oxygen Transfer of Pyrazinedicarboxylato Peroxo Titanium Derivatives. Molecular and Crystal Structure of Peroxo(Pyrazine 2-Carboxylato 3-Carboxyl)(Acetylacetonato)(Hexamethylphosphortriamide) Titanium(IV). *Inorg. Chim. Acta*, **1986**, 113, 173–180.

(70) Qu, L.-Y.; Shan, Q.-J.; Gong, J.; Lu, R.-Q.; Wang, D.-R. Synthesis, Properties and Characterization of Dawson-Type Tungstophosphate Heteropoly Complexes Substituted by Titanium and Peroxotitanium. *J. Chem. Soc*., *Dalton Trans*., **1997**, 4525–4528.

(71)Bordiga, S.; Damin, A.; Bonino, F.; Ricchiardi, G.; Lamberti, C.; Zecchina, A. The Structure of the Peroxo Species in the TS-1Catalyst as Investigated by Resonant RamanSpectroscopy. *Angew. Chem. Int. Ed*. **2002**, *41*, 4734–4737.

(72) López, X.; Carbó, J. J.; Bo, C.; Poblet, J. M. Structure, Properties and Reactivity of Polyoxometalates: a Theoretical Perspective. *Chem*. *Soc*. *Rev*. **2012**, *41*, 7537–7571.

(73) Skobelev, I. Y.; Zalomaeva, O. V.; Kholdeeva, O. A.; Poblet, J. M.; Carbó, J. J. Mechanism of Thioether Oxidation over Di-and Tetrameric Ti Centres: Kinetic and DFT Studies Based on Model Ti–Containing Polyoxometalates.*Chem*.*–Eur*. *J*. **2015**, *21*, 14496–14506.

(74) Skobelev, I. Y.; Evtushok, V. Y.; Kholdeeva, O. A.; Maksimchuk, N. V.; Maksimovskaya, R. I.; Ricart, J. M.; Poblet, J. M.; Carbó, J. J.Understanding the Regioselectivity of Aromatic Hydroxylation over Divanadium–Substituted γ–Keggin Polyoxotungstate. *ACS Catal*. **2017**, *7*, 8514–8523.

(75) Antonova, N.; Carbó, J. J.; Kortz, U.; Kholdeeva, O.A.; Poblet, J. M. Mechanistic Insights into Alkene Epoxidation with H_2O_2 by Ti- and other TM-Containing Polyoxometalates: Role of the Metal Nature and Coordination Environment *J. Am. Chem. Soc*.**2010**, *132*, 7488–7497.

(76) Donoeva, B. G.; Trubitsina, T. A.; Antonova, N. S.; Carbó, J. J.; Poblet, J. M.; Al-Kadamany, G.; Kortz, U.; Kholdeeva, O. A. Epoxidation of Alkenes with H_2O_2 Catalyzed by Dititanium-Containing 19-Tungstodiarsenate(III): Experimental and Theoretical Studies, *Eur. J. Inorg. Chem*. **2010**, 5312–5317.

(77) Jiménez-Lozano, P.; Skobelev, I. Y.; Kholdeeva, O. A.; Poblet, J. M.; Carbó, J. J. Alkene Epoxidation Catalyzed by Ti-Containing Polyoxometalates: Unprecedented β-Oxygen Transfer Mechanism*Inorg. Chem*. **2016**, *55*, 6080–6084.

(78) Jiménez-Lozano, P.; Ivanchikova, I. D.; Kholdeeva, O. A.; Poblet, J. M.; Carbó, J. J. Alkene Oxidation by Ti–Containing Polyoxometa-lates. Unambiguous Characterization of the Role of the Protonation State. *Chem. Commun*. **2012**, *48*, 9266–9268.

(79) DFT calculations were performed with Gaussian09 using B3LYP functional. The basis set was lanl2dz for W, Ti and Nbatoms, and 6-31g(d,p) for the rest of atoms. The solvent effects of acetonitrile were included using the IEF-PCM implicit solvation model. See the Supporting Information and ref. [39] for details.

(80) Nikoloudakis, E.; Karikis, K.; Laurans, M.; Kokotidou, C.; Solé-Daura, A.; Carbó, J. J.; Charisiadis, A.; Charalambidis, G.; Izzet, G.; Mitraki, A.; Douvas, A. M.; Poblet, J. M.; Proust, A.; Coutsolelos, A. G. Self-assembly study of nanometric spheres from polyoxometalate-phenylalanine hybrids, an experimental and theoretical approach. *Dalton Trans.* **2018**, *47*, 6304—6313.

(81) Shul'pin, G. B.; Kozlov, Y. N.; Nizova, G. V.; Süss-Fink, G.; Stanislas, S.; Kitaygorodskiyc, A.; Kulikova, V. S. Oxidations by the reagent "O_2–H_2O_2–vanadium derivative–pyrazine-2-carboxylic acid". Part 12.1 Main features, kinetics and mechanism of alkane hydroperoxidation. *J. Chem. Soc., Perkin Trans.* **2001**, *2*, 1351-1371.

(82) Kirillova, M. V.; Kuznetsov, M. L.; Romakh, V. B.; Shul'pina, L. S.; Fraústo da Silva, J. J. R.; Pombeiro, A. J. L.; Shul'pin, G. B. Mechanism of oxidations with H_2O_2 catalyzed by vanadate anion or oxavanadium(V) triethanolaminate (vanadatrane) in combination with pyrazine-2-carboxylic acid (PCA): Kinetic and DFT studies. *J. Catal.* **2009**, *267*, 140-157.

For Table of Contents (TOC)

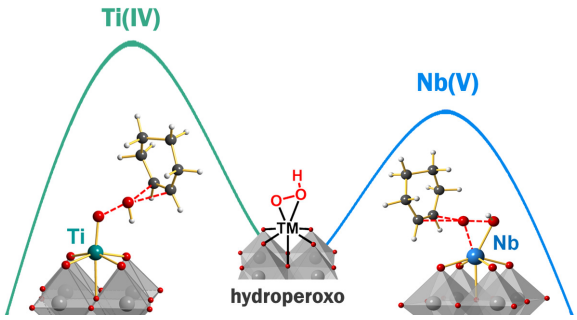

Supporting Information

Why does Nb(V) show higher heterolytic pathway selectivity than Ti(IV) in epoxidation with H_2O_2? Answers from model studies on Nb- and Ti-substituted Lindqvist tungstates

Nataliya V. Maksimchuk[†,‡] Irina D. Ivanchikova,[†] Gennadii M. Maksimov,[†] Ilia V. Eltsov,[‡] Vasilii Yu. Evtushok,[†,‡] Oxana A. Kholdeeva,[†,‡,*] Daniel Lebbie,[§] R. John Errington,[§,*] Albert Solé-Daura,[‖] Josep M. Poblet,[‖] and Jorge J. Carbó[‖,*]

[†] Boreskov Institute of Catalysis, Pr. Lavrentieva 5, Novosibirsk 630090, Russia

[‡] Novosibirsk State University, Pirogova str. 2, Novosibirsk 630090, Russia

[§] Chemistry, School of Natural and Environmental Sciences, Bedson Building, Newcastle University, NE1 7RU, UK

[‖] Departament de Química Física i Inorgànica, Universitat Rovira i Virgili, 43005 Tarragona, Spain

* Corresponding authors: khold@catalysis.ru; j.carbo@urv.cat; john.errington@newcastle.ac.uk

Table of Contents

Experimental details

Materials. Diethyl ether was dried over and distilled from sodium benzophenone ketyl and acetonitrile was dried over and distilled from calcium hydride. 10% ^{17}O-enriched water and deuterated acetonitrile were purchased from Goss Scientific Instruments, and the latter was degassed and stored under nitrogen over calcium hydride. Acetonitrile (Panreac, HPLC grade) that was used as a solvent in catalytic reactions was dried and stored over activated 3Å molecular sieves. Cyclohexene (CyH) and cyclooctene (CyOct) were purchased from Sigma-Aldrich and purified prior to use by passing through a column filled with neutral alumina to remove traces of possible oxidation products. The concentration of hydrogen peroxide (30 or 77% in water) was determined iodometrically prior to use. All the other compounds were the best available reagent grade and were used without further purification.

Synthesis and Characterization of POMs. $WO(OCH_3)_4$[S1] and $(n\text{Bu}_4\text{N})_2WO_4$[S2] were prepared using literature procedures. $Ti(OCH_3)_4$ was prepared by repeated treatment of $Ti(O\textit{i}Pr)_4$ with methanol under reflux.[S3]The synthesis of **TiW$_5$** was carried out under an atmosphere of dry, oxygen-free nitrogen using Schlenk and dry-box techniques.[S4] **TiW$_5$** enriched in ^{17}O was prepared by hydrolysis of a mixture of $Ti(OCH_3)_4$, $WO(OCH_3)_4$, and $(Bu_4N)_2WO_4$ in dry acetonitrile using 10% ^{17}O-enriched water according to the procedure reported earlier.[S5] The presence of one terminal Ti–OCH_3 group and the absence of Ti=O group was confirmed by ^{1}H NMR spectroscopy that revealed one singlet at δ 4.10 (in addition to the resonances of Bu_4N cation) which integrated for 3H with reference to the triplet of CH_3-group in Bu_4N at δ 1.00 (36H). Anal. calcd (%) for $C_{49}H_{111}N_3TiW_5O_{19}$: C, 29.22; H, 5.55; N, 2.09. Found: C, 28.72; H, 5.60; N, 2.11. IR (KBr, 1200-400 cm^{-1}): 1152 (m, CO), 1096 (m, CO), 966 (w), 947 (s, W=O), 929 (w, sh), 904 (m), 883 (m), 777 (vs, WOW), 736 (sh, WOW), 592 (m, Ti-OC), 567 (sh), 537 (w, Ti-OC), 424 (s). ^{1}H NMR (ppm, in CD_3CN): 4.10 (s, 3H, OCH_3), 3.23 (m, 24H, NCH_2), 1.68 (m, 24H, CH_2), 1.44 (m, 24H, CH_2), 1.00 (t, 36H, CH_3). ^{17}O NMR (ppm, in CH_3CN): 724 (W=O), 716 (W=O), 527 (TiOW), 393 (WOW), 383 (WOW), and –55 (μ_6-O).

$(Bu_4N)_2[W_6O_{19}]$ (**W_6**) was prepared and characterized as described elsewhere.[S5]

$(Bu_4N)_4[((\mu\text{-}O)(NbW_5O_{18})_2]$ (**$(NbW_5)_2O$**) and $(Bu_4N)_2[(O_2)NbW_5O_{18}H]$ (**$HNb(O_2)W_5$**) were synthesized and characterized as described previously.[S6]

The synthesis of $(Bu_4N)_2[(CH_3O)NbW_5O_{18}]$ (**NbW_5**) was adapted from ref.[S7] To a solution of **$(NbW_5)_2O$** (1.75 g, 0.49 mmol) in 13 mL CH_3CN, methanol (20 mL total) was added stepwise until all of the solid had dissolved. The resulting mixture was stirred for 2 days at room temperature and then evaporated at ambient conditions during 5 days to give a white solid. The ^{1}H NMR spectrum of the methoxide **NbW_5** exhibited signs of hydrolysis as indicated by a methanol peak at δ 3.25. Anal. calcd (%) for $C_{33}H_{74}N_2NbW_5O_{19}$: C, 21.82; H, 4.16; N, 1.54; O, 16.73; Nb, 5.12; W, 50.62. Found: C, 21.11; H, 4.11; N, 1.57; O, 15.51; Nb, 4.82; W, 47.7. IR (KBr, 1200-400 cm^{-1}): 1152 (w, CO), 1109 (w, CO), 991 (w), 971 (s, W=O), 879 (w), 811 (vs, WOW), 795 (sh, WOW), 739 (w), 713 (w), 687 (w), 581 (m, Nb-OC), 531 (m, Nb-OC), 445 (s). ^{1}H NMR (ppm, in CH_3CN): 4.36 (s, 1.7H, $NbOCH_3$), 3.25 (s, 1.3H C*H*$_3$OH), 3.10 (m, 24H, NCH_2), 1.60 (m, 24H, CH_2), 1.34 (m, 24H, CH_2), 0.95 (t, 36H, CH_3).

Catalytic reactions. Catalytic experiments were performed under vigorous stirring (600 rpm) in thermostated glass vessels. Typical reaction conditions were as follows: alkene 0.2 mmol, H_2O_2 0.2 mmol (30% aqueous solution), POM 0.004 mmol, CH_3CN 1 mL, 50 °C. Reactions were started by the addition of 30% H_2O_2 to the reaction mixture containing acetonitrile solvent, alkene, and POM. Samples of the reaction mixture (0.5 μL) were withdrawn periodically during the reaction course by a syringe. The oxidation products were identified by gas chromatography–mass spectrometry (GC–MS). The product yields and substrate conversions were quantified by gas chromatography (GC) using biphenyl as an internal standard. For quantification of allylic oxidation products by GC, the method described by Shul'pin was employed.[S8] Semiquantitative Quantofix peroxide test sticks were used for estimation of the amount of H_2O_2 at the end of catalytic reactions. Each experiment was repeated at least twice.

H_2O_2 decomposition. Decomposition of H_2O_2 (0.2 *M*) was studied in the absence of organic substrate at 40–80 °C in CH_3CN (2 mL) in the presence of either **NbW_5** or **TiW_5** catalyst (0.008 mmol POM). Aliquots of 0.2 mL were taken during the reaction course, and H_2O_2 concentration was determined by iodometric titration. Two or three experiments were carried out in parallel.

Kinetic experiments. Kinetic experiments were performed in temperature-controlled glass vessels under vigorous stirring (600 rpm). Reactions were initiated by the addition of 30 or 77% H_2O_2 to a CH_3CN solution containing CyOct substrate, POM, and an internal standard for GC (biphenyl). The total volume of the reaction mixture was 1 mL. Samples (0.5 μL) of the reaction mixture were withdrawn periodically during the reaction with a syringe and analyzed by GC. Each experiment was repeated two or three times. To rule out the possibility of evaporative losses of the substrate, blank experiments without catalyst and oxidant were carried out at the reaction temperature using the internal standard.

Reaction order in catalyst. The POM concentration was varied in the range 0.002–0.01 *M*. Concentrations of other reactants were held constant: [CyOct] = 0.1 *M*, [H_2O_2] = 0.1 *M*. The reaction temperature was kept at 50 °C.

Reaction order in substrate. The initial substrate concentration was varied between 0.02 and 0.4 *M* while maintaining constant concentrations of H_2O_2 (0.1 *M*) and catalyst (0.004 *M*). The reaction temperature was kept at 50 °C.

Reaction order in H_2O_2. The initial oxidant concentration was varied in the range of 0.05–0.4 *M*. 77% H_2O_2 was employed in order to reduce the amount of water in the reaction mixture. The concentration of water in these experiments was kept constant (0.34 *M*) by the addition of corresponding amounts of H_2O. The concentrations of other reactants were as follows: [CyOct] = 0.1 *M*, [POM] = 0.004 *M*. The reaction temperature was kept at 50 °C.

Reaction order in H_2O. The initial concentration of water was varied from 0.05 to 2.0 *M*. Other parameters were held constant: [CyOct] = 0.1 *M*, [H_2O_2] = 0.1 *M*, and [POM] = 0.004 *M*. The reaction temperature was kept at 50 °C.

Determination of activation energies. The temperature dependence of the epoxidation rate was studied in the range of 40–80 ºC in CH_3CN using the following reaction conditions: [CyOct] = 0.1 *M*, [H_2O_2] = 0.1 *M*, and [POM] = 0.004 *M*.

Stoichiometric interaction with CyH. Stoichiometric reactions between CyH and peroxo complex **HTi(O$_2$)W$_5$** was performed under Ar in thermostated glass vessels equipped with a magnetic stirrer at [POM] = 0.016 *M* and [CyH] = 0.08 *M* in dry CH_3CN (1 mL) at 50 °C. The reaction course was monitored using both UV-vis and GC. The oxidation products were identified by GC–MS and quantified by GC using biphenyl as internal standard.

Computational Details. The DFT analysis of the reaction pathway was carried out with Gaussian09 rev. C01 software.[S9] Geometry optimization of reagents, intermediates, transition states and products was made using B3LYP density functional.[S10–S12] LANL2DZ pseudopotential[S13] was used for W, Ti and Nb atoms and 6–31g(d,p) basis set[S14–S16] was used for other atoms. The geometry optimization was full and without any symmetry constrains, and solvent effects of acetonitrile were included using the IEF-PCM implicit solvation model as implemented in Gaussian09.[S17] This level of theory has been proved to be accurate and reliable enough to study the reactivity concerning POMs and their transition metal-substituted analogues, always showing a high degree of consistency with experimental outcomes and kinetic studies.[S18–S20] . The free-energies were converted from 1 atm to the standard state of 1 mol·L^{-1} at 25ºC.

References:

(S1) Clegg, W.; Errington, R. J.; Kraxner, P.; Redshaw, C. Solid State and Solution Studies of Tungsten(VI) Oxotetraalkoxides. *J. Chem. Soc., Dalton Trans.*, **1992**, 1431-1438.

(S2) Che, T. M.; Day, V. W.; Francesconi, L. C.; Fredrich, M. F.; Klemperer W. G.; Shum, W. Synthesis and Structure of the [η5-C5H5)Ti(Mo5O18)]3- and [η5-C5H5)Ti(W5O18)]3- Anions. *Inorg. Chem.*, 1985, **24**, 4055-4062.

(S3) Bradley, D. C.; Mehrotra R. C.; Gaur, D. P. *Metal Alkosides*. Academic Press: London, **1978.**

(S4) Errington, R. J. *Advanced Practical Inorganic and Metalorganic Chemistry*. Blackie Academic & Professional: London, **1997**.

(S5) Clegg, W.; Elsegood, M. R. J.; Errington, R. J.; Havelock, J. Alkoxide Hydrolysis as a Route to Early Transition-Metal Polyoxometalates: Synthesis and Crystal Structures of Heteronuclear Hexametalate Derivatives, *J. Chem. Soc. Dalton Trans*. **1996**, 681-690.

(S6) Maksimchuk, N. V.; Maksimov, G. M.; Evtushok, V. Yu.; Ivanchikova, I. D.; Chesalov, Yu. A.; Maksimovskaya, R. I.; Kholdeeva, O. A.; Solé-Daura, A.; Poblet, J. M.; Carbó, J. J. Relevance of Protons in Heterolytic Activation of H_2O_2 over Nb(V). Insights from Model Studies on Nb-substituted Polyoxometalates. *ACS Catal*., **2018**, *8*, 9722–9737.

(S7) Lu, Y. J.; Lalancette, R.; Beer. R. H. Deoxygenation of Polynuclear Metal-Oxo Anions: Synthesis, Structure, and Reactivity of the Condensed Polyoxoanion $[(C_4H_9)_4N]_4(NbW_5O_{18})_2O$. *Inorg. Chem*. 1996, *35*, 2524–2529.

(S8) Shul'pin, G. B. Metal–Catalyzed Hydrocarbon Oxygenations in Solutions: The Dramatic Role of Additives: A Review. *J. Mol. Catal. A: Chem.* **2002**, *189*, 39–66.

(S9) *Gaussian 09, Revision C.01*; Frisch, M. J., Trucks, G. W., Schlegel, H. B., Scuseria, G. E., Robb, M. A., Cheeseman, J. R., Scalmani, G., Barone, V., Mennucci, B., Petersson, G. A., Nakatsuji, H., Caricato, M., Li, X., Hratchian, H. P., Izmaylov, A. F., Bloino, J., Zheng, G., Sonnenberg, J. L., Hada, M., Ehara, M., Toyota, K., Fukuda, R., Hasegawa, J., Ishida, M., Nakajima, T., Honda, Y., Kitao, O., Nakai, H., Vreven, T., Montgomery Jr., J. A., Peralta, J. E., Ogliaro, F., Bearpark, M., Heyd, J. J., Brothers, E., Kudin, K. N., Staroverov, V. N., Kobayashi, R., Normand, J., Raghavachari, K., Rendell, A., Burant, J. C., Iyengar, S. S., Tomasi, J., Cossi, M., Rega, N., Millam, J. M., Klene, M., Knox, J. E., Cross, J. B., Bakken, V., Adamo, C., Jaramillo, J., Gomperts, R., Stratmann, R. E., Yazyev, O., Austin, A. J., Cammi, R., Pomelli, C., Ochterski, J. W., Martin, R. L., Morokuma, K., Zakrzewski, V. G., Voth, G. A., Salvador, P., Dannenberg, J. J., Dapprich, S., Daniels, A. D., Farkas, O., Foresman, J. B., Ortiz, J. V., Cioslowski, J., Fox, D. J., Eds.; Gaussian Inc.: Wallingford CT, 2010.

(S10) Lee, C.; Yang, W.; Parr, R. G. Development of the Colle–Salvetti Correlation–Energy Formula into a Functional of the Electron Density. *Phys. Rev. B* **1988**, *37*, 785–789.

(S11) Becke, A. D. Density-Functional Thermochemistry. III. The Role of Exact Exchange. *J. Chem. Phys*. **1993**, *98*, 5648–5652.

(S12) Stephens, P. J.; Devlin, F. J.; Chabalowski, C. F.; Frisch, M. J. Ab Initio Calculation of Vibrational Absorption and Circular Dichroism Spectra Using Density Functional Force Fields. *J. Phys. Chem*. **1994**, *98*, 11623–11627.

(S13) Hay, P. J.; Wadt, W. R. Ab Initio Effective Core Potentials for Molecular Calculations. Potentials for K to Au Including the Outermost Core Orbitals. *J. Chem. Phys*. **1985**, *82*, 299–310.

(S14) Francl, M. M.; Pietro, W. J.; Hehre, W. J.; Binkley, J. S.; Gordon, M. S.; DeFrees, D. J.; Pople, J. A. Self-Consistent Molecular Orbital Methods. XXIII. A Polarization-Type Basis Set for Second-Row Elements. *J. Chem. Phys*. **1982**, *77*, 3654–3665.

(S15) Hehre, W. J.; Ditchfield, R.; Pople, J. A. Self—Consistent Molecular Orbital Methods. XII. Further Extensions of Gaussian—Type Basis Sets for Use in Molecular Orbital Studies of Organic Molecules. *J. Chem. Phys*. **1972**, *56*, 2257–2261.

(S16) Hariharan, P. C.; Pople, J. A. The Influence of Polarization Functions on Molecular Orbital Hydrogenation Energies. *Theoret. Chim. Acta* **1973**, *28*, 213–222.

(S17) Cancès, E.; Mennucci, B.; Tomasi, J. A New Integral Equation Formalism for the Polarizable Continuum Model: Theoretical Background and Applications to Isotropic and Anisotropic Dielectrics. *J. Chem. Phys*. **1997**, *107*, 3032−3041.

(S18) López, X.; Carbó, J. J.; Bo, C.; Poblet, J. M. Structure, Properties and Reactivity of Polyoxometalates: a Theoretical Perspective. *Chem. Soc. Rev*. **2012**, *41*, 7537–7571.

(S19) Skobelev, I. Y.; Zalomaeva, O. V.; Kholdeeva, O. A.; Poblet, J. M.; Carbó, J. J. Mechanism of Thioether Oxidation over Di-and Tetrameric Ti Centres: Kinetic and DFT Studies Based on Model Ti–Containing Polyoxometalates. *Chem.–Eur. J*. **2015**, *21*, 14496–14506.

(S20) Skobelev, I. Y.; Evtushok, V. Y.; Kholdeeva, O. A.; Maksimchuk, N. V.; Maksimovskaya, R. I.; Ricart, J. M.; Poblet, J. M.; Carbó, J. J. Understanding the Regioselectivity of Aromatic Hydroxylation over Divanadium–Substituted γ–Keggin Polyoxotungstate. *ACS Catal*. **2017**, *7*, 8514–8523.

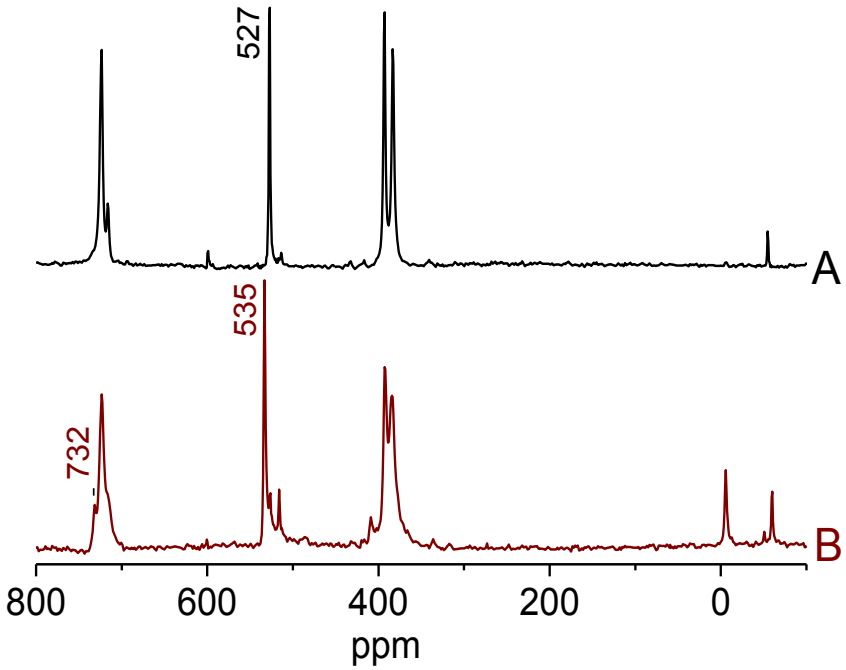

Figure S1. ^{17}O NMR spectra of **TiW_5**: (A) initial and (B) after catalytic reaction of CyH oxidation (reaction conditions as in Table 1). POM 0.02 *M*, CH_3CN, 50 ºC.

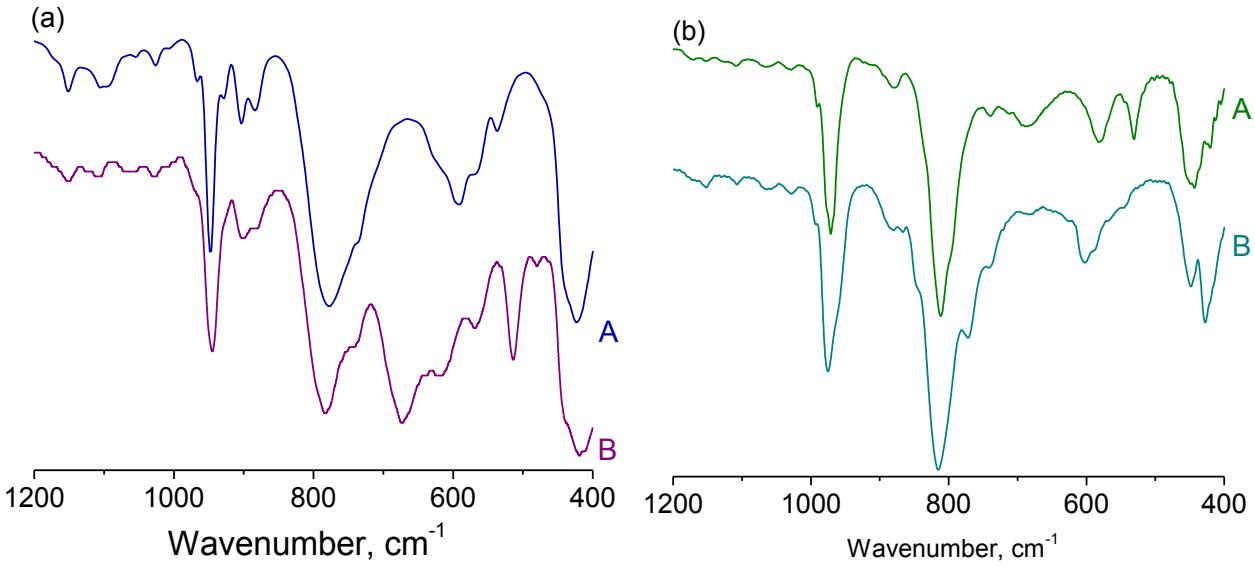

Figure S2. FTIR spectra of (a) **TiW_5** and (b) **NbW_5:** (A) initial and (B) after catalytic reaction of CyH oxidation. Reaction conditions: CyH 0.2 *M*, 30% H_2O_2 0.2 *M*, POM 0.004 *M*, CH_3CN, 50ºC, 4 h for **TiW_5** and 2 h for **NbW_5**.

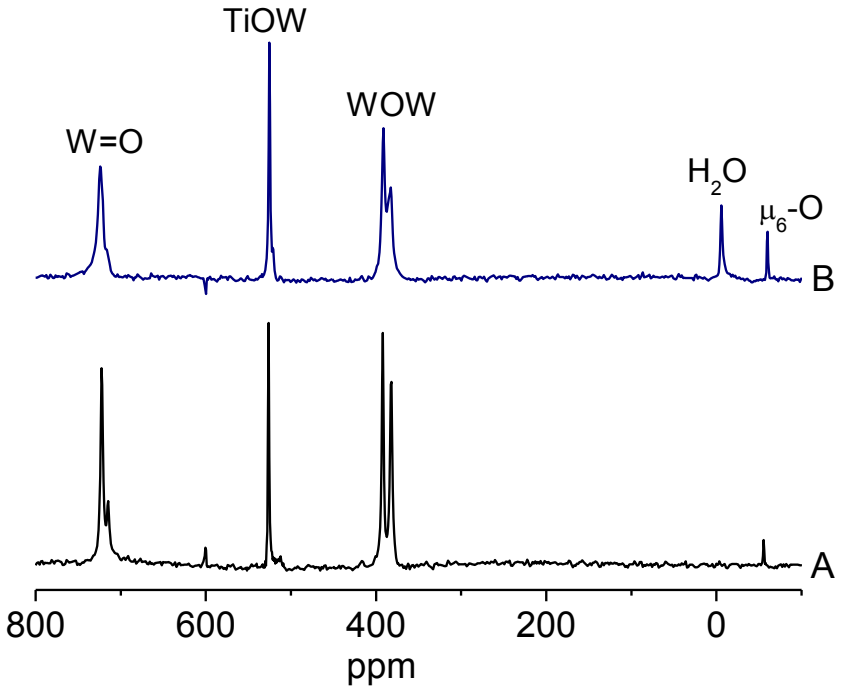

Figure S3. ^{17}O NMR spectra of (A) **TiW$_5$** and (B) **TiW$_5$** after 24 h of hydrolysis. POM 0.02 *M*, H_2O 10 vol%, CD_3CN, 50 ºC.

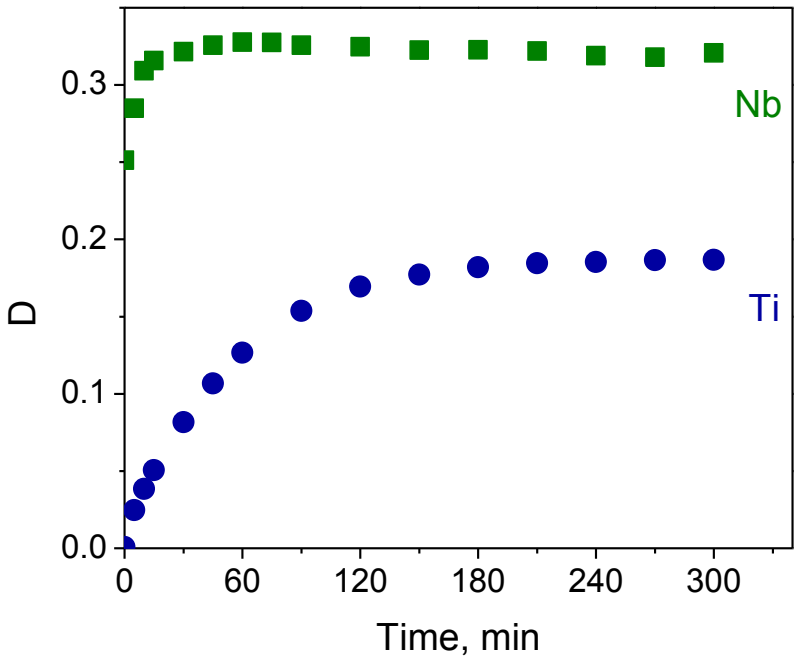

Figure S4. UV-vis absorbance vs time upon interaction of **MW$_5$** with 5 equiv. of 30% H_2O_2: 315 nm for **NbW$_5$** and 375 nm for **TiW$_5$**. POM 0.5 m*M*, H_2O_2 2.5 m*M*, CH_3CN, 20 ºC, l = 0.1 cm.

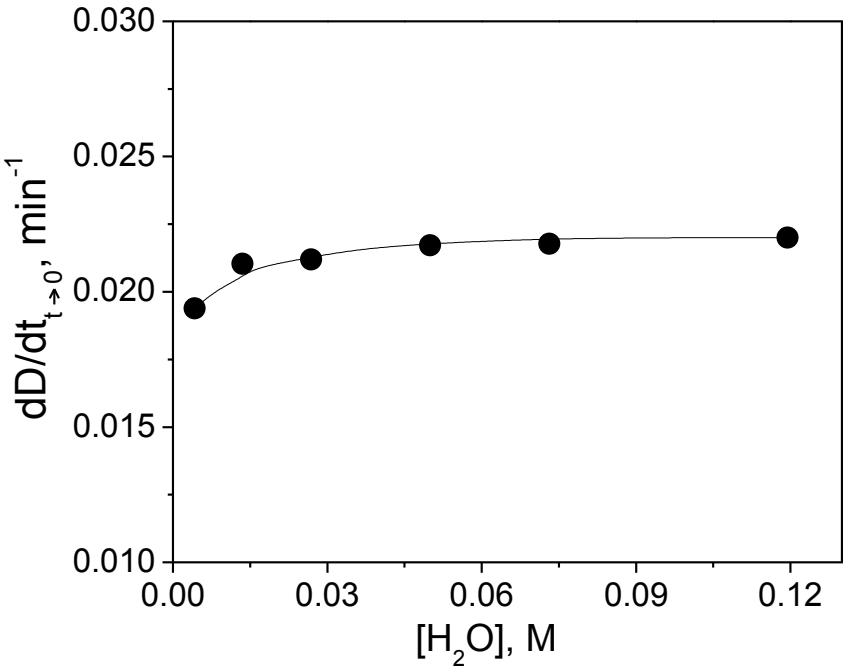

Figure S5. Effect of water concentration on the rate of Ti peroxo complex formation upon interaction of **TiW$_5$** with 5 equiv. of H_2O_2: dD/dt at t→0 at 375 nm versus [H_2O]. POM 1.5·m*M*, H_2O_2 7.5·m*M*, CH_3CN, 20 ºC, l = 0.1 cm.

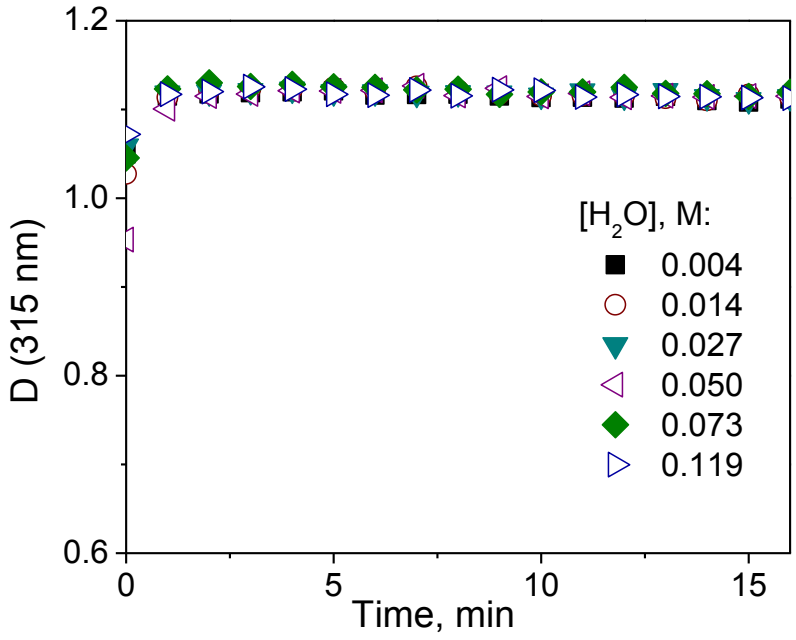

Figure S6. Effect of water concentration on the rate of Nb peroxo complex formation upon interaction of **NbW$_5$** with 5 equiv. of H_2O_2: UV-vis absorbance at 315 nm vs time at different [H_2O]. POM 1.5·m*M*, H_2O_2 7.5·m*M*, CH_3CN, 20 ºC, l = 0.1 cm.

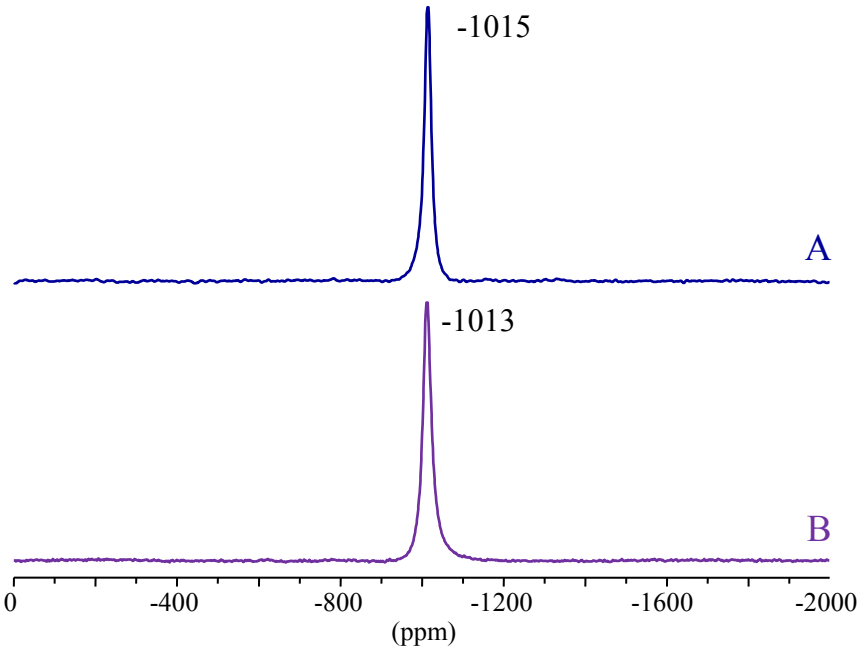

Figure S7. ^{93}Nb NMR spectra of (A) **HNb(O$_2$)W$_5$** and (B) **NbW$_5$** in the presence of 5 equiv of 30% H_2O_2. POM 0.01 *M*, CH_3CN, 20 °C.

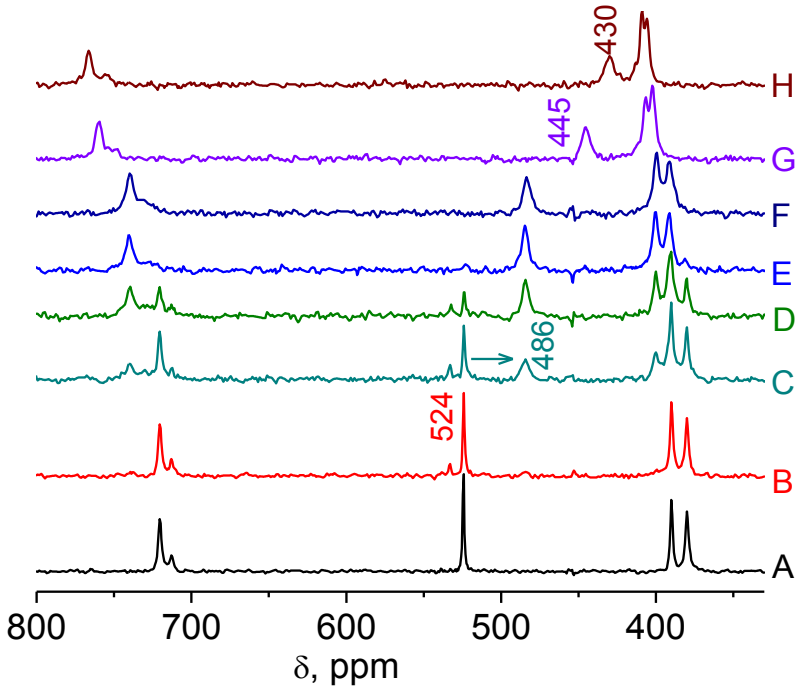

Figure S8. ^{17}O NMR spectra of **TiW$_5$**: (A) initial and after interaction with (B) 0.1, (C) 0.2, (D) 0.3 (E) 0.4, (F) 0.5, (G) 0.8, and (H) 1.0 equiv. of $HClO_4$. POM 0.02 *M*, $HClO_4$ 0.002–0.02 *M*, CH_3CN, 20 °C.

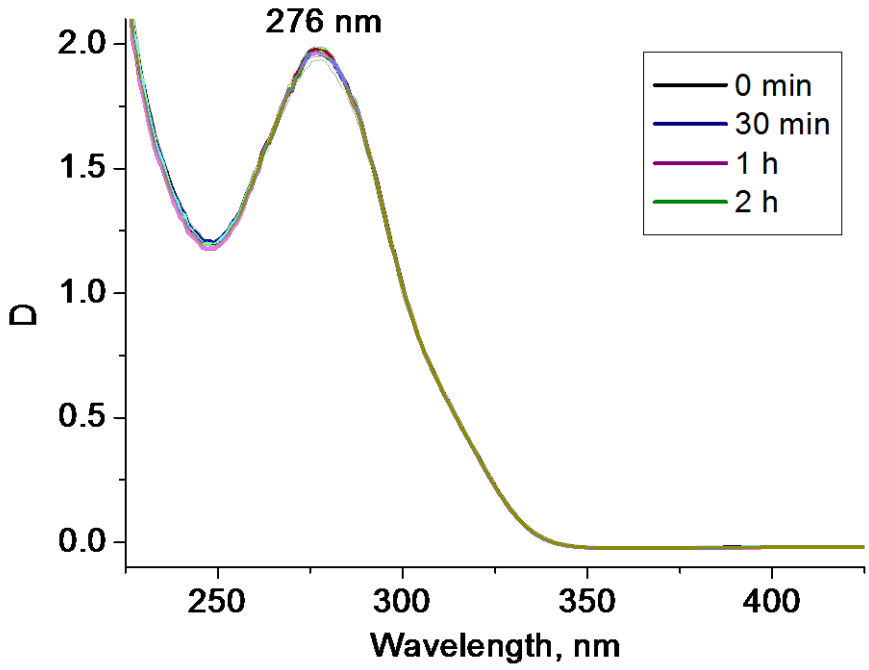

Figure S9. UV spectra of **W6** upon interaction with 40 equiv. of 30% H_2O_2. POM 0.002 *M*, H_2O_2 0.08 *M*, CH_3CN, 20 °C.

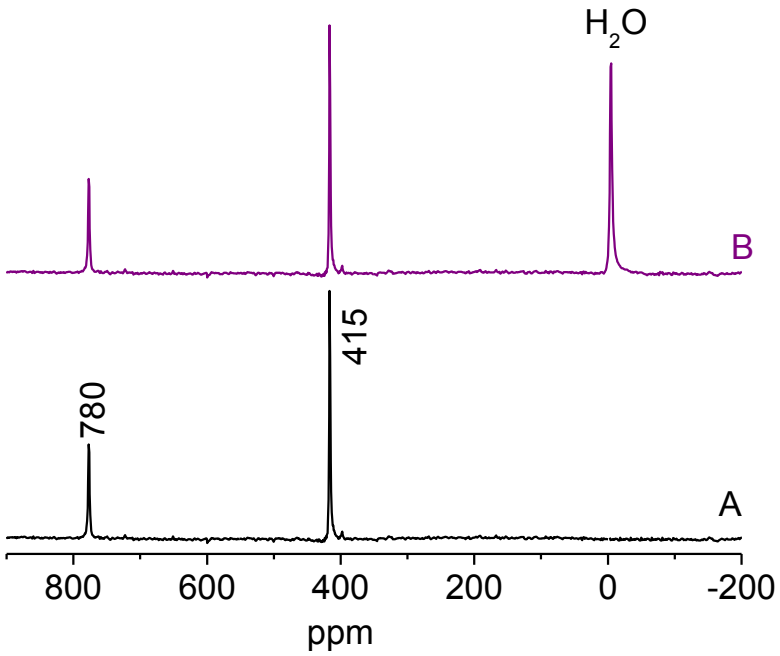

Figure S10. ^{17}O NMR spectra of **W6**: (A) initial and (B) after interaction with 20 equiv. of 30% H_2O_2. POM 0.02 *M*, H_2O_2 0.4 *M*, CH_3CN, 50°C, 5 h.

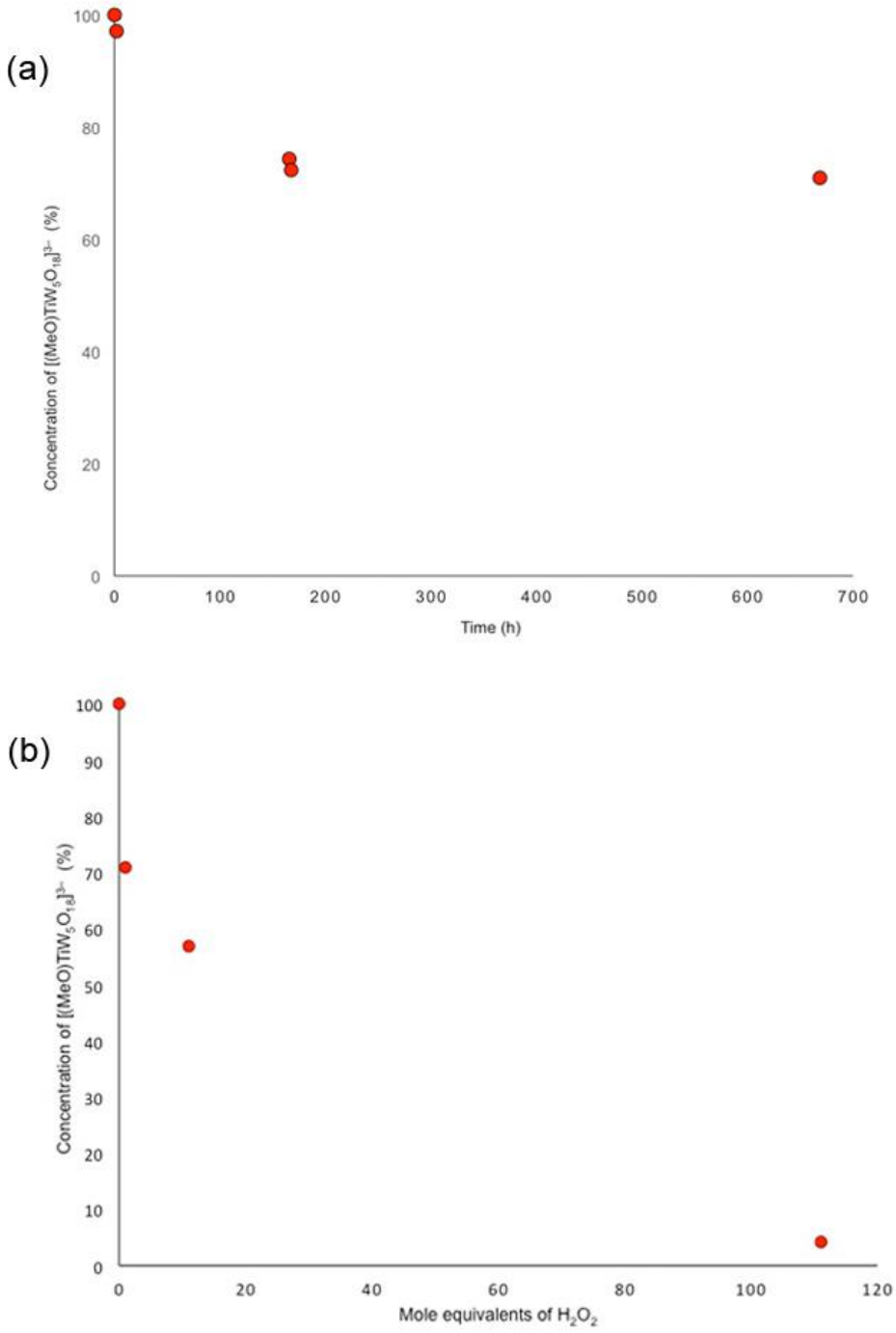

Figure S11. Plots of the conversion of **TiW$_5$** upon treatment with (a) one mole-equivalent and (b) an excess of dried H_2O_2. POM 0.03 *M*, CH_3CN, RT.

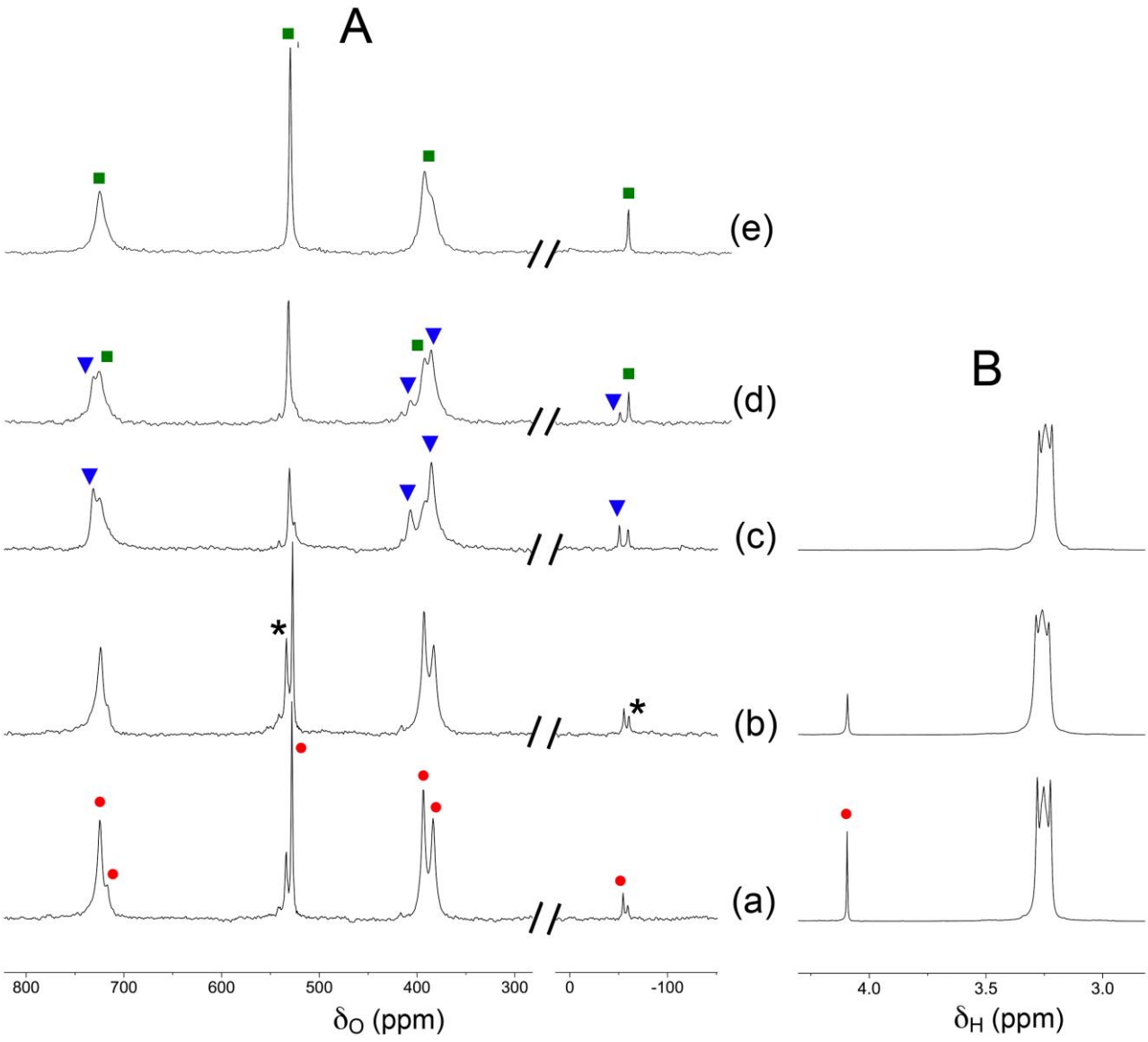

Figure S12. ^{17}O (**A**) and ^{1}H (**B**) NMR spectra of the products after treatment of **TiW_5** with (a) 1, (b) 11 and (c) 111 mole equivalents of dried H_2O_2. Spectra (d) and (e) were recorded 22 and 44 h respectively after spectrum (c). Peaks assigned to **TiW_5**, **$HTi(O_2)W_5$** and **$(TiW_5)_2O$** are indicated by ●, ▼and ■, respectively. Peaks due to an apparent intermediate prior to formation of **$HTi(O_2)W_5$** are marked with an asterisk. POM 0.03 *M*, CH_3CN, RT.

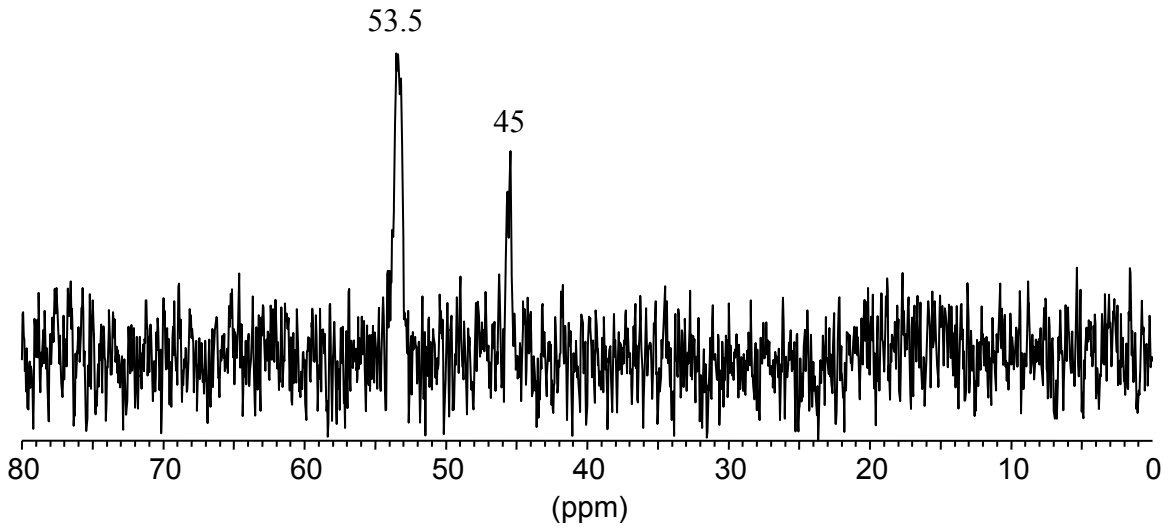

Figure S13. ^{183}W NMR spectrum of **TiW$_5$** in the presence of 5 equiv. of 30% H_2O_2 in CD_3CN. POM 0.07 M, 20 ^{o}C.

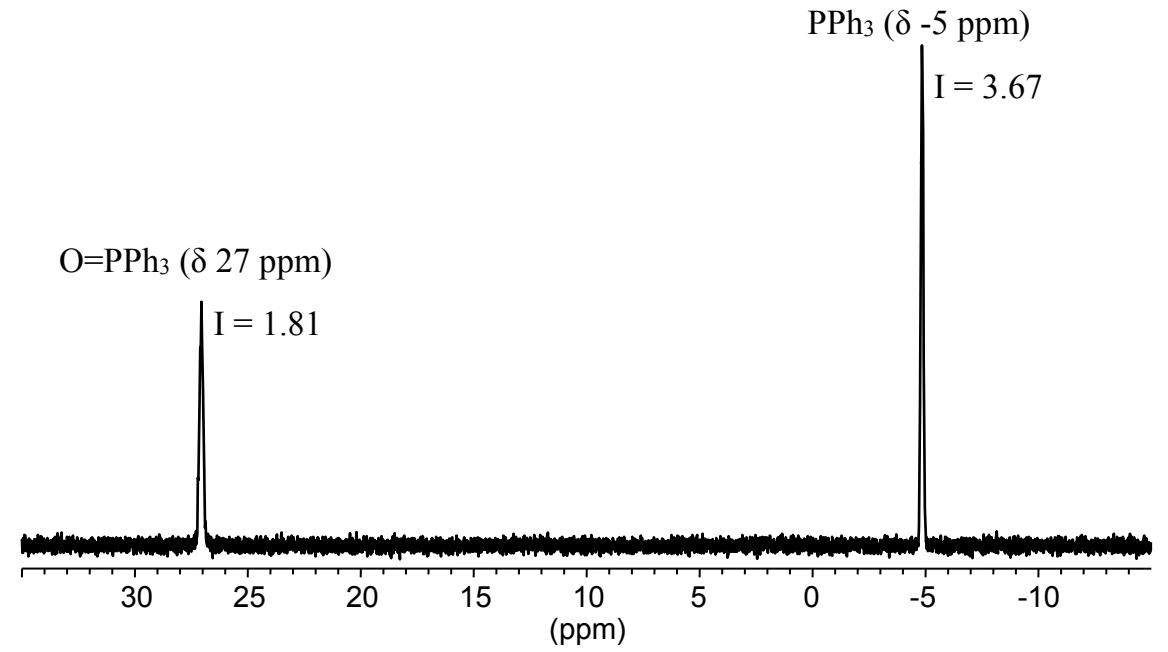

Figure S14. ^{31}P NMR spectrum recorded 1 h after addition of 3 equiv. of PPh_3 to **HTi(O$_2$)W$_5$** in CH_3CN. POM 0.014 *M*, PPh_3 0.041 *M*, 20 ^{o}C.

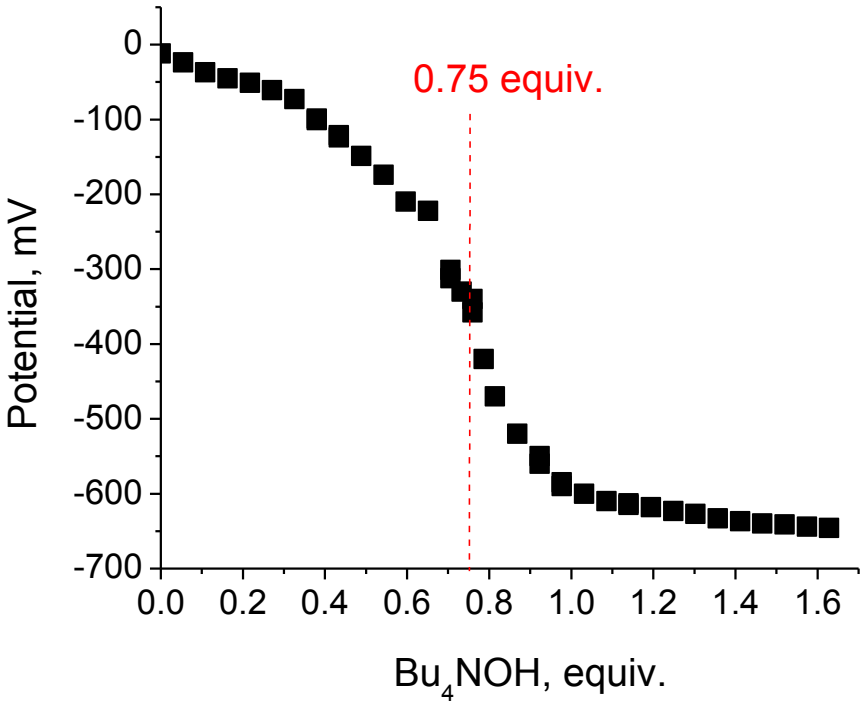

Figure S15. Potentiometric titration of **HTi(O$_2$)W$_5$** (0.007 mmol) in CH_3CN (7 mL) with aqueous Bu_4NOH (0.38 *M*). The potentials are relative to a standard Ag/AgCl electrode.

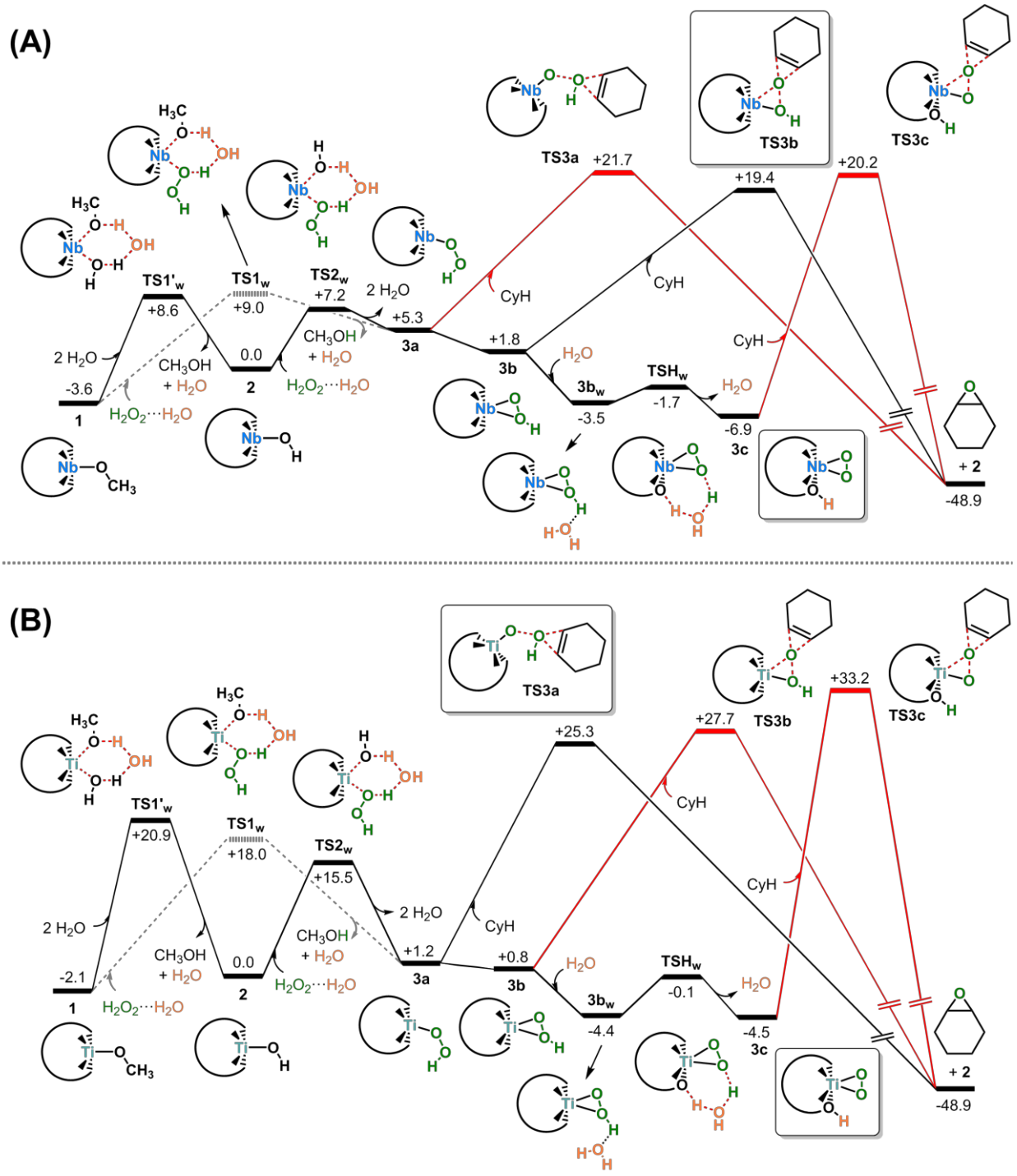

Figure S16. Full version of calculated free energy profiles (kcal·mol^{-1}) for the epoxidation of CyH catalyzed by **NbW$_5$** (A) and **TiW$_5$** (B). Black lines depict the most favorable reaction pathway, while less favorable ones are shown in red lines.

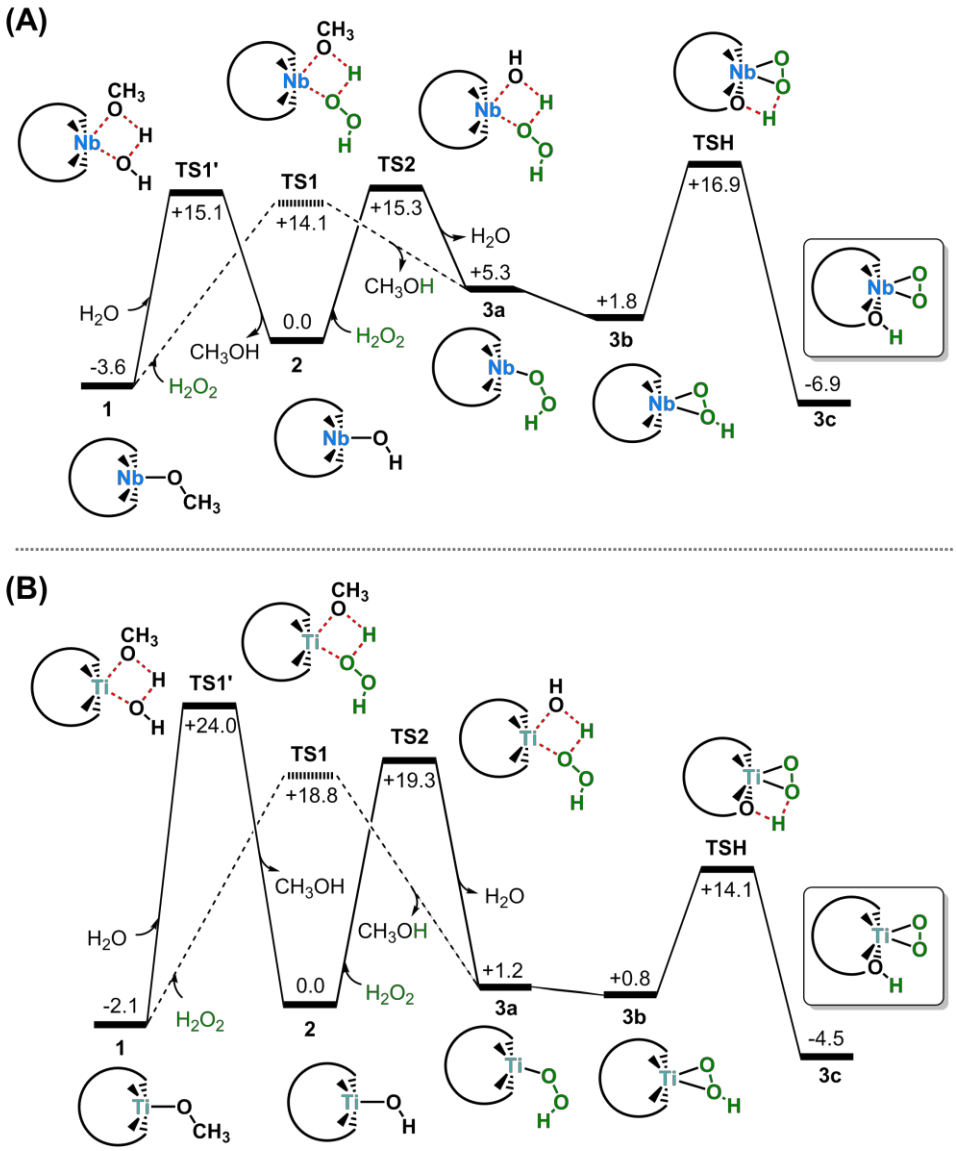

Figure S17. Alternative reaction paths for the formation of resting state **3c** from the active catalytic species **2** and from the methoxy precursor **1**.

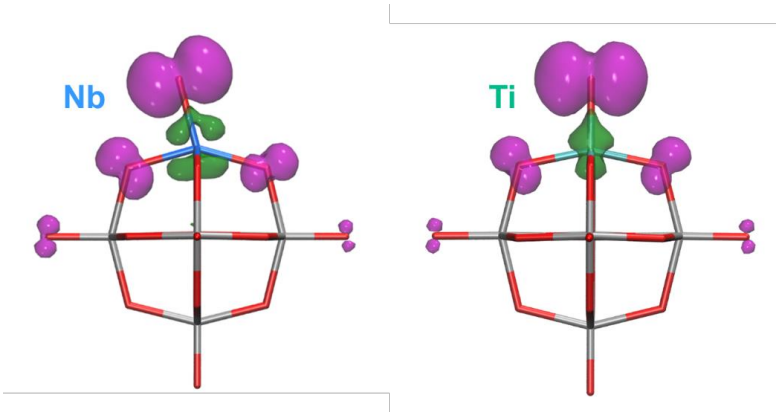

Figure S18. Spin densities computed for Nb- and Ti-oxyl species (isovalue = 0.002). Atomic spin densities on oxygen atoms are 0.95 and 0.97 for Nb and Ti, respectively.

Cartesian coordinates in Å and Gibbs free-energies in a.u. of the most representative DFT-derived structures:

1^{Nb}: ΔG = -1866.11438 a.u.

O	-0.001574	-0.027874	-0.351395
W	-1.416092	0.482377	-2.164585
W	1.743849	-0.527405	-1.853880
W	1.379304	-0.645551	1.455803
W	-1.778485	0.366262	1.145089
W	-0.724668	-2.336397	-0.510337
Nb	0.682513	2.156209	-0.196355
O	-2.545610	0.701621	-0.604003
O	0.262740	-0.012925	-2.996998
O	-0.314942	-0.197665	2.285415
O	2.494122	-0.911584	-0.108107
O	1.685876	1.225632	1.255241
O	0.526724	-2.323231	0.954955
O	1.982267	1.322787	-1.462655
O	0.812424	-2.229680	-1.667297
O	-0.611864	2.151887	-1.714757
O	-1.689778	-1.430190	-1.911406
O	-0.907061	2.058086	1.003264
O	-1.975036	-1.521642	0.709342
O	2.387864	-1.098659	2.769198
O	-2.450389	0.853622	-3.483493
O	3.015947	-0.892467	-2.947591
O	-3.076819	0.651041	2.231913
O	-1.235969	-3.969763	-0.622957
O	1.239456	3.929011	-0.078435
C	1.661353	5.274829	0.014338
H	1.851756	5.664580	-0.990002
H	0.876554	5.865993	0.495470
H	2.577685	5.326523	0.609893

TS1^{Nb}: ΔG = -2017.62657 a.u.

O	-0.041696	-0.007317	-0.156552
W	-1.350776	0.718915	-1.968665
W	1.817654	-0.228959	-1.601391
W	1.224313	-0.933386	1.601037
W	-1.942062	0.017294	1.235877
W	-0.664509	-2.332877	-0.782876
Nb	0.540914	2.118907	0.404110
O	-2.589305	0.649216	-0.481628
O	0.397393	0.418301	-2.748976
O	-0.542199	-0.694851	2.367047
O	2.453476	-0.897856	0.104532
O	1.447735	0.952328	1.739596
O	0.472828	-2.520032	0.755286
O	1.954282	1.523600	-0.894603

O	0.935965	-1.969100	-1.772151
O	-0.614953	2.305595	-1.188412
O	-1.567812	-1.208981	-2.064442
O	-1.132415	1.733472	1.467139
O	-2.027808	-1.760437	0.458921
O	2.154511	-1.567672	2.896649
O	-2.294374	1.297796	-3.279958
O	3.171222	-0.374272	-2.646801
O	-3.321361	0.071726	2.254877
O	-1.100164	-3.934014	-1.209347
O	-0.195101	4.172951	0.907254
O	1.959998	3.614238	0.862950
H	1.051694	4.300259	1.041499
O	-0.915064	4.281816	2.165759
H	-1.348853	3.398254	2.177078
C	3.260184	3.972089	0.382903
H	3.592163	3.214124	-0.328720
H	3.209350	4.947566	-0.108504
H	3.952631	4.021285	1.227707

TS1'^{Nb}: ΔG = -1942.50378 a.u.

O	-0.052334	0.032478	-0.233124
W	-1.508222	0.601252	-1.989003
W	1.715294	-0.185561	-1.782293
W	1.359996	-0.721573	1.484937
W	-1.859259	0.075776	1.279779
W	-0.607123	-2.340010	-0.681837
Nb	0.465482	2.231027	0.174284
O	-2.652565	0.553724	-0.427092
O	0.196595	0.336306	-2.869837
O	-0.356820	-0.526004	2.354057
O	2.495106	-0.714478	-0.082977
O	1.501008	1.188166	1.509661
O	0.644493	-2.390335	0.782055
O	1.809868	1.604150	-1.187546
O	0.913578	-1.967107	-1.795984
O	-0.812250	2.258115	-1.340421
O	-1.636061	-1.338610	-1.969478
O	-1.121572	1.809422	1.359455
O	-1.906518	-1.760774	0.608545
O	2.403808	-1.232627	2.749214
O	-2.564488	1.060998	-3.262623
O	3.006698	-0.330242	-2.906204
O	-3.171694	0.120024	2.387790
O	-0.990799	-3.981640	-0.995720
O	-0.226972	4.223612	0.680916
O	1.918818	3.770282	0.399149
H	0.995355	4.383175	0.791476
C	3.260351	3.702767	0.876265
H	3.851018	3.102298	0.180257

H	3.669805	4.715562	0.921585
H	3.295036	3.241080	1.868607
H	-0.771988	4.211282	1.481441

2^{Nb}: ΔG = -1826.83290 a.u.

O	-0.069782	0.012687	-0.282853
W	-1.457392	0.554468	-2.103094
W	1.755687	-0.216908	-1.745364
W	1.311086	-0.573338	1.529718
W	-1.906167	0.177787	1.168408
W	-0.580733	-2.298299	-0.610882
Nb	0.432045	2.287277	0.041308
O	-2.649685	0.576410	-0.573865
O	0.281563	0.255927	-2.908082
O	-0.439839	-0.323074	2.327222
O	2.492573	-0.641912	-0.005473
O	1.455892	1.326062	1.452760
O	0.619868	-2.282332	0.897656
O	1.806349	1.627094	-1.214936
O	0.981716	-1.996880	-1.705881
O	-0.806553	2.247980	-1.518157
O	-1.577548	-1.387964	-1.985310
O	-1.158665	1.952729	1.148190
O	-1.941438	-1.681520	0.618658
O	2.315709	-1.015597	2.849181
O	-2.477181	0.929554	-3.431803
O	3.088038	-0.383487	-2.813800
O	-3.245648	0.310963	2.232451
O	-0.948427	-3.956945	-0.848361
O	0.848370	4.126654	0.300476
H	1.551193	4.664445	-0.092286

TS2^{Nb}: ΔG = -1978.34872 a.u.

O	-0.017585	0.045471	-0.277489
W	-1.549082	0.571413	-1.983707
W	1.678270	-0.232814	-1.902832
W	1.469362	-0.680682	1.392848
W	-1.758004	0.113188	1.308601
W	-0.601808	-2.345582	-0.646975
Nb	0.530133	2.233277	0.041553
O	-2.614901	0.582286	-0.367664
O	0.113117	0.272681	-2.929534
O	-0.210131	-0.446250	2.329830
O	2.525150	-0.728862	-0.227479
O	1.622715	1.226138	1.360937
O	0.700004	-2.359559	0.766494
O	1.807875	1.572150	-1.355554
O	0.862025	-2.009406	-1.835644

O	-0.802994	2.245343	-1.407480
O	-1.689372	-1.362245	-1.902399
O	-0.992207	1.865155	1.302953
O	-1.849284	-1.720329	0.690192
O	2.564054	-1.169776	2.620057
O	-2.657296	1.010976	-3.217032
O	2.916738	-0.412844	-3.076796
O	-3.015489	0.210087	2.471085
O	-1.010993	-3.989378	-0.898303
O	-0.213248	4.310769	0.543344
O	1.975477	3.824438	0.232433
H	2.702294	3.683339	0.856553
H	1.024879	4.420524	0.585103
O	-0.711938	4.412718	1.907411
H	-1.145911	3.532721	1.987219

3a^{Nb}: ΔG = -1901.94564 a.u.

O	-0.055058	0.079346	-0.292720
W	-1.616017	0.539636	-2.003863
W	1.647415	-0.173153	-1.916705
W	1.462657	-0.578553	1.394898
W	-1.801338	0.116526	1.302378
W	-0.562149	-2.333734	-0.627572
Nb	0.422843	2.231859	-0.018912
O	-2.677722	0.507381	-0.381676
O	0.070230	0.297583	-2.935837
O	-0.228563	-0.390628	2.319050
O	2.513578	-0.598096	-0.241918
O	1.568024	1.318425	1.342982
O	0.756394	-2.286630	0.767812
O	1.733743	1.679315	-1.384911
O	0.898938	-1.959074	-1.833795
O	-0.969075	2.244203	-1.445434
O	-1.666236	-1.403298	-1.901533
O	-1.111059	1.893331	1.272245
O	-1.815478	-1.737650	0.701977
O	2.571998	-1.034768	2.620902
O	-2.740799	0.898348	-3.247654
O	2.889143	-0.320771	-3.089376
O	-3.060456	0.165209	2.464701
O	-0.913177	-3.993964	-0.857311
O	0.388663	4.030349	0.720111
O	-0.465655	4.446266	1.787595
H	-0.998866	3.625761	1.925867

3b^{Nb}: ΔG = -1901.95118 a.u.

O	0.019068	0.064652	-0.297919
W	-1.532444	0.593598	-1.991351

W	1.695502	-0.226365	-1.940381
W	1.526616	-0.652309	1.362106
W	-1.696381	0.208188	1.314785
W	-0.594518	-2.301692	-0.617237
Nb	0.577623	2.234664	0.009003
O	-2.577783	0.630847	-0.361478
O	0.112410	0.256307	-2.954208
O	-0.129795	-0.340424	2.319182
O	2.560186	-0.718595	-0.266974
O	1.712854	1.270868	1.277454
O	0.734898	-2.319396	0.792732
O	1.859310	1.573669	-1.430369
O	0.861335	-2.004049	-1.818728
O	-0.771258	2.264567	-1.448678
O	-1.692153	-1.342535	-1.873991
O	-0.950290	1.961373	1.263169
O	-1.802050	-1.646777	0.737806
O	2.637217	-1.121917	2.582435
O	-2.657740	1.018298	-3.214906
O	2.912792	-0.456092	-3.128731
O	-2.942111	0.320697	2.489982
O	-1.021268	-3.947431	-0.831336
O	1.492562	4.003600	-0.209163
O	0.906033	4.178541	1.125255
H	0.193126	4.831926	0.981410

TS3a^{Nb}: ΔG = -2136.45782 a.u.

O	-0.014496	0.053535	-0.417776
W	-1.448719	0.565045	-2.205898
W	1.642515	-0.608072	-1.943150
W	1.426066	-0.446653	1.361794
W	-1.667395	0.726117	1.099428
W	-0.851564	-2.143719	-0.368373
Nb	0.847035	2.313773	-0.468395
O	-2.501531	0.978390	-0.632301
O	0.154949	-0.093849	-3.072072
O	-0.197526	0.165886	2.229377
O	2.459177	-0.908642	-0.210965
O	1.829216	1.379573	0.996072
O	0.460507	-2.112276	1.046190
O	1.993947	1.252059	-1.700896
O	0.636555	-2.240290	-1.595863
O	-0.517261	2.205911	-1.915923
O	-1.832351	-1.301422	-1.806298
O	-0.702466	2.343341	0.781766
O	-2.010091	-1.173882	0.834620
O	2.464652	-0.846898	2.670566
O	-2.507420	0.913581	-3.513030
O	2.845900	-1.116396	-3.059241
O	-2.889011	1.184004	2.217062

O	-1.467810	-3.747897	-0.331320
O	1.487114	4.071190	-0.706654
O	1.620783	4.408818	0.966221
H	0.881073	5.044022	0.941254
C	1.403819	4.392980	3.244055
C	2.217541	5.458362	2.999526
H	1.826930	3.393252	3.250238
H	3.266366	5.282393	2.779916
C	-0.049090	4.532949	3.597668
C	-0.592489	5.946465	3.332477
H	-0.628326	3.778502	3.051614
C	0.398778	7.018856	3.806222
H	-1.560794	6.070094	3.827925
H	-0.782669	6.075393	2.256716
C	1.753446	6.886753	3.088784
H	0.554123	6.906703	4.886825
H	-0.010685	8.021854	3.647030
H	2.524362	7.472315	3.604925
H	1.700415	7.317055	2.077015
H	-0.159009	4.279429	4.663046

TS3b^{Nb}: ΔG = -2136.46146 a.u.

O	0.072457	0.038360	-0.215904
W	-1.337448	0.750459	-1.955195
W	1.845095	-0.197141	-1.750094
W	1.445099	-0.802796	1.492252
W	-1.734343	0.161215	1.289413
W	-0.585435	-2.256053	-0.720399
Nb	0.702234	2.225358	0.267915
O	-2.500144	0.708899	-0.412581
O	0.365127	0.430993	-2.831460
O	-0.267507	-0.520333	2.359045
O	2.588827	-0.821542	-0.066270
O	1.701371	1.091535	1.553550
O	0.645990	-2.416502	0.755853
O	2.036840	1.564588	-1.090832
O	0.960975	-1.939790	-1.818029
O	-0.577022	2.354896	-1.251202
O	-1.557000	-1.182574	-1.995022
O	-0.940524	1.873209	1.388835
O	-1.869213	-1.655380	0.579869
O	2.450421	-1.401613	2.749786
O	-2.357190	1.297130	-3.225209
O	3.139933	-0.376295	-2.865832
O	-3.055763	0.245107	2.385116
O	-1.047192	-3.870287	-1.075641
O	1.417779	4.109098	0.033336
O	0.936329	3.829472	1.666108
H	0.126711	4.369465	1.704213
C	1.440794	4.723698	-2.243243

C	2.716030	4.544755	-1.803506
H	0.878919	3.866423	-2.600195
H	3.152081	3.551613	-1.851561
C	3.586315	5.673204	-1.328634
C	0.775230	6.070434	-2.300163
C	1.780181	7.228668	-2.184333
C	2.797229	6.965900	-1.065622
H	4.131200	5.358044	-0.430247
H	4.359357	5.847902	-2.093314
H	3.487777	7.810418	-0.966476
H	2.266540	6.873431	-0.110303
H	2.312522	7.341039	-3.138259
H	1.246928	8.169229	-2.008631
H	0.198536	6.147903	-3.230484
H	0.034445	6.127396	-1.488674

TSH^{Nb}: ΔG = -1901.92706 a.u.

O	0.027536	0.091743	-0.283906
W	-1.541887	0.607080	-1.975786
W	1.675788	-0.292606	-1.970225
W	1.547551	-0.662847	1.348594
W	-1.694144	0.155516	1.331940
W	-0.613809	-2.335041	-0.627403
Nb	0.670635	2.216880	-0.076702
O	-2.569097	0.625066	-0.329034
O	0.110406	0.246180	-2.949477
O	-0.128706	-0.382765	2.312364
O	2.552427	-0.758347	-0.316681
O	1.766939	1.198577	1.297595
O	0.714676	-2.332231	0.748987
O	1.888577	1.574496	-1.457700
O	0.838107	-2.038188	-1.855893
O	-0.793803	2.257001	-1.473499
O	-1.692373	-1.342729	-1.857143
O	-0.942514	1.959308	1.322726
O	-1.820367	-1.668543	0.739065
O	2.654471	-1.196831	2.546268
O	-2.679013	1.006488	-3.196929
O	2.877775	-0.520705	-3.168458
O	-2.935816	0.258729	2.505851
O	-1.056917	-3.974362	-0.842212
O	1.059682	3.777552	1.079390
O	-0.279887	4.039694	0.541890
H	-0.941410	3.117070	1.168251

3c^{Nb}: ΔG = -1901.96500 a.u.

O	0.026512	0.074758	-0.250683
W	-1.479419	0.679402	-1.913912

W	1.730307	-0.217230	-1.945857
W	1.536352	-0.658722	1.349843
W	-1.712576	0.088439	1.354188
W	-0.581839	-2.291367	-0.660363
Nb	0.730611	2.293683	0.015360
O	-2.530062	0.716539	-0.269993
O	0.133879	0.291217	-2.912452
O	-0.138340	-0.324343	2.336460
O	2.559347	-0.777915	-0.268764
O	1.768424	1.239703	1.317931
O	0.675386	-2.314908	0.795829
O	1.987328	1.546708	-1.446584
O	0.849494	-2.011000	-1.839727
O	-0.691069	2.324792	-1.372082
O	-1.704407	-1.262762	-1.822717
O	-0.930982	2.028348	1.417704
O	-1.856775	-1.673719	0.755113
O	2.618552	-1.183567	2.571681
O	-2.612541	1.136767	-3.116835
O	2.918740	-0.495939	-3.149245
O	-2.948783	0.242177	2.529927
O	-1.039212	-3.923215	-0.902015
O	1.723893	3.948532	-0.283651
O	0.685944	4.105897	0.742234
H	-1.596826	2.729528	1.349461

TS3c^{Nb}: ΔG = -2136.46018 a.u.

O	-0.030249	0.066682	-0.221921
W	-1.530266	0.714940	-1.846630
W	1.714211	0.003139	-1.896440
W	1.507285	-0.588072	1.361253
W	-1.776711	-0.083629	1.365078
W	-0.469286	-2.257465	-0.752537
Nb	0.564584	2.437427	0.181309
O	-2.618301	0.583942	-0.230945
O	0.100456	0.473988	-2.859332
O	-0.187630	-0.449768	2.350703
O	2.563640	-0.588584	-0.244211
O	1.630566	1.309016	1.432859
O	0.771611	-2.288062	0.712357
O	1.856713	1.741370	-1.307113
O	0.950242	-1.845831	-1.911341
O	-0.867068	2.379577	-1.211180
O	-1.647849	-1.245540	-1.876695
O	-1.106342	1.862359	1.538134
O	-1.808502	-1.818619	0.675783
O	2.611036	-1.107179	2.570644
O	-2.675591	1.165454	-3.045054
O	2.930619	-0.137204	-3.101440
O	-3.036021	-0.063922	2.530179

O	-0.827561	-3.903026	-1.083031
O	1.550257	4.161954	-0.188045
O	0.270448	4.028394	1.079452
H	-1.794994	2.543099	1.507973
C	2.528525	4.584498	-2.112693
H	2.076978	3.777795	-2.680402
C	3.465934	4.274454	-1.165756
H	3.756218	3.236743	-1.041197
C	4.208093	5.317071	-0.380354
C	3.561267	6.708316	-0.472713
H	4.295659	4.992533	0.663396
C	3.151129	7.030006	-1.916183
H	4.255184	7.465823	-0.092577
H	2.673969	6.734714	0.170552
C	2.146195	5.996571	-2.453357
H	4.044873	7.029889	-2.554321
H	2.719894	8.034806	-1.979812
H	2.042422	6.085208	-3.542058
H	1.144152	6.188763	-2.043859
H	5.239246	5.352494	-0.765563

3-rad^{Nb}: ΔG = -1826.14540 a.u.

O	0.009257	0.006586	-0.287845
W	-1.521824	0.630916	-1.957350
W	1.683454	-0.234320	-1.910418
W	1.527935	-0.648304	1.379651
W	-1.698671	0.159202	1.330178
W	-0.586736	-2.284393	-0.624418
Nb	0.591461	2.276291	0.049955
O	-2.572128	0.642077	-0.323039
O	0.125647	0.308277	-2.923754
O	-0.140373	-0.382690	2.336322
O	2.563549	-0.720610	-0.258593
O	1.720559	1.244027	1.334380
O	0.732518	-2.328378	0.772683
O	1.827192	1.600760	-1.339848
O	0.874090	-1.996489	-1.852537
O	-0.781495	2.292753	-1.390944
O	-1.685495	-1.311745	-1.871216
O	-0.887875	1.925978	1.271968
O	-1.826197	-1.667046	0.743283
O	2.630240	-1.155204	2.592680
O	-2.645919	1.067173	-3.177715
O	2.916516	-0.385651	-3.093192
O	-2.930975	0.314089	2.512823
O	-1.019420	-3.926067	-0.862060
O	0.726060	4.117282	0.671299

Ti-complexes:

1^{Ti}: ΔG = -1868.04871 a.u.

O	-0.072266	-0.037435	-0.167130
W	-1.442144	0.902774	-1.855146
W	1.743588	-0.121222	-1.684989
W	1.311814	-0.936165	1.536618
W	-1.874250	0.088860	1.365903
W	-0.743929	-2.237022	-0.813460
Ti	0.558680	2.016149	0.433838
O	-2.631736	0.735267	-0.314694
O	0.260848	0.567780	-2.752284
O	-0.431040	-0.734552	2.393721
O	2.458878	-0.901805	-0.045480
O	1.559471	0.893898	1.699668
O	0.481562	-2.508346	0.656135
O	1.907021	1.560279	-0.908232
O	0.822420	-1.865699	-1.885020
O	-0.675095	2.386527	-1.046984
O	-1.692197	-1.058172	-2.017538
O	-1.021851	1.724997	1.562725
O	-2.032485	-1.700036	0.525038
O	2.314196	-1.653698	2.779081
O	-2.465969	1.545729	-3.120566
O	3.071821	-0.233564	-2.818688
O	-3.223227	0.127867	2.480109
O	-1.237511	-3.847158	-1.286647
O	1.021501	3.642034	0.967172
C	1.055088	4.786506	1.784977
H	1.087823	5.686520	1.160704
H	1.947031	4.763515	2.421763
H	0.162520	4.824062	2.420574

TS1^{Ti}: ΔG = -2019.55578 a.u.

O	0.019498	0.013144	-0.267502
W	-1.420256	0.869535	-1.881801
W	1.718153	-0.193087	-1.865902
W	1.454261	-0.839458	1.358855
W	-1.690817	0.190623	1.337406
W	-0.716594	-2.199902	-0.782347
Ti	0.710468	2.156991	0.234652
O	-2.545792	0.788549	-0.308510
O	0.213938	0.515775	-2.871814
O	-0.216053	-0.602436	2.322326
O	2.529083	-0.918260	-0.253306
O	1.739173	1.005517	1.430970
O	0.574100	-2.450867	0.612894
O	1.983735	1.509681	-1.146253
O	0.780308	-1.912573	-1.968448
O	-0.594646	2.398249	-1.139905
O	-1.713571	-1.064183	-1.992437

O	-0.830916	1.826869	1.421483
O	-1.934762	-1.619038	0.581199
O	2.505762	-1.498582	2.558900
O	-2.482082	1.495630	-3.089606
O	2.960435	-0.364922	-3.051688
O	-2.957557	0.286858	2.507597
O	-1.249050	-3.794828	-1.167579
O	0.939012	3.727787	1.540138
C	0.125468	4.346517	2.527881
H	0.763699	4.861190	3.254773
H	-0.461579	3.578197	3.033492
H	-0.556153	5.073831	2.070969
O	1.599130	3.999262	-0.574953
O	3.037874	3.859485	-0.770795
H	1.371543	4.259139	0.648615
H	3.033345	2.951254	-1.150043

TS1'^{Ti}: ΔG = -1944.42634 a.u.

O	-0.075311	0.024111	-0.272403
W	-1.432911	0.607695	-2.066610
W	1.770125	-0.139163	-1.710624
W	1.293351	-0.529380	1.528474
W	-1.915598	0.196759	1.169602
W	-0.562297	-2.270216	-0.625942
Ti	0.393841	2.286901	0.087651
O	-2.682147	0.551841	-0.583184
O	0.293396	0.296457	-2.899901
O	-0.459172	-0.339966	2.342365
O	2.505258	-0.643550	0.022317
O	1.414326	1.343867	1.430045
O	0.624160	-2.268366	0.898174
O	1.814803	1.621990	-1.157005
O	0.998510	-1.959550	-1.702199
O	-0.813691	2.257096	-1.434199
O	-1.557244	-1.363072	-2.000495
O	-1.215765	1.913708	1.150824
O	-1.931449	-1.689926	0.600111
O	2.299672	-0.960799	2.864846
O	-2.446908	1.005241	-3.407676
O	3.118235	-0.308383	-2.779806
O	-3.278913	0.284503	2.229172
O	-0.916837	-3.941126	-0.880522
O	0.435253	3.910300	1.366904
C	0.725890	3.929305	2.751403
H	-0.068589	3.409085	3.295155
H	0.771368	4.967942	3.100618
H	1.677716	3.429429	2.967224
O	1.229839	4.052135	-0.685677
H	2.108871	3.810549	-1.008472
H	1.099041	4.324993	0.496050

2^{Ti}: ΔG = -1828.76960 a.u.

O	-0.075469	0.005690	-0.283486
W	-1.460734	0.608850	-2.109298
W	1.779766	-0.143985	-1.744084
W	1.331577	-0.521822	1.550967
W	-1.910555	0.229098	1.186058
W	-0.571041	-2.288599	-0.613619
Ti	0.389311	2.189728	0.036422
O	-2.670431	0.581701	-0.574398
O	0.281893	0.272608	-2.922924
O	-0.443170	-0.319414	2.344992
O	2.510721	-0.628562	-0.000322
O	1.439278	1.327590	1.448770
O	0.630239	-2.259250	0.901944
O	1.795288	1.635931	-1.205788
O	0.991235	-1.962750	-1.704662
O	-0.815718	2.241965	-1.509278
O	-1.573454	-1.366776	-1.985930
O	-1.167563	1.947987	1.148773
O	-1.932661	-1.663083	0.619887
O	2.355361	-0.973135	2.896004
O	-2.500636	0.987228	-3.464398
O	3.137131	-0.312244	-2.834374
O	-3.279526	0.349474	2.267448
O	-0.939321	-3.980736	-0.858951
O	0.811081	3.934864	0.258977
H	1.568429	4.399434	-0.122848

TS2^{Ti}: ΔG = -1980.27906 a.u.

O	-0.018998	0.014392	-0.280233
W	-1.531613	0.623987	-1.951859
W	1.670902	-0.182371	-1.900214
W	1.498368	-0.624803	1.378415
W	-1.715065	0.148296	1.324843
W	-0.585383	-2.298823	-0.636894
Ti	0.511078	2.196218	0.036120
O	-2.611374	0.611870	-0.336823
O	0.097181	0.275764	-2.944989
O	-0.178731	-0.439395	2.348698
O	2.546986	-0.727619	-0.251429
O	1.637158	1.231202	1.335628
O	0.717106	-2.339701	0.767973
O	1.769876	1.582736	-1.350384
O	0.860990	-1.992955	-1.846880
O	-0.770694	2.249362	-1.393482
O	-1.700868	-1.331499	-1.879503
O	-0.933385	1.868727	1.297307

O	-1.841202	-1.694767	0.718797
O	2.607167	-1.125887	2.602411
O	-2.658797	1.066155	-3.180905
O	2.907592	-0.352527	-3.092275
O	-2.967401	0.261663	2.505201
O	-1.007988	-3.951504	-0.883041
O	-0.234440	4.259345	0.393778
O	1.962908	3.678336	0.325432
H	2.483443	3.460146	1.111335
H	1.024423	4.294419	0.519782
O	-0.733913	4.410708	1.757561
H	-1.105324	3.506114	1.879179

3a^{Ti}: ΔG = -1903.88887 a.u.

O	-0.080660	0.017018	-0.270641
W	-1.633704	0.607566	-1.972396
W	1.652675	-0.089848	-1.888339
W	1.472507	-0.572207	1.432519
W	-1.813914	0.115728	1.344919
W	-0.558516	-2.321862	-0.644763
Ti	0.381324	2.109554	0.032757
O	-2.710674	0.489477	-0.348472
O	0.063210	0.350030	-2.918586
O	-0.243261	-0.449427	2.356029
O	2.523508	-0.586824	-0.221377
O	1.540713	1.276187	1.388248
O	0.765446	-2.298442	0.757890
O	1.680964	1.706275	-1.291148
O	0.914391	-1.910105	-1.845519
O	-0.985188	2.235826	-1.375979
O	-1.666307	-1.373294	-1.909735
O	-1.128711	1.846187	1.320455
O	-1.821433	-1.762292	0.699557
O	2.603825	-1.052965	2.675584
O	-2.781929	0.993249	-3.233021
O	2.922981	-0.186098	-3.082847
O	-3.098664	0.138773	2.528387
O	-0.901231	-4.012706	-0.916793
O	0.483577	3.871763	0.546519
O	-0.394136	4.451965	1.521029
H	-0.944803	3.669693	1.757022

3b^{Ti}: ΔG = -1903.88947 a.u.

O	0.027714	0.028394	-0.308491
W	-1.514305	0.651855	-1.953068
W	1.672054	-0.255187	-1.970899
W	1.566236	-0.615683	1.324936
W	-1.629594	0.282468	1.340213

W	-0.620242	-2.263617	-0.586998
Ti	0.636042	2.150944	-0.050167
O	-2.565527	0.673236	-0.322134
O	0.080462	0.235878	-2.976863
O	-0.066555	-0.335031	2.330177
O	2.577598	-0.767285	-0.324838
O	1.772820	1.259169	1.218946
O	0.745011	-2.311353	0.781439
O	1.853952	1.521280	-1.475014
O	0.818176	-2.031654	-1.839117
O	-0.723044	2.271388	-1.436999
O	-1.722612	-1.309061	-1.838554
O	-0.852223	1.959333	1.246488
O	-1.795356	-1.604107	0.784536
O	2.698579	-1.110170	2.529424
O	-2.661651	1.084715	-3.167355
O	2.868759	-0.502040	-3.191331
O	-2.856893	0.422549	2.547345
O	-1.084787	-3.913626	-0.779129
O	1.925248	3.949481	-0.156336
O	0.666502	3.936395	0.584172
H	2.594781	3.871049	0.548708

TS3a^{Ti}: ΔG = -2138.38889 a.u.

O	-0.039844	0.055446	-0.373114
W	-1.523104	0.570530	-2.115191
W	1.613936	-0.485619	-1.943257
W	1.469085	-0.390139	1.367236
W	-1.672636	0.652260	1.194799
W	-0.781382	-2.166361	-0.348836
Ti	0.707882	2.209785	-0.421087
O	-2.580256	0.867190	-0.509545
O	0.075963	-0.047938	-3.040181
O	-0.173247	0.093857	2.293534
O	2.482643	-0.817511	-0.239993
O	1.777513	1.409937	1.036682
O	0.557554	-2.112867	1.032248
O	1.896181	1.357322	-1.679635
O	0.682997	-2.185008	-1.609300
O	-0.679361	2.198959	-1.827064
O	-1.824469	-1.349001	-1.744076
O	-0.798233	2.283936	0.895428
O	-1.951320	-1.276155	0.900204
O	2.552580	-0.797376	2.650126
O	-2.640938	0.872196	-3.397742
O	2.812019	-0.942511	-3.099420
O	-2.899054	1.021635	2.352312
O	-1.328824	-3.805473	-0.330452
O	1.127811	3.918141	-0.304444
O	0.256423	4.791954	0.989398

H	-0.296089	3.984352	1.146475
C	-1.191996	6.009094	2.004089
C	-0.318770	5.570534	2.965841
H	-2.083093	5.424186	1.789893
H	-0.511818	4.623831	3.464007
C	-1.062238	7.345495	1.333805
C	0.322059	7.978303	1.540792
H	-1.293130	7.239632	0.267659
C	0.768551	7.855484	3.003927
H	0.297507	9.029142	1.233653
H	1.048545	7.471871	0.894337
C	0.852281	6.382585	3.440505
H	0.049206	8.381422	3.645382
H	1.738485	8.340977	3.154086
H	0.916020	6.303962	4.532822
H	1.770602	5.917872	3.055587
H	-1.845563	8.000775	1.745160

TS3b^{Ti}: ΔG = -2138.38494 a.u.

O	-0.222809	0.046914	-0.265576
W	-1.915162	0.437922	-1.817476
W	1.377518	0.354343	-1.940980
W	1.474293	-0.279338	1.300956
W	-1.816331	-0.197301	1.426479
W	-0.294888	-2.256837	-0.713892
Ti	-0.146712	2.376621	0.179497
O	-2.888088	0.081756	-0.170498
O	-0.306398	0.512855	-2.901602
O	-0.133125	-0.523026	2.353463
O	2.446887	-0.043817	-0.368782
O	1.190878	1.565539	1.356515
O	1.091915	-2.088512	0.617343
O	1.119197	2.079295	-1.293513
O	1.003568	-1.581329	-1.971723
O	-1.524199	2.148540	-1.193122
O	-1.643642	-1.518550	-1.874210
O	-1.443342	1.614275	1.484657
O	-1.555805	-2.029665	0.718650
O	2.737290	-0.565101	2.447300
O	-3.177817	0.671410	-2.975542
O	2.559803	0.526926	-3.191699
O	-2.997833	-0.447680	2.664821
O	-0.343041	-3.953228	-1.045771
O	0.625832	4.163697	0.431061
O	-1.141711	4.076368	0.642071
H	-1.203328	4.121287	1.610418
C	2.561760	4.663010	-0.465874
C	2.741842	4.186863	0.802041
H	2.507486	3.953884	-1.285036
H	2.869658	3.121419	0.955718

C	2.879282	5.084657	1.999673
C	2.418138	6.523341	1.719295
H	2.324596	4.651346	2.840747
C	2.961829	7.019744	0.372623
H	2.739281	7.184251	2.531991
H	1.322377	6.546618	1.696652
C	2.476574	6.129067	-0.784029
H	4.059832	7.009148	0.401458
H	2.662628	8.058346	0.193885
H	3.051450	6.332347	-1.696591
H	1.431100	6.362234	-1.033051
H	3.936668	5.080444	2.308092

TSH^{Ti}: ΔG = -1903.86822 a.u.

O	-0.001887	0.015719	-0.278586
W	-1.533474	0.627536	-1.956520
W	1.677109	-0.205681	-1.917734
W	1.533658	-0.647706	1.368182
W	-1.698953	0.136856	1.332981
W	-0.582605	-2.305947	-0.642174
Ti	0.591231	2.143642	-0.024981
O	-2.588022	0.624993	-0.313201
O	0.109723	0.256013	-2.944990
O	-0.152924	-0.415131	2.338985
O	2.556499	-0.765097	-0.289697
O	1.731589	1.176025	1.314014
O	0.710761	-2.349562	0.763141
O	1.833399	1.596912	-1.372858
O	0.856865	-2.011478	-1.857595
O	-0.785518	2.234589	-1.447060
O	-1.703899	-1.337624	-1.860053
O	-0.941842	1.934229	1.364616
O	-1.835026	-1.682878	0.737746
O	2.639752	-1.189571	2.577755
O	-2.675319	1.034882	-3.184945
O	2.899038	-0.397966	-3.116358
O	-2.953506	0.224871	2.506724
O	-1.020012	-3.955366	-0.877471
O	1.191942	3.703435	0.805610
O	-0.207235	3.961177	0.466334
H	-0.852039	3.066336	1.166027

3c^{Ti}: ΔG = -1903.89799 a.u.

O	0.019256	0.016749	-0.262753
W	-1.450627	0.730212	-1.882539
W	1.725650	-0.187531	-1.933044
W	1.546495	-0.600992	1.337299
W	-1.704801	0.094994	1.364140

W	-0.567565	-2.257768	-0.659581
Ti	0.728721	2.286342	0.029431
O	-2.540374	0.727358	-0.249341
O	0.128256	0.290430	-2.921890
O	-0.138050	-0.314799	2.351576
O	2.572554	-0.795397	-0.277593
O	1.776401	1.243821	1.304648
O	0.673980	-2.299983	0.801527
O	1.963023	1.538174	-1.421919
O	0.852607	-2.021399	-1.854342
O	-0.678490	2.329477	-1.347723
O	-1.709921	-1.244477	-1.807462
O	-0.915316	2.003901	1.393136
O	-1.869343	-1.667438	0.775980
O	2.625721	-1.148806	2.566801
O	-2.599025	1.180623	-3.089008
O	2.920290	-0.460934	-3.147386
O	-2.945230	0.252898	2.548014
O	-1.046928	-3.898675	-0.885230
O	1.680496	3.849317	-0.263892
O	0.650862	3.994749	0.755090
H	-1.576707	2.670966	1.156914

TS3c^{Ti}: ΔG = -2138.37619 a.u.

O	-0.001115	-0.022056	-0.259813
W	-1.464265	0.745098	-1.826909
W	1.739490	0.004480	-1.901813
W	1.545340	-0.503323	1.336215
W	-1.732088	-0.047228	1.370979
W	-0.426406	-2.230499	-0.730410
Ti	0.623117	2.503368	0.154016
O	-2.588539	0.605807	-0.226070
O	0.126339	0.431135	-2.890681
O	-0.148239	-0.389810	2.360724
O	2.612264	-0.602574	-0.261677
O	1.660933	1.351174	1.363352
O	0.803117	-2.260567	0.743927
O	1.868227	1.712011	-1.334039
O	0.984797	-1.890223	-1.912932
O	-0.787216	2.366194	-1.222857
O	-1.627303	-1.250544	-1.854331
O	-1.052998	1.877131	1.473961
O	-1.788850	-1.792500	0.717919
O	2.650707	-1.015462	2.562160
O	-2.624594	1.186490	-3.029685
O	2.959135	-0.155998	-3.117625
O	-2.993855	-0.007734	2.545883
O	-0.818542	-3.892716	-1.011362
H	-1.738765	2.516283	1.231213
O	1.674637	4.124797	-0.224879

O	0.299064	4.001399	0.976679
C	2.738367	4.478445	-2.011320
H	2.293993	3.699147	-2.619793
C	3.572966	4.112255	-0.986081
H	3.799200	3.060684	-0.851732
C	4.329075	5.110865	-0.154818
C	3.788620	6.541915	-0.302736
H	4.316504	4.794140	0.894797
C	3.519324	6.875584	-1.776292
H	4.499988	7.254528	0.129348
H	2.855512	6.632404	0.265060
C	2.484435	5.913023	-2.384139
H	4.458965	6.798430	-2.339993
H	3.173340	7.909693	-1.882255
H	2.471612	6.001914	-3.477926
H	1.472624	6.182852	-2.050206
H	5.385451	5.074835	-0.464779

3-rad^{Ti}: ΔG = -1828.08727 a.u.

O	-0.076053	0.011477	-0.281742
W	-1.448056	0.589107	-2.084184
W	1.765431	-0.139198	-1.732676
W	1.305740	-0.526004	1.526732
W	-1.904116	0.221988	1.177250
W	-0.561986	-2.261303	-0.612243
Ti	0.390403	2.189946	0.036701
O	-2.667909	0.574940	-0.578428
O	0.277859	0.280795	-2.913092
O	-0.441594	-0.320766	2.340144
O	2.502667	-0.613419	0.005839
O	1.411594	1.365436	1.425170
O	0.639669	-2.257879	0.905970
O	1.802890	1.647122	-1.212787
O	0.992631	-1.956952	-1.700174
O	-0.793015	2.255948	-1.470793
O	-1.571720	-1.365213	-1.994636
O	-1.191453	1.943954	1.161279
O	-1.924087	-1.667112	0.613013
O	2.319025	-0.948302	2.855709
O	-2.467487	0.981417	-3.417700
O	3.101849	-0.320798	-2.808057
O	-3.259628	0.311704	2.240264
O	-0.920712	-3.930828	-0.854032
O	0.775237	3.991453	0.298052